Developing and validating a high-throughput drug screen in a zebrafish model of amyotrophic lateral sclerosis

Alexander McGown

Department of Neuroscience (SITraN)

Supervisors: Dr Tennore Ramesh and Prof Pamela Shaw

PhD Thesis

Submitted February 2014

Abstract

Amyotrophic Lateral Sclerosis (ALS) is a progressive neurodegenerative disorder that rapidly leads to paralysis and death. Currently the treatment options for ALS are limited and there is a desperate need for new therapeutic agents to combat the disease. Zebrafish were highlighted as having the potential of being both an excellent model for ALS and as a drug screening system due to their rapid development, large numbers, optical clarity and susceptibility to genetic manipulation. This work describes the use of a zebrafish model of ALS that overexpresses the mutant G93R SOD1 gene alongside a hsp70-DsRed stress readout. This has been used to demonstrate that the hsp70- DsRed readout is activated by sod1 toxicity and that in the embryo stages it is characterised by expression in the glycine positive inhibitory interneurons. Further investigation of these neurons identified defective glycinergic transmissions from the stressed neurons. In the adults, the motor neurons of the spinal cord are primarily affected, and also show defective neuromuscular junctions (NMJ's). This suggests that ALS is a disease which does not start at symptom onset but is a progressive disorder, where specific neuronal subtypes are initially dysregulated, followed by the dysregulation within other neuronal subtypes. Based upon this fluorescence readout, a high-throughput drug screen using the zebrafish was designed, optimised and validated which has the capability to screen 100's of compounds with a sensitivity and specificity of over 90%. This assay has been utilized to screen a small molecule library of 2000 compounds in order to identify potential therapeutics for ALS. This screen highlighted novel therapeutics that can potentially ameliorate sod1 toxicity and some that upregulate the heat shock response, a known cellular repair pathway. Selamectin, a macrocyclic lactone with known neuroprotective properties, was identified as the most promising hit from the screen. By combining Selamectin and Riluzole, a reduction in neuronal stress was seen, which offered the potential for a therapy with reduced side effects e.g. sedation. In conclusion, this work has highlighted the potential of a novel therapeutic for the treatment of ALS that should be taken towards mouse trials.

Statement of contribution

I state that all work in this thesis is my own. The only exception to this is the electrophysiology experiments outlined in chapter 3.4 which were performed in a collaboration with Jonathan R. McDearmid and his lab from the University of Leicester and has been published in (McGown et al 2013).

Acknowledgments

This work is dedicated to my Grandad and Uncle whose words of wisdom, laughs and guidance have given me the drive to succeed

I would like to thank Dr Tennore Ramesh and Professor Dame Pamela Shaw for all their guidance and support throughout the years, without their insight and knowledge this would not have been possible. Dr Niki Panagiotaki deserves a special mention for her help and patience with me and for making my time in the lab enjoyable and rewarding. I would also like to thank Danielle for putting up with my moaning, working weekends and endless science chatter! Finally a special mention for my parents who have been so supportive over the years, they are amazing people who have always gone the extra mile and further to help me.

Contents

List of abbreviations

- ADP- Adenosine Diphosphate
- ALS – Amyotrophic Lateral Sclerosis
- ApoR – Apomorphine R
- ApoS – Apomorphine S
- ATP- Adenosine Tiphosphate
- BAC- Bacterial artificial chromosome
- BBB- Blood brain barrier
- BSA- Bovine serum albumin
- CHAT- Choline acetyltransferase
- CNS – Central Nervous System
- CSF- Cerebrospinal fluid
- Cu-Copper
- DAPI- 4',6-diamidino-2-phenylindole
- DMSO- Dimethyl sulfoxide
- Dpf – days post fertilisation
- EGCG- Epigallocatechin gallate
- ER – Endoplasmic reticulum
- FDA- Food Drug Administration
- FRET- Fluorescence resonance energy transfer
- FTD – Fronto-temporal dementia
- FUS – Fused in Sarcoma

- GABA – Gamma-amino butyric acid
- GFP- Green fluorescent protein
- GWAS – Genome wide association study
- Hpf- hours post fertilisation
- IC – inhibitory concentration
- LD – Lethal dose
- HSF1- Heat shock factor 1
- HSP- Heat Shock protein
- Kda- Kilo Daltons
- MND - Motor Neuron Disease
- NF-κB- Nuclear factor kappa B
- NDS- Normal donkey serum
- NGS- Normal goat serum
- NICE- National Institute For Clinical Excellence
- NMJ – Neuro-muscular junction
- NTG – Non-Transgenic organism
- PBS – Phosphate buffered saline
- PBDT- PBS, DMSO, BSA and Tween-20 mixture
- PFA- Paraformaldehyde
- qPCR- Quantitative polymerase chain reaction
- ROS- Reactive oxygen species
- SD – Standard deviation
- SSMD – strictly standardised median difference

- SOD1- Superoxide dismutase 1
- SV2 – Synaptic vesicle protein 2
- TARDBP - Transactivating response element DNA binding protein-43
- TG – Transgenic organism
- TILLING – targeting induced local lesions in genomes
- UPR – Unfolded protein response
- UV – Ultraviolet
- VCP- Valosin Containing Protein
- VEGF – Vascular endothelial growth factor
- WT - Wildtype
- Zn- Zinc

List of tables and figures

1. Introduction

Motor Neuron Disease (MND) is a rapid onset neurodegenerative disorder where typically sufferers die within 3-5 years from the onset of disease symptoms, usually from respiratory failure due to muscle paralysis (Pasinelli & Brown 2006). The initial symptoms of MND include rapidly progressing muscular weakness and atrophy throughout the body together with symptoms of dysarthria (speech difficulties), dysphagia (difficulty swallowing), dyspnea (breathing problems) and paralysis. 25% of MND cases are bulbar in onset which usually presents as slurred speech and difficulty swallowing. The other 75% of MND cases present with individual limb weakness in an arm or leg which over time progresses to other limbs. MND onset usually occurs at around 55 years of age and is more commonly seen in males with a male/female ratio of 1.5:1 (Johnston et al 2006). The incidence rate of MND is ~2 in 100,000 based on various population studies (Abhinav et al 2007, Chio et al 2009). MND was first identified and documented in France in 1869 by Jean-Martin Charcot and was initially labelled *la maladie de Charcot* (Charcot's disease) (Krajewski et al 2000). In most commonwealth countries the disease is known as motor neuron disease but is more commonly known worldwide as Amyotrophic Lateral Sclerosis (ALS) or in the USA as its common household name Lou Gehrig disease after the famous baseball player who was diagnosed with the disease in 1939. There is no cure for ALS and very limited treatment options. Currently there is only one FDA and NICE approved drug for the treatment of the disease, Riluzole, which is believed to function by decreasing glutamate excitotoxicity but the method of action is poorly understood. The majority of treatments for ALS are palliative treatments such as assisted ventilation. ALS is caused by a progressive loss of motor neurons in the brain and spinal cord which leads to muscle dennervation, paralysis and death. The exact causes of ALS remain unclear with only approximately 10% of cases occurring due to an identifiable genetic cause. ALS has been linked to fronto-temporal dementia (FTD) which is a progressive neuronal loss in the frontal and temporal cortex leading to behavioural changes and is the second most common form of young-onset dementia after Alzheimer's disease (Van Langenhove et al 2012). FTD and

ALS have been linked by common genetic causes of TDP-43, FUS and C9orf72 and it is predicted that 15% of FTD positive patients also showed features of MND (DeJesus-Hernandez et al 2011, Lagier-Tourenne et al 2012, Ringholz et al 2005) . TDP-43 mis-localisation has been shown as a linked mechanism between FTD and ALS as TDP43 positive inclusions are seen in both ALS and FTD (Arai et al 2006, Neumann et al 2006). Fused in Sarcoma (FUS) mutations are also seen in familial ALS and rare cases of FTD suggesting another genetic link between the two diseases (Kwiatkowski et al 2009). ALS and FTD can now be brought together under a broad spectrum neurodegenerative disorder with overlapping clinical symptoms.

1.1 Sporadic ALS

95% of ALS cases are sporadic in nature and the exact causes of the disease are unknown, though several genetic and environmental factors have been potentially identified in disease pathogenesis. Factors such as diet, geographical location and smoking have been implicated as causative factors in ALS (Armon 2003). One potential factor is occupational hazards such as prolonged exposure to heavy metals, which has been implicated in causing an increased risk of developing ALS (Mitchell 1987). Furthermore a trend has been identified between people who engage in high levels of physical activity and ALS. In Italy footballers have been shown to have a higher risk of developing ALS in later life in comparison to the normal population (Chio et al 2005). In addition, it has been shown that people who spend their career in the armed forces also have an increased incidence rate of ALS, suggesting that physical exercise may be linked to the development of ALS (Weisskopf et al 2005). Although multiple studies suggest a link between physical exercise and ALS this theory is unproven and may be purely coincidental. One possible link between physical activity and ALS is that increased physical strain and exercise may lead to higher neuronal stress levels and in people with an underlying genetic predisposition for ALS this may be a trigger that leads to the development of the disease in later in life. Another feature of sporadic ALS is the more common occurrence of the

disease in males. A combinatorial study looked at 2 possibilities of the effect of gender on disease. They looked at the incidence and the prevalence of the disease in men and women and showed that the incidence was higher in males with a rate of 1.11-1.39 compared to females (Uruguay omitted with a ratio of 2.32). The study also showed that men had an earlier onset than women, but that gender did not have an effect on survival (McCombe & Henderson 2010). This suggests that in sporadic ALS there are multiple factors that influence the disease and it is a cumulative effect of multiple factors that may ultimately lead to disease onset.

1.2 Familial ALS

5-10% of ALS cases are familial in nature and usually show an autosomal dominant inheritance pattern (Bento-Abreu et al 2010). The genes were identified by various techniques including linkage, Sanger sequencing, Homozygosity mapping and newer techniques such as whole exsome sequencing, repeat-primed PCR and genome wide association studies (GWAS). GWAS studies in ALS are difficult as they require large sample sizes and this is challenging in rarer diseases, such as ALS. More recently GWAS is being used to identify pathways involved in disease allowing a better understanding of disease pathogenesis. Below is a table summarising the major familial genes associated with ALS.

Locus	Chromosome	Gene ID	Protein/function	Inheritance	Onset
ALS1	21q22.11	SOD1	Superoxide dismutase 1, oxidative stress	AD & AR	Adult
ALS2	2q33.2	ALS2	Alsin/Rho Nucleotide exchange factor	AR	Juvenile
ALS4	9q34.13	SETX	Senataxin, RNA/DNA helicase	AD	Juvenile
ALS5	15q21.1	SPG11	Spatacsin protein, transmembrane protein	AR	Juvenile
ALS6	16p11.2	FUS	Fused in sarcoma, RNA binding protein	AD	Adult
ALS7	20p13	*	*	AD	Adult
ALS8	20q13.33	VAPB	Vesicle associated membrane protein, vesicular trafficking	AD	Adult
ALS10	1p36.22	TARDBP	TAR DNA binding protein, transcriptional processing, splicing regulation	AD	Adult
ALS12	10p13	OPTN	Optineurin, membrane and vesicle trafficking	AD & AR	Adult
ALS14	9p13.3	VCP	Valosin containing protein, vesicle transport and fusion	AD	Adult
ALS15	Xp11.21	UBQLN2	Ubiquilin 2, degredation	X Linked	Juvenile & Adult
ALS16	9p13.3	SIGMAR1	Sigma non-opiod intracellular receptor 1, ER chaperone	AR	Juvenile
ALS-FTD	9p21.2	C9ORF72	Chromosome 9 open reading frame 72	AD & Sporadic	Adult

Table 1.1: Summary of the major known genes implicated as causative in ALS. (*= currently unknown data)

1.2.1 SOD1

The most common familial genetic cause of ALS is mutation in the superoxide dismutase 1 gene (*SOD1*) which was identified in 1993 and found at chromosome position 21q22.1 (Rosen et al 1993). SOD1 is one of three human superoxide dismutase enzymes. The *SOD1* gene one of the most common causative factor of familial ALS and is also the most researched. SOD1 is implicated in approximately 20% of familial cases and 2% of all ALS cases (Rosen et al 1993). SOD1 is an enzyme consisting of 153 amino acids and is active when expressed as a homodimer. It is a Cu/Zn binding protein whose function is to facilitate the conversion of superoxide free radicals to hydrogen peroxide which is then further catalysed to water and oxygen by glutathione peroxidase or catalase. More than 150 mis-sense mutations occurring throughout the SOD1 protein have been identified as causative for familial ALS with the majority of these are dominant mutations (Turner & Talbot 2008). The majority of mutations are missense mutations and include mutations in regions that have no effect on the catalytic activity of the protein, which suggests that the cause of neuronal death is not only due to altered dismutase activity, but also to altered protein structure and folding (Rosen et al 1994). This is further supported by mouse data where a complete knockout of SOD1 protein did not lead to the onset of ALS and the mice lived an uncompromised lifespan (Reaume et al 1996). This suggests that altered protein function rather than non-functional protein is a causative factor for ALS and that mutant SOD1 leads to a toxic gain of function. More recently this theory has been brought into question as SOD1 knockout mice showed denervation, muscle atrophy and weakness comparable with SOD1 mutant models (Fischer et al 2012). These studies ran for longer and show a progressive degeneration of the motor neurons. This data supports the idea that a loss of SOD1 is enough to lead to ALS and loss of SOD1 function may cause disease. SOD1 has been shown to become misfolded, leading to its targeting for degradation via the ubiquitylation pathway, although this has been shown to fail, somehow allowing mutant SOD1 to form aggregates (Basso et al 2006). Misfolded SOD1 appears to be resistant to the degradation pathways leading to impairment of the proteosomal and

autophagy pathways, with increased numbers of autophagosomes detectable in rodent models and ALS patients (Morimoto et al 2007, Sasaki 2011). The mutant SOD1 aggregates have also been shown to induce a stress response in affected cells, leading to activation of the unfolded protein response (UPR) and microglial activation (Saxena et al 2009, Saxena & Caroni 2011). Mutant SOD1 has then been shown to cause cellular toxicity via multiple pathways to lead to disease (See chapter 1.3 What causes ALS?). In mutant SOD1 the aggregates appear as TDP-43 negative cytoplasmic inclusions (Mackenzie et al 2007). This may suggest that SOD1 and TDP-43 mediated ALS are mediated through different pathways, although evidence suggests that TDP-43 interacts with mutant SOD1 specifically (Higashi et al 2010). WT SOD1 has also been shown to have an increased propensity to become misfolded, aggregation prone and toxic to motor neurons when oxidised, which implicates WT SOD1 as a potential cause of sporadic ALS after a secondary modification leading to misfolding (Bosco et al 2010, Ezzi et al 2007). This has been confirmed in some sporadic ALS cases where SOD1 positive aggregates were observed in cases with no SOD1 mutation present (Bosco et al 2010). This is still a controversial finding and other groups have failed to replicate these findings in different sporadic ALS cohorts, so a SOD dependant pathway common to sporadic and familial ALS is still unconfirmed (Brotherton et al 2012). In general *SOD1* mutations are less associated with fronto-temporal dementia (FTD) than other familial causes of ALS e.g. C9orf72

.

1.2.2 ALS2

More recently other genes have been implicated in ALS. Juvenile forms of ALS have been associated with the *ALS2* gene found on chromosome 2q33 which encodes the alsin protein (Hadano et al 2001). Juvenile ALS is a rare form of ALS which has an early onset and slightly different disease course compared to the adult disease progression. It occurs under both sporadic and familial circumstances (Grunnet et al 1989, Lerman-Sagie et al 1996). The *ALS2* gene encodes a 1657 amino acid protein alsin which acts via

activation of small GTPases. Alsin mutation is a relatively rare cause of ALS resulting in juvenile and infantile onset and has been detected in consanguineous families from Europe, North Africa and the Middle East (Devon et al 2003). Generally juvenile onset ALS patients will have a slower disease progression with a far longer survival compared to patients who develop the adult-onset disease. A common feature of mutations in ALS2 is decreased protein stability, which suggests that the resulting loss of ALS2 is causative for the motor neuron death seen in these patients (Yamanaka et al 2003). ALS2 deficient mice show a range of defects such as age dependent loss of motor ability, increased anxiety and susceptibility to stress, although little neuropathology was seen (Cai et al 2005). When the cellular mechanisms involved were further probed in the mouse model, progressive axonal degeneration could be seen in the lateral spinal cord particularly affecting the descending axons of the upper motor neurons, but the lower motor neurons were preserved (Yamanaka et al 2006). Taken into context this suggests that these juvenile forms of ALS are quite distinct to the classical forms and that these disease pathways sit somewhere between hereditary spastic paraparesis and ALS.

1.2.3 TDP-43

Recently the *TARDBP* (Transactivating response element DNA binding protein-43) gene on chromosome 1p36 was identified as a causative gene for ALS (Sreedharan et al 2008). *TARDBP* encodes the TDP-43 protein and mutations in the glycine rich carboxyl-terminal encoded in the 6th exon have been linked to ALS, although the pathway by which TDP-43 causes the disease is still unknown. TDP-43 has been identified as a major component of the ubiquitinated inclusions seen in sporadic ALS and mutations in the TARDBP gene are present in ~4% of familial ALS cases (Mackenzie et al 2010, Neumann et al 2006). TDP-43 positive inclusions are present in a range of neurological disorders including ALS and have a probable role in the disease pathogenesis. TDP-43 is known to be highly conserved and to have a key role in transcription and splicing regulation (Kuo et al 2009). Mouse

models of TDP-43 mutations showed significant alterations in splicing even in the absence of TDP-43 aggregation (Arnold et al 2013). TDP-43 has been shown to bind approximately 30% of the mouse transcriptome which shows the wide range of regulation that TDP-43 controls (Tollervey et al 2011). TDP-43 function is auto-regulated via a negative feedback loop to control mRNA degradation mechanisms (Ayala et al 2011). The majority of pathogenic mutations are found in the C-terminus and this is required for the auto-regulation so potentially it is this dysregulation that leads to aggregation and pathogenesis. This has been further proven by overexpression of normal TDP-43 in mice which leads to an overall reduction in functional protein (Igaz et al 2011, Xu et al 2010).The mechanisms of TDP-43 proteinopathy and toxicity are poorly understood. Given the range of binding partners, it is predicted that neuronal function could easily be altered by mutations. Full length TDP-43 has been shown to intrinsically aggregate, a process which requires all of the C domain, N terminus and RNA binding domain, suggesting that RNA binding and aggregation lead to toxicity (Voigt et al 2010). TDP-43 structural analysis highlighted prion like domains within the C terminus which suggests that TDP-43 toxicity may spread in a prionoid- like dispersion which has been observed in ALS patients (Ravits & La Spada 2009). Although aggregation as a disease mechanism has supporting evidence from human data, the animal models continue to show toxicity in the absence of aggregates. This suggests that aggregation may not be a pre-requisite for TDP-43 mediated toxicity. It is hypothesised that the aggregates may accelerate the disease progression as has been shown in sporadic ALS patients (Nishihira et al 2009). Recently, multiple labs have shown in a zebrafish model of Tdp-43 mediated ALS, knockdown of Tdp-43 did not show a phenotype and this was due to a compensatory mechanism by a novel splice isoform, known as *tardbpl*, which had the capability to produce the full length protein. By knocking down both genes, a severe phenotype was seen with shortened motor axons, locomotor defects and death at around 10 days post fertilisation (Hewamadduma et al 2013, Schmid et al 2013). These data suggest that the two genes work in tandem to auto-regulate themselves and that mutations are needed in both to induce the phenotype in zebrafish.

1.2.4 FUS

Another gene implicated in ALS is the *FUS* gene, a 526 amino acid protein which is also known as translocated in liposarcoma (TLS) and is found on chromosome 16 and is present in ~2% of familial ALS cases (Kwiatkowski et al 2009). *FUS* has also been implicated in cancer as an oncogene, but mutations in *FUS* lead to aggregation and accumulation of mutant proteins which is associated with neuronal toxicity and neuronal death in the spinal cord (Valdmanis et al 2009). Both FUS and TDP-43 are proteins which bind RNA/DNA, suggesting this could be a major pathway in ALS pathogenesis, possibly via alternative splicing (Kwiatkowski et al 2009, Vance et al 2009). FUS protein has been found to accumulate and aggregate in the cytoplasm of FUS positive ALS cases (Vance et al 2009). The FUS protein also contains a SYGQ domain which has been implicated as having prion like properties which may explain why aggregates of FUS are seen (Cushman et al 2010, Kato et al 2012). Alongside increased FUS protein in the cytoplasm, reduced nuclear staining is seen in FUS positive cases, which suggests that problems in nuclear transport may occur (Dormann & Haass 2011). FUS positive inclusions also contain stress granule markers such as ubiquitin and p62, suggesting that cellular stress and autophagy are common mechanisms of FUS-mediated ALS. In mice, wild-type FUS overexpression leads to an aggressive neurodegenerative phenotype in the homozygous mouse, but no degeneration was seen in the heterozygous animals. Both the homozygous and heterozygous FUS overexpressing mice showed higher protein levels both in the nucleus and in the cytoplasm. Despite only small differences in FUS expression between the heterozygous and the homozygous mice, only the homozygous showed the motor dysfunction alongside FUS positive inclusions and gliosis (Mitchell et al 2013). More work is needed to fully understand the pathways by which FUS mediated toxicity leads to disease.

1.2.5 VCP

Other recently identified mutations in ALS are mutations in valosin containing protein (VCP). *VCP* mutations have been shown to lead to TDP-43 depositions which are a hallmark of ALS pathology (Shaw 2010). It has been identified in some forms of fronto- temporal dementia (FTD) associated with Paget's disease and was found to be a candidate gene of ALS through next generation sequencing of families in Italy and the USA (Johnson et al 2010). The ALS phenotype arising from *VCP* mutations appears to be a rare manifestation and VCP is a low risk factor for ALS (Koppers et al 2012, Tiloca et al 2012). Heterozygous knock in VCP mutations have been performed in mice but they did not lead to a reduction in lifespan, although weakness and weight loss were seen at the later stages of life and a loss of 50% of motor neurons was seen in the spinal cord at 20 months of age (Yin et al 2012). Upon further inspection of the spinal cords of these mice, gliosis, TDP-43 positive inclusions and evidence of oxidative stress were present. Homozygous expression of human mutant *VCP* mutations in mice leads to a much more severe phenotype, with average survival only 21 days and severe motor defects observed (Nalbandian et al 2012). These data appear to show the very strong deleterious effect of *VCP* mutations in ALS.

1.2.6 OPTN

Optineurin is a protein encoded by the *OPTN* gene and has been implicated as causative in open angle glaucoma. Mutations in *OPTN* leading to ALS were first identified in Japanese patients (Maruyama et al 2010). Optineurin has many known functions including cellular morphogenesis, membrane trafficking, vesicle trafficking and various mutations have been identified in optineurin that stop it from inhibiting the activation of nuclear factor kappa B (NF-κB) (Maruyama et al 2010). This upregulated NF-κB has been highlighted as causative for ALS and also as a major target for new

therapeutic development. Optineurin positive inclusions have also been seen to co-localise in familial and sporadic cases with SOD1 mutations (Hortobagyi et al 2011). *OPTN* mutations may be linked to longer survival as various studies showed family members with survival over ten years although some OPTN patients had a rapid disease progression (Tumer et al 2012)

1.2.7 C9orf72

Two groups identified the C9ORF72 mutations as causative for ALS. They found a hexanucleotide repeat (GGGGCC)n within intron 1 to be causative for ALS and FTD (DeJesus-Hernandez et al 2011, Renton et al 2011a). Controls are found to have up to 30 hexanucleotide repeats, but in ALS patients between 700-4400 have been seen, suggesting that large numbers of repeats lead to disease, although an exact pathogenic number is unknown (Beck et al 2013) (Gómez-Tortosa et al 2013). ALS cases containing the C9ORF72 expansion have been shown to express TDP-43 positive inclusions and have a generally faster disease progression when compared to non-C9ORF72 ALS patients (Cooper-Knock et al 2012). C9ORF72 is implicated as causative in 39.7% of familial ALS cases in Caucasian patients and 7% of sporadic ALS cases (Majounie et al 2012). The mutation therefore accounts for approximately 10% of all ALS cases and is the most common causative gene for both familial and sporadic ALS. C9ORF72 is expressed across the CNS in most tissues and has its highest expression within the cerebellum (Renton et al 2011b). Three transcripts of ALS have been identified. The 1 and 3 transcripts encode a long isoform of 481 amino acids, whereas transcript 2 encodes a shorter form 222 amino acids in length (Gijselinck et al 2012). Multiple pathways have been implicated as disease causing in C9ORF72 positive ALS cases which link in with the causative factors in non-C9ORF72 ALS. The exact way in which the hexanucleotide expansion causes disease is unknown, but 3 potential pathways have been hypothesised: haploinsuffciency, RNA toxicity and repeat associated non-ATG (RAN) translation of dipeptide repeat (DPR) proteins. Haploinsuffciency has been highlighted as, in cells expressing the expansion, levels of

transcript 1 mRNA were found to be decreased by 38% (DeJesus-Hernandez et al 2011). Also, reduced levels of C9ORF72 mRNA have been seen in the cerebellum and the frontal cortex of patient tissue (Gijselinck et al 2012, Mori et al 2013b). The second hypothesis suggests that the expansion leads to a toxic gain of function via an alteration of RNA processing. Nuclear and cytoplasmic RNA foci were identified in the frontal cortex and spinal cord of C9ORF72 positive patients (Cooper-Knock et al 2012). Evidence has also suggested that the hexanucleotide repeat RNA has the ability to fold and form G-quadruplexes which may sequester and silence RNA binding proteins (RBP) (Reddy et al 2013). Further supporting evidence for this hypothesis of RNA toxicity comes from other diseases such as Fragile X associated tremor/ataxia and Myotonic Dystrophy where repeat expansions are seen and RNA sequestration has been shown to be a causative factor. The final hypothesis suggests that the repeat sequence is translated into a toxic DPR protein (Ash et al 2013). DPR proteins have previously been shown to aggregate and be involved in the formation of p62 positive, tdp-43 negative inclusions in multiple CNS tissues (Mori et al 2013a).

1.3 Pathogenesis of ALS?

ALS is seen clinically as the progressive degeneration of motor neurons resulting in muscle weakness, fatigue and eventually in muscle paralysis. This progressive degeneration has been shown in mutant SOD1 mouse models of ALS where 40% denervation of neuromuscular junctions was seen by day 47, 60% denervation by day 80 and widespread motor neuron loss by day 100 (Fischer et al 2004). The symptoms of ALS include muscle weakness initially followed by atrophy, spasticity and eventually paralysis. This muscular paralysis shows clinically as wasting of the cranial muscles (Bulbar onset) or in the limbs (Spinal onset) (Eisen 2009). In ALS there is not a complete loss of all motor neurons but a loss of specific subtypes/populations of neurons. Motor neurons innervating the eye muscles and pelvic floor muscles (Onuf's nucleus) are less vulnerable to the disease process compared to spinal motor neurons. Also in the neurons that

degenerate there are certain neuronal subtypes that degenerate faster than others (Pun et al 2006). It has been shown that neurons innervating fast muscle fibres degenerate much faster than neurons innervating slow muscle fibres. This observation has led to the hypothesis about a pathway where the neurons innervating the fast muscle fibres undergo progressive degeneration and are affected earlier in the disease progression before the onset of slow muscle fibre neuron degeneration. This hypothesis is supported by studies which show higher levels of slow fibre neurons in the mutant in comparison to the wildtype SOD1 mouse, suggesting a decrease in fast muscle fibres. It is suggested that this is caused by a progression where fast muscle neurons change into slow muscle neurons, leading to higher levels of slow muscle neurons (Frey et al 2000, Pun et al 2006). ALS is a disease that also affects other neuronal pathways, for example, in the frontal region of the brain, Approximately 5% of ALS patients show signs of fronto-temporal dementia and up to 50% of cases show subtle evidence of fronto-temporal dysfunction (Phukan et al 2007).

1.3.1 Oxidative stress

Oxidative stress is caused by the production of reactive oxygen species (ROS) usually as a by-product of aerobic metabolism (Coyle & Puttfarcken 1993). This leads to an incomplete reduction of oxygen leaving O_2^- and H_2O_2 which are further reacted to make strong oxidants causing protein, lipid and DNA damage. Evidence from ALS post-mortem tissue shows increased oxidative stress in the spinal cord and motor cortex of sporadic ALS patients (Ferrante et al 1997). Increased levels of oxidised DNA were also seen, using 9-OHdG staining, in the spinal cord of ALS patients (Fitzmaurice et al 1996). These data suggest that at some stage of ALS progression oxidative stress is causing cellular damage. Oxidative stress has also been linked to other pathogenic mechanisms as increased oxidative stress has been shown to increase glutamate levels in ALS patients, leading to potential excitotoxicity (Shaw et al 1995). ROS exposure has also been shown in glial and neuronal cell models to reduce glutamate transporter function (Trotti et al

1996, Volterra et al 1994). Mitochondrial dysfunction is also linked to oxidative stress in ALS. Mitochondria are an important site for creating and dealing with ROS and cumulative damage from ROS over time may lead to decreased mitochondrial efficiency over time (Mecocci et al 1993). SOD1 mutations have also been shown to cause damage to mitochondria before symptom onset, also leading to higher levels of ROS (Higgins et al 2002). As the function of SOD1 is to remove oxygen free radicals to prevent accumulation of oxidative stress, it can be hypothesised that mutations in SOD1 would lead to increased free radical levels in the motor neurons and the supporting cells. Increased oxidative stress has been identified by proteomic analysis in SOD1 models via a dysregulation in the NRF2-ARE stress response pathway (Bergemalm et al 2009). This has been confirmed by over expressing NRF2, which led to delayed disease onset and an extended lifespan in a SOD1 mouse model (Vargas et al 2008). It is widely agreed that oxidative stress has a major role in motor neuron death, but this is most likely a downstream effect due to defects in organelles of the motor neurons and the surrounding supporting cells, leading to an increase in reactive oxygen species or a decrease in clearance. Anti-oxidants have been identified as potential therapeutic agents in cell and *in vivo* studies suggesting they may have a role in slowing down ALS disease progression but currently all have failed to show positive effects in clinical trials. Future trials may work to exploit the NRF2-ARE pathway to find compounds that activate the pathway to mimic the beneficial effects seen with NRF2 over-activation.

1.3.2 Axonal transport defects

Axonal transport is an integral part of all mammalian cells and is the process of moving cellular cargos from one part of the cell to another. This is particularly important for neurons, as cellular cargos are made in the cell body and need to be transported along axons and dendrites. Axonal transport defects have been identified in ALS (De Vos et al 2007) where SOD1 has been shown to slow axonal transport (Williamson & Cleveland

1999). SOD1 effects on axonal transport are likely to be mediated via multiple pathways including mitochondrial dysfunction, reduced ATP supply to the neurons and dysfunctional signalling. Studies in the G93R SOD1 mouse model showed defects in the fast retrograde axonal transport of the sciatic nerve motor neurons. This corresponds with the defective anterograde axonal transport seen in mice of the same age, suggesting a link between defective axonal transport mechanisms (Bilsland et al 2008, Pun et al 2006). Defects have also been shown in the axonal transport of mitochondria which links SOD1 with mitochondrial defects seen in 85 day old G93A SOD1 mice (Perlson et al 2009). Proteomic analysis revealed that the SOD1 mutants show increased expression of axonal proteins involved in the death/stress pathway (Caspase 8 and $p75^{NTR}$), decreased expression of axonal transport survival proteins (P-Trk) and extracellular signal regulated kinases (P-Erk) (Perlson et al 2009).

1.3.3 Mitochondrial defects

Mitochondria are a key organelle involved in energy production, cellular homeostasis and apoptosis. Mitochondrial defects have been implicated in ALS progression and abnormal pathology can be seen in the form of vacuoles and swelling within the mitochondria in combination with respiratory pathway defects in rodent and human ALS (Jung et al 2002, Mattiazzi et al 2002). Mitochondrial clustering and aggregation of the membranes has been observed in tdp-43 and SOD1 mouse models (Guo et al 2010, Sotelo-Silveira et al 2009). When looking at changes in mitochondrial function, alterations in NAD(P)H and Ca^{2+} buffering capacity both led to an increased risk of Ca^{2+} overloading in the motor neurons (Jaiswal & Keller 2009, Loizzo et al 2010). Dysfunctional mitochondria are not just motor neuron specific. Defects in the mitochondria of astrocytes lead to defective respiratory function, decreased O_2 consumption and decreased membrane potential (Zhou et al 2010). This suggests that defective mitochondrial function may be present in many cells including muscle, glia, astrocytes and motor neurons and that this may lead to decreased motor neuron survival (Joyce et al 2011). Mitochondrial

dysfunction may cause motor neuron death via hypersensitivity to deficient energy production and in motor neurons this may lead to an upregulation of pro-apoptotic factors and activation of the apoptosis pathway (Soriano & Scorrano 2010).Evidence of increased apoptosis has been seen downstream of the mitochondria by upregulation of caspase 3 which has been seen in SOD1 and tdp-43 rodent models (Nagai et al 2001).

1.3.4 Protein aggregation

Another hypothesis for the cause of ALS is the intracellular accumulation of proteins which was highlighted by live cell imaging and showed that two SOD1 mutations led to protein aggregation (Matsumoto et al 2005). SOD1 accumulation has also been shown in motor neurons of patients, mouse and cell models of ALS (Shibata et al 1994). Antibody staining for misfolded SOD1 also showed strong staining for aggregates in the motor neurons of familial ALS patients. These accumulations are a key feature seen in ALS sufferers. Another ALS linked gene, TDP-43 a mainly nuclear protein, has been identified as a major component of the inclusions seen in the cytoplasm of ALS patient cells (Neumann et al 2006). It is not clear how SOD1 and TDP-43 cause protein aggregation, but altered protein folding seems the most likely cause. Another hypothesis is that the aggregates seen may have a toxic effect on the cells and in particular the motor neurons. It has been suggested that initially the aggregation formation is slow and in low abundance but that the number of aggregates increase rapidly towards the disease end stage via aggregate interactions which may explain the rapid onset of symptoms and death seen in ALS patients (Chia et al 2010, Johnston et al 2000, Karch & Borchelt 2008). This has been brought into question by drug treatments such as edaravone which decreased the aggregate size and reduced the motor phenotype but failed to alter survival in the G93A mouse, suggesting that aggregates may not lead to the ALS disease phenotype and are more likely a secondary effect (Ito et al 2008). Arimoclomol is a drug which up-regulates the unfolded protein response (UPR) via activation of heat shock factor 1 (HSF1). HSF1 is present as

monomers with the inactive heat shock proteins, but upon cellular stress, trimerisation occurs and the HSF1 translocates into the nucleus and activates the heat shock response (Shamovsky & Nudler 2008). Arimoclomol has been shown to delay the disease progression in SOD1 transgenic mice by reducing the amount of misfolded protein being generated (Kalmar et al 2008). Evidence for upregulation of the UPR has been shown by activation of the HSP27 protein which delayed symptom onset by 11days but had no effect on survival (Sharp et al 2008).

1.3.5 Excitotoxicity

Another causative factor implicated in ALS pathogenesis is neuronal excitotoxicity. The normal role of glutamate is as an excitatory neurotransmitter in the CNS which mediates its effects via cellular receptors and ion channels. Excitotoxicity is a process that leads to neuronal damage caused by excessive glutamate receptor activation either by excessive glutamate release, defective reuptake or receptor over expression (King et al 2007). This excess of glutamate causes neuronal damage by disrupting intracellular homeostasis, ROS generation and altered mitochondrial function (Arundine & Tymianski 2003). A role for glutamate excitotoxicity in the motor neurons of ALS sufferers has been identified due to their high expression of Ca++ permeable AMPA receptors which leads to increased calcium levels in the neurons (Van Den Bosch et al 2000). It is suggested that neuronal death could arise due to over-stimulation of the AMPA receptors, leading to increased intracellular calcium, causing excitotoxicity in the neuron and that the high numbers of AMPA receptors in motor neurons underpin susceptibility to excitotoxicity (Van Den Bosch et al 2006). This links into the early degeneration of fast muscle neurons, as these express the highest levels of the AMPA receptors, suggesting a link between the AMPA receptors and degeneration in ALS (Hollmann & Heinemann 1994). Neuronal excitability has been identified in G93A mice by electrophysiology which showed the hypoglossal motor neurons and superior colliculus interneurons showed hyperexcitiability as early as postnatal day 4 (van Zundert et al

2008). Excitotoxicity as a primary disease mechanism in ALS is questionable, as neuronal loss will lead to increased glutamate levels and it is currently unknown if excitotoxicity is a cause or consequence of neuronal loss in ALS (Foran & Trotti 2009).The function of Riluzole is most likely by modulation of the excitotoxicity pathway as it is known to block presynaptic glutamate release (Cheah & Kiernan 2010). However other anti-gluatamatergic agents have not shown the same effect, which suggests that Riluzole may act on multiple pathways in ALS.

1.3.6 Activation of non-neuronal cells

Motor neuron death has been shown to be a non-cell autonomous process with glial cells playing a crucial role. Neuronal death in ALS via non neuronal cells has been shown as activation of these cell types in ALS patients and has been shown to accelerate the disease (Beers et al 2008). It has been shown that glial cells expressing mutant SOD1 can lead to the death of normal motor neurons when surrounding them (Clement et al 2003). When mutant SOD1 expressing motor neurons were surrounded by normal glial cells, disease progression was slowed by 50% (Boillée et al 2006). Expressing mutant SOD1 in astrocytes has been shown not to cause an ALS phenotype, but astrocytes expressing mutant SOD1 from rats had toxic effects on motor neurons from mouse and humans (Di Giorgio et al 2008, Nagai et al 2007). This suggests that mutant SOD1 inhibits the astrocyte's ability to provide the trophic support required by the motor neurons. The role of non-neuronal cells needs to be further investigated to identify exactly what roles these cells play in the disease and to improve the possibility of using these cell types as a potential therapeutic target in ALS.

1.3.7 Dysregulated transcription and RNA processing

TDP-43 is a protein identified in ALS with a known role as a RNA-DNA binding protein and as a major component of the inclusions seen in ALS, although this is not seen in SOD1 or FUS related ALS (Mackenzie et al 2010, Neumann et al 2006). This highlighted the role of RNA processing as a disease mechanism in ALS, as TDP-43 has roles in RNA processing, mRNA processing, transcriptional regulation and alternative splicing. FUS is also implicated in this pathway as it is another RNA-DNA binding protein found to be mutated in ALS cases with FUS positive stress granules seen in patient cells (Ito et al 2011). How these mutant proteins mediated the toxic effect is unknown. One hypothesis is that loss of normal nuclear function in both types of mutation causes cytoplasmic accumulation and depleted nuclear expression. The other hypothesis is that a toxic gain of function mutation leads to toxicity. Both are involved in the transport complexes for mRNA and thus neuronal damage may occur due to defective mRNA transport in the cells. Other evidence suggests that mutant TDP-43 causes alternative splicing defects in the mRNA (Kirby et al 2010). It was shown that mutant TDP-43 in fibroblasts led to widespread RNA splicing changes which include splicing changes in genes known to be implicated in ALS disease pathogenesis. As previously discussed, C9orf72 also causes major changes in RNA processing. The exact way in which the hexanucleotide expansion causes disease is unknown but 3 potential pathways have been hypothesised: haploinsuffciency, RNA toxicity and repeat associated non-ATG (RAN) translation of dipeptide repeat (DPR) proteins. These data suggest strongly that in certain ALS subtypes, major changes in RNA processing are occurring and contributing to motor neuron injury.

1.3.8 Endoplasmic Reticulum (ER) Stress

Protein misfolding and aggregation (Kaufman 2002) is known to induce ER stress and activate the unfolded protein response (UPR) in an attempt to

rectify aberrant proteins. The ER has a central role in lipid synthesis, protein folding and protein maturation and stress leads to dysregulation of these pathways. ER stress signals have been shown to be upregulated in patient tissue samples and CSF, as well as in SOD1 mice, with strong colocalization to SOD1 positive inclusions (Atkin et al 2006, Atkin et al 2008). Further evidence is seen in NSC-34 cell lines exposed to CSF of ALS patients that led to upregulation of ER stress markers including the UPR and caspase activation although it is not understood what in the CSF causes the ER stress (Vijayalakshmi et al 2011). Although the UPR is thought to be neuroprotective, as it works to correct cellular stress mice lacking X-box binding protein 1, a key component of the UPR, show improved ER protein degradation, enhanced autophagy and reduced aggregation of mSOD1 (Hetz et al 2009). Recently, further support for this hypothesis of reducing the UPR has come from the neurodegenerative field where inhibitors of PERK, a key translational inhibitor in the UPR pathway, leads to the prevention of neurodegeneration in prion infected mice (Moreno et al 2013). This suggests that sustained activation of the UPR in the prion-infected cells leads to translational inhibition which effectively leads to the death of the cells by loss of key proteins needed for survival. By inhibiting PERK-mediated translation silencing the cell has the ability to cope with the prion proteins and survive, thus preventing cellular loss. In ALS this may mean that by preventing the UPR in neurons, the cells may be able to cope with mSOD1 and continue to survive as repression of key neuronal proteins would be inhibited, thus reducing neurodegeneration.

1.3.9 Neuro-inflammation

In ALS patients, inflammatory component activation with activated microglia and infiltrating lymphocytes (Henkel et al 2004), as well as increased pro-inflammatory signalling is seen in the CSF (Mantovani et al 2009). Further evidence for neuro-inflammation in ALS comes from reduced numbers of T_{REG} cells and monocytes in early ALS patients, suggesting the neurodegeneration is leading to recruitment of these cells to the CNS (Kipnis

et al 2004). This is further supported by CD4 knockout mice carrying mSOD1 that develop a much more aggressive disease phenotype which it is possible to rescue via bone marrow transplantation (Beers et al 2008). Further supporting evidence is provided by intra-peritoneal injections of CD40L-specific monoclonal antibody into $SOD1^{G93A}$ mice which delayed disease onset, extended survival and led to reduced expression of neuro-inflammatory markers (Lincecum et al 2010). These data suggest that activation of the immune response leads to neuro-inflammation and ultimately neuronal death and modulation of these pathways may be neuroprotective in ALS models.

1.3.10 Deregulated endosomal trafficking

Endosomal trafficking is the process of taking extracellular molecules into the cell via a network of organelles known as the endosomal network. Dysregulation of this pathway is seen in multiple diseases, including ALS, with a higher prevalence in rarer mutations such as ALS2, VAPB, VCP and CHMPB2. Dysregulation of the endosomal pathways in ALS is still not a completely understood pathway, but most likely arises because of the susceptibility of motor neurons due to the large size of the axons and dendrites and the high metabolic needs of the cells.

1.4 Current treatments

Riluzole is the only FDA and NICE approved drug for the treatment of ALS. Riluzole is a drug from the benzothiazole class of compounds which slows down the degeneration of the motor neurons and typically gives sufferers a life extension of 3-5months (Bensimon et al 1994). The IUPAC name for Riluzole is 6-(trifluoromethoxy) benzothiazol-2-amine. The exact function of Riluzole is not fully understood, but it is hypothesised that it exerts its neuroprotective effect by having an anti-glutamatergic role. Riluzole is a

sodium channel blocker which inhibits the release of glutamate from pre-synaptic terminals, thereby ameliorating excitotoxicity caused by excessive stimulation of post-synaptic neuronal glutamate receptors (Irifune et al 2007). This hypothesis has been brought into question as other anti-excitotoxic drugs such as topiramate and gabapentin have not shown the same extension of lifespan as Riluzole (Gurney et al 1996, Skradski & White 2000). This suggests that Riluzole may function by other pathways such as modulation of NMDA receptors and the blocking of TTX sensitive sodium channels which have been linked to damaged neurons (Song et al 1997). Although there are several hypotheses for how Riluzole functions, the exact pathways and mechanisms remain unknown.

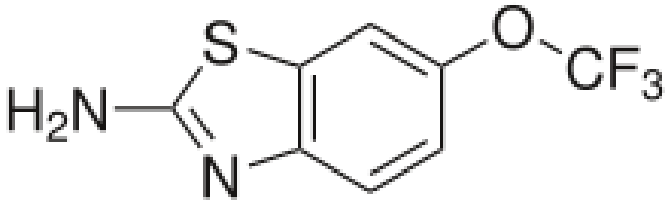

Fig 1: Structure of the Riluzole molecule. Although its exact neuroprotective pathway is unknown, it is known to increase the lifespan of ALS sufferers by 3-5 months.

Other drugs have been tested for efficacy in treating ALS such as anti-excitotoxic agents, anti-oxidants, anti-apoptotic and anti-inflammatory drugs, but none have been shown to have a clinical response. Current clinical trials include NMDA receptor antagonists, anti-oxidants, glutamate antagonists and SOD1 inhibitors and it is hoped that some of these may show a positive effect in human ALS (Aggarwal & Cudkowicz 2008). A number of drugs targeting disease pathways highlighted in ALS have undergone clinical trials with some examples shown in Table 1.2.

Clinical trial	Outcome
Dexpramipexole	An enantiomer of pramipexole, a current treatment for Parkinson's Disease. It functions by scavenging reactive oxygen species and by inhibiting the caspase cascade (Cheah & Kiernan 2010). Failed to show efficacy in a phase 3 ALS trial.
Olesoxime	Binds the mitochondrial permeability transition pore and is hypothesised to stabilise the mitochondria (Bordet et al 2007). Failed to show efficacy in phase 2/3 ALS clinical trial. Currently in a phase 2 clinical trial for SMA.
Creatine	Stimulates mitochondrial respiration and showed a positive effect in SOD1 mouse models (Klivenyi et al 1999). Clinical trials have failed to replicate this effect in ALS patients, but the safety of this compound means it has the possibility of being used in combination therapies.
Edaravone	Reduces lipid peroxides and hydroxyl radicals in the G93A mouse model(Ito et al 2008). Currently undergoing phase 3 studies in Japan
AEOL-10150	Manganese porphryin molecule currently undergoing a phase 2 trial. Has been shown to reduce oxidative stress and extend disease duration of G93A SOD1 mice by upto 3-fold (Benatar 2007).
L-745870	A dopamine receptor agonist with a hypothesised role in inhibiting oxidative stress. Has been shown to delay disease onset and extend survival in SOD1 mouse models (Okada et al 2005). Showed no effect in clinical trials.
Sodium phenylbutyrate	A histone deacetylase inhibitor with a role in aggregate clearance and preventing transcriptional irregularities (Chuang et al 2009). Has shown efficacy in animal models of ALS and is currently in a phase 3 trials (Cudkowicz et al 2009).

Table 1.2: Clinical trials in ALS and the study outcomes. Composed from data included in (Joyce et al 2011)

In the clinic, Riluzole is usually prescribed alongside symptomatic treatments such as nutritional and respiratory support measures. In ALS the main cause of death is by respiratory failure and one of the major treatment options used in the USA and Japan is assisted/mechanical ventilation. Assisted ventilation has been shown to be very effective in extending the lifespan of sufferers as the respiratory muscles are supported (Borasio et al 1998, Bourke et al 2003). It is important to remember that assisted ventilation may extend survival but does not slow down the disease progression.

Riluzole is among a group of drugs which activate the NF-E2-related factor 2/antioxidant response element (Nrf2/ARE) pathway (Chang et al 2010). Nrf2 is a transcription factor which has been shown to bind the ARE, a cis-acting enhancer sequence which up-regulates gene expression in cells undergoing oxidative stress (Moi et al 1994, Rushmore et al 1991). Nrf2 functions by forming a translation complex with musculo-aponeurotic fibrosarcoma proteins (Maf) that bind to the promoter region of ARE which leads to up-regulation of 250 genes involved in encoding detoxifying proteins and antioxidant enzymes (Kwak et al 2003, Neymotin et al 2011). Reduced Nrf2 mRNA levels were seen in the brain and spinal cord and it is suggested that this reduction in Nrf2 may cause the increased stress seen in ALS motor neurons (Sarlette et al 2008). This pathway may be an exciting avenue for investigation of new treatments for ALS by reducing the neuronal stress seen in ALS patients by up-regulating the Nrf2 pathway. In a study using the G93A SOD1 mouse model, treatment with Nrf2/ARE activators caused a significant increase in survival, further highlighting the Nrf2 pathway as a strong drug target (Neymotin et al 2011). The study used CDDO-EA and CDDO-TFEA (Triterpenoids) as they had been highlighted to induce activation of the Nrf2 pathway in cell and mouse models of ALS. The cell models show that both drugs increased Nrf2 activation and in the mouse model, the drugs had a neuroprotective effect and extended survival.

1.5 Current drug screen studies

One of the major steps in drug development is to test therapeutic agents in an *in vivo* model. Currently the process of drug development takes on average 12-15 years and costs tens of millions of dollars for each drug, with only a 1% success rate. This is due to the current method of drug discovery which is target driven. A major limitation to this process is the lack of useful *in vivo* high throughput screening systems.

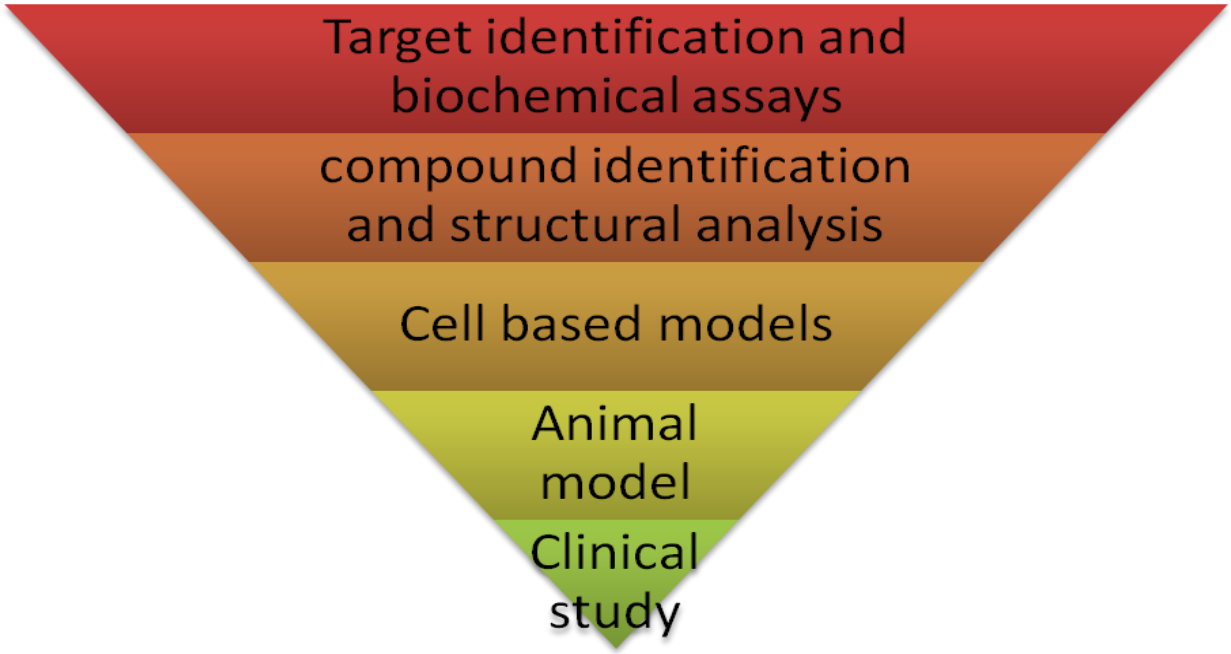

Fig 2: Diagram of the current pathway of drug discovery. This process takes up to 15 years and compounds fail at every stage due to problems such as toxicity and low specificity. Diagram adapted from (Bowman & Zon 2010).

The idea of using an *in vivo* model to perform high throughput drug screening raises the possibility of shortening the time taken to get a potential therapeutic agent through to a clinical trial and reducing the number of drugs that fail at later stages due to problems that occur *in vivo*. Drugs that have toxic effects or efficacy issues in the early high throughput screen could be eliminated, meaning less money and time is spent on ineffective drugs. This has huge implications for drug companies, as the potential to not only find

drugs faster but to identify any biological properties at an earlier stage makes these models both scientifically interesting and potentially lucrative. This is where the advantages of using a zebrafish model to pre-screen compounds are highlighted. Zebrafish have the potential to allow screening of thousands of compounds in an *in vivo* model as a pre-clinical screen before taking hit compounds into a mouse model. The zebrafish has the advantage in that it can be used to screen large numbers of compounds more quickly and economically compared to mice, with the advantage of being a vertebrate organism compared to Drosophila and C.elegans. The use of zebrafish in drug screening is currently of great interest to commercial companies due to the potential of reducing the costs incurred in generating hit compounds compared to murine screening systems. One such drug study looking at aortic coarctation in zebrafish screened 5000 drugs for an effect in the gridlock mutant, yielding lead molecules which affected the VEGF pathway and angiogenesis (Peterson et al 2004). If a zebrafish model of ALS could be developed as a high throughput drug screening system for ALS disease modifiers, it would raise the possibility of identifying novel treatments.

Drug screens have been performed in various ALS models. One such study looked at compounds which activated the glial glutamate transporter EAAT2 which plays a key role in glutamate clearance from the synaptic cleft (Colton et al 2010). Using an astrocyte cell model they screened 140,000 compounds and identified 293 initial hits which caused an upregulation in EAAT2 expression. This has implications for the field of ALS, as reducing glutamate levels will decrease excitotoxicity and potentially reduce neuronal stress. Due to the limited number of screens performed in ALS models, it is important that new models are generated to further understand the biological processes of the disease so that new drug targets can be identified.

1.6 Models of ALS

Human models of ALS are difficult to use as it is a disease of the CNS and thus no patient tissue is available until after death when most of the motor

neurons have already been lost to the disease. This presents researchers with a problem when investigating the early stages of disease and possible causative factors in the early stages of disease progression as no early stage human CNS tissue is available. Cell models can be generated from tissue samples such as skin to generate fibroblast lines and blood or cerebrospinal fluid (CSF) can be taken from patients, but none of these are the tissues directly affected by the disease. Animal models of ALS are used as surrogates and one of the most commonly used models in ALS research is the mouse model. The first ALS mouse model developed showed a similar phenotype to the human form of the disease by showing muscle tremor, weakness, paralysis and early death (Gurney 1994). This mouse model had a mutation of glycine (residue 93) to alanine (G93A) and is the most commonly used mutant SOD1 mouse model and has been used extensively in the testing of therapeutic agents (Turner & Talbot 2008). Although this mutation is a relatively rare form, it is one of the most studied and best understood. This model has been questioned as a viable tool for testing therapeutic agents because compounds identified as active in the mouse model have failed to show positive effects in human trials (Aggarwal & Cudkowicz 2008). These differences are blamed on poor experimental design such as not being significantly powered (low n-numbers used in the study) and over-extrapolating effects seen in mice as a positive result, which would be clinically insignificant. Also many murine studies commence before disease onset which is clearly not possible in patients thus making the relevance and value of these animal studies open to question. Mouse models are also often highly inbred and over-express the mutant proteins which may not accurately reflect the human condition. This brings the animal model in to question and raises the need for the development and validation of new ALS models. Currently there are 12 different human SOD1 mutations expressed in the mouse, some of which affect copper binding or truncate the protein (Joyce et al 2011, Turner & Talbot 2008). An interesting observation in the SOD1 mouse is that over expression of the wild-type protein does induce a motor phenotype and this is caused by axonopathy (Jaarsma et al 2008). This suggests that over expression of SOD1 can lead to neuronal defects without the presence of pathogenic mutations. Rat models of ALS have also

been generated with mutations in SOD1 at G93A and H46R (Howland et al 2002, Nagai et al 2001). The rat models show a similar phenotype to the mouse, but have a more aggressive and variable disease course.

Another animal model of ALS is the invertebrate model *Caenorhabditis elegans. C.elegans* is a useful model for studying ALS as it has transparent embryos, allowing easy visualisation and a simple, fully mapped nervous system comprised of 302 neurons (Watts & Strogatz 1998). It also has the advantages of being an inexpensive model to keep and is easily manipulated by genetic techniques such as RNA interference. SOD1 mutants have been shown to cause locomotor defects in *C.elegans* (Wang et al 2009). The locomotor defects in the mutants were linked to the presence of soluble and insoluble SOD1 aggregates. Another group screened 75000 compounds in inducible TDP-43 expressing PC12 cells to identify compounds that reduced TDP-43 inclusion size without causing cellular toxicity. The 16 hits were then screened in a *C. elegans* model to replicate the hit effects in a simple model to identify potential ALS therapeutics (Boyd et al 2013). *C.elegans* was also used to show that methylene blue had the ability to supress toxicity and rescue the toxic phenotype in both TDP-43 (A315T and G348C) and FUS models (S57Δ and R521H) (Vaccaro et al 2012).

Another key model in ALS research is the *Drosophila melanogaster.* This invertebrate fly model is a useful tool in research due to its fully sequenced genome, short generation time and its susceptibility to genetic manipulation (Adams et al 2000). *Drosophila* models which express the mutant human SOD1 protein have been generated (Watson et al 2008). These models showed defects in climbing, accumulation of stress in glial cells, defective neural circuits and SOD1 protein aggregation. The problems with these models are that they do not show the motor neuron loss, paralysis and death that are seen in the human disease. TDP-43 models in *Drosophila,* either overexpression WT TDP-43 or mutant forms, led to vacuolar degeneration in the photoreceptors in the retina with more degeneration in the mutants (Ihara et al 2013). By abolishing the RNA binding motif on TDP-43 they showed complete normalisation, highlighting the key role of the RNA binding domain in TDP-43 toxicity.

Cell models of ALS are useful as they give a uniform population of one cell type with a characterised, specific genetic background to screen compounds for effect. Cells also have the advantage in compound screening with large numbers of cells available for screening and the ability to screen 1000's of compounds in a matter of weeks, as well as the ability to genetically alter cell lines to carry transgenes and fluorescent readouts. Cells usually show less variability as they are from a defined genetic background unlike *in vivo* models and they are easy to use for readouts with imaging and other well characterised techniques. Cell models have been used to identify potential therapeutics for the treatment of ALS. One screen used mouse and patient fibroblast models to identify compounds working on the NRF2-ARE pathway in ALS (Mead et al 2013). Two thousand compounds from the Spectrum library were screened for NRF2 activation and S[+]-Apomorphine was identified. This was then taken into the $SOD1^{G93A}$ mouse model where CNS penetrance was shown, NRF2 induction was seen and attenuation of motor dysfunction occurred. Another cell based screen in ALS used NSC34 motor neuron cells expressing mutant SOD1 to identify antioxidant compounds with potentially neuroprotective effects (Barber et al 2009). Using cell based assays, *in silico* analysis and a review of the published literature they identified three possible new therapeutics which could be taken forward for *in vivo* testing.

	Neural groove	Neural tube	Spontaneous movement	Free living
Human	23dpf	4wpf	9-10wpf	40wpf
Mouse	8.5dpf	9.5dpf	12dpf	21dpf
	Neural thickening	**Neural keel**	**Spontaneous movement**	**Free living**
Zebrafish	10.3hpf	11-16hpf	17-24hpf	56-72hpf

Table 1.3: Comparison of neural development stages in Humans, Mice and Zebrafish. Dpf – Days post fertilisation, wpf – weeks post fertilisation, hpf- hours post fertilisation

1.7 Zebrafish model of Neurodegeneration

The Zebrafish (*Danio rerio*) is an excellent model for neurological disorders such as ALS because it has transparent embryos, allowing visualisation of the nervous system. The zebrafish is also a vertebrate which gives it advantages over invertebrate models such as *C.elegans* and *Drosophila*. The zebrafish nervous system is also simpler than other higher vertebrate models (Doyon et al 2008). Zebrafish also have the advantage of reaching sexual maturity at 3-4 months of age and can produce viable embryos all year round, giving it an advantage over other higher vertebrate models which have long gestation periods. Zebrafish also produce large numbers of embryos with each cross and these embryos develop externally, allowing easy manipulation from larval stages. Large numbers of embryos make the zebrafish an ideal choice for large scale drug studies and mutagenesis screens. The zebrafish also has a conserved and simplified nervous system, allowing the generation of transgenic and knock-out models of disease which closely model the human nervous system. Zebrafish have been used to model various neurological disorders such as a model of DJ-1 mutations in Parkinson's Disease (Bretaud et al 2007), poly-glutamine mutations in

Huntington's Disease (Karlovich et al 1998), knockout mutations of the survival motor neuron gene in Spinal Muscular Atrophy (Bertrandy et al 1999) and studying presenilin mutations in Alzheimer's Disease (Campbell et al 2006).

As with all models, there are limitations when modelling a disease in an organism or cell. Modelling disease is a double edged sword in which simplicity can be an advantage, but it can also mean the relevance of findings is brought into question, whereas complexity can introduce difficulty in elucidating real effects. It is important to remember that the zebrafish still has the limitations of being a more simplistic model than higher models such as mouse or primates. Also the genetics are highly conserved but not identical, likewise the architecture of the nervous system and other organs has subtle differences. As with all models there are advantages and limitations and it is important to recognise and understand both so that all results can be understood and interpreted correctly.

1.7.1 Zebrafish models of ALS

Several genetic models of ALS in zebrafish exist for *sod1* as well as other genetic causes. Zebrafish transiently overexpressing *sod1*^{A4V} were shown to develop an axonopathy in a dose-dependent manner (Lemmens et al 2007). Further from this they showed that vascular endothelial growth factor (VEGF), a known ALS disease modifier, had a role in modulation of the axonopathy. Reduction in VEGF levels led to a more severe phenotype, whereas overexpression of VEGF rescued the axonopathy. A stable Sod1 model that was generated expressed T70I mutant Sod1 in zebrafish generated by TILLING (targeting induced local lesions in genomes) (Da Costa et al 2013). The model has the advantage over murine models of having mutant SOD1 expression level as a physiological level that is much closer to the expression in human ALS patients. The model also showed an NMJ phenotype and a susceptibility to oxidative stress, highlighting the potential of this model for further investigation into the mechanisms of ALS

and therapeutic development. Another group showed that transient expression of G93A SOD1 by microinjection in zebrafish led to early defects including defective axon growth and branching (Sakowski et al 2012). Upregulation of the growth factor IGF-1 was then shown to have the ability to rescue the early defects. They took this model further and generated a stable G93A-SOD1 mutant model and showed that the model has behavioural defects including decreased activity, NMJ defects, neuronal loss and altered patterning. FUS has also been modelled in zebrafish where morphlino knockdown of FUS and expression of mutant FUS (R521H) both led to impaired motor activity and reduced NMJ synaptic fidelity in embryos (Armstrong & Drapeau 2013). It was also possible to rescue the knockdown phenotype by injection of WT FUS but not mutant FUS. As previously discussed Tdp-43 has also been modelled in zebrafish where mutants of *tardbp* or *tardbpl* show no phenotype but the double mutants show muscle degeneration, reduced circulation, reduced motor neuron length and early death (Hewamadduma et al 2013, Schmid et al 2013). Recently C9orf72 has also been modelled using zebrafish. Knockdown of zebrafish C9orf72 was performed using morphlino injection and led to a significant axonopathy and showed rescue of the axonopathy with injection of the long transcript human C9orf72 (Ciura et al 2013). They also showed that knockdown of C9orf72 led to reduced swimming in the embryos but co-injection with human C9orf72 rescued the swimming defect. These models of ALS show that zebrafish are an important model for neurodegeneration and ALS modelling and have the potential to play a key role in further understanding the disease and the potential to screen therapeutic agents due to the beneficial properties of zebrafish over other *in vivo* models.

1.8 Background to the project

A transgenic fish expressing the fish form of mutant Sod1 protein was generated in Ohio (Ramesh et al 2010). This model expresses the mutant form of fish Sod1 at moderate levels. The wildtype Sod1 was not used as humans regulate their temperature at 37°C whereas

zebrafish regulate around 28°C. To generate the mutant line, a bacterial artificial chromosome (BAC) which contained the zebrafish *sod1* gene was used. To track the transgene expression, heat shock protein 70 (HSP70) was used to drive the fluorescent protein Ds-Red. It is important to note that in this construct the sod1 gene is driven from a sod1 promoter and the DsRed fluorescence is driven by the hsp70 promoter. This means that each gene is driven independently so that the DsRed signal is not just a result of increased sod1 expression but a true readout of hsp70 up regulation. This is confirmed by comparison of the mutant sod1 and wild type sod1 lines where increased sod1 expression leads to increased DsRed in the mutant line, but doesn't lead to an increase in DsRed expression in the wild type overexpression line. This shows us that it is a mutant specific effect, not an overexpression effect caused by readthrough.

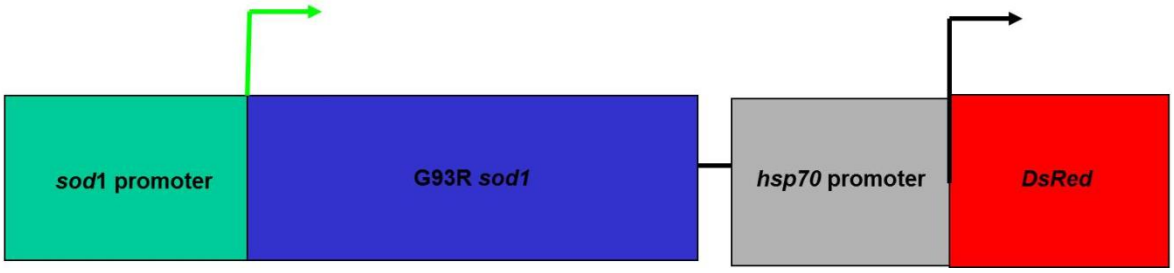

Fig 3: Structure of the hsp70-DsRed tagged to the sod1 transgene to facilitate the tracking of cellular stress mediated by mutant sod1 protein expression (Ramesh et al 2010).

Various zebrafish lines were generated which expressed different levels of mutant Sod1 and wild-type Sod1. By performing quantitative PCR (qPCR) and western blots, the steady-state protein expression levels could be determined. The G93Ros10 line was shown to have a 4x higher Sod1 expression level in comparison to the WT. To confirm that over-expression of the mutant protein led to a mutant phenotype, the neuromuscular junctions were visualised using immunohistochemistry by co-localising for the SV2 antibody (motor neuron) and α-bungaro-toxin (Muscle ACh receptors). It was shown that at both larval and adult stages of development, alterations in neuromuscular junctions could be seen, with reduced co-localisation in

comparison to over-expressing wild type fish. In the larval stages there was a significant decrease in colocalization and post synaptic volume and at adult stages the total NMJ volume was significantly decreased. To examine changes in the motor ability of the mutant sod1 model, the fish were examined using a swim tunnel. This functions by testing the ability of the fish to swim against an increasing current over time (Pagala et al 1998, Plaut 2000). The swim tunnel test showed that the mutant sod1 lines could not maintain performance in the swim tunnel and had endurance defects in comparison to the wild type lines. The study also measured the optimal force and fatigability of muscles by direct stimulation of the muscles. Neither of these were affected, which corresponds with the disease progression in humans in that it is not a muscular defect but a degeneration of the neural inputs to the muscle. At disease end stage the G93Ros10 spinal cord showed a significant reduction in ChAT positive motor neurons compared to the non-transgenic fish. The mutant lines also showed reduced survival in comparison to the wild type expression lines, another hallmark of ALS. Electron microscopy also revealed significant alterations to the muscle and the mitochondria of spinal cord motor neurons in the mutant sod1 zebrafish. Now that this model has been validated as over-expressing the mutant sod1 protein and as a model for ALS, the next step is to develop its use to set up a high throughput drug screen for drug development in ALS. One measurable way of detecting changes caused by therapeutic agents would be to detect changes in protein expression such as altered sod1 level, or changes in DsRed expression.

1.9 Heat shock proteins

Heat shock proteins (HSP's) are ubiquitously expressed proteins found in all organisms. These proteins are up-regulated in response to increased temperature as well as other forms of stress. (De Maio 1999). Heat shock proteins were first identified in 1962 in a *Drosophila* model where an increase in temperature was seen to induce new RNA synthesis (Ritossa 1996). The

different forms of HSP are named after their molecular size such as HSP70 which is 70KDa and HSP90 which is 90KDa.

HSP70 has 3 functional domains (Flaherty et al 1990):

1. N-terminal ATPase domain which hydrolyses ATP to ADP.
2. Substrate binding domain which has an amino acid binding region which can hold peptides in place.

3. C-terminal domain which has 2 roles dependent on its binding state:

    a. ATP bound-binds and releases peptides rapidly

    b. ADP bound- tightly binds and holds peptides

HSP70 has many functions in the body and acts as a regulatory protein. One of its major roles is as a chaperone protein which binds tightly to partially synthesised peptides, stabilising the peptide until complete synthesis occurs (Tavaria et al 1996). HSP70 has been shown to prevent protein aggregation, a hallmark of ALS, as well as preventing non-functional protein assembly and promotion of neurite outgrowth (Takeuchi et al 2002). HSP70 has also been shown to play a key role in protecting cells from damage by thermal and oxidative stress. This is done by HSP70 binding partially unfolded and denatured proteins caused by the stress which in turn prevents further misfolding and aggregation, giving proteins and peptides time to refold. Recently, heat shock proteins have been highlighted as a potential therapeutic target due to their ability to protect neurons from stress, aggregation and damage. In the G93A mouse model of ALS, it has been shown that over-expression of HSP70 confers a neuroprotective role and increases the lifespan of the mice (Gifondorwa et al 2007). By injecting recombinant human HSP70 three times per week from postnatal day 50, the mice showed increased survival, delayed onset of symptoms, prolonged motor neuron survival and maintained motor function. A follow- up study showed that administration of recombinant human HSP70 from postnatal day 30 did not prevent the denervation of NMJ's and did not maintain the morphology of the peripheral nerve axons compared to the control (Gifondorwa et al 2012). In addition, it was shown that recombinant human

HSP70 injections led to increased glia and astrocyte activation which may be a key mechanism in maintaining neuronal integrity. Inhibition of glia has been shown to be neuroprotective and give an extension in survival for SOD1 mice which were treated with minocycline, a microglial activation suppressor (Edgar & Nave 2009, Kriz et al 2002). In contrast to this, injection of minocycline in symptomatic late stage mice led to increased gliosis and altered astrocyte activity (Keller et al 2011). This suggests that a balance exists between when suppression of glia is beneficial in slowing disease progression and when adverse effects occur. The pathway by which HSP70 confers a neuroprotective role is not understood, but it is suggested that it may function by maintaining neuromuscular junction integrity and skeletal muscle innervation. Muscle cells have been shown to secrete HSP70 and expression is seen in muscle and peripheral tissue but not spinal cord and brain, suggesting that any effect of increased HSP70 expression is due to effects at the NMJ (Hoshino et al 2011, Robinson et al 2005). This has also been shown in cell models and mouse models by using drugs which upregulate the heat shock response. In symptomatic mice dosed from 75 days with arimoclomol an extension in survival and motor performance was seen and in mice dosed from 90 days, improved motor performance but no extension in survival was seen (Kalmar & Greensmith 2009, Kalmar et al 2008). Using arimoclomol, primary motor neuron cultures were protected from chemical stresses such as hydrogen peroxide, whereas other HSP70 inducers like celastrol conferred no protective effect. This suggests that, although the heat shock response is upregulated, this does not necessarily mean it is neuroprotective. HSP70 has been shown to increase the number of chaperone proteins in SOD1 mouse models by binding the BAG1 protein (Rohde et al 2008). It was hypothesised that this would prevent toxicity due to reduced aggregate formation, although this was not the case and no extension in mouse survival was seen. Elevated levels of HSP70 have also been shown to have no effect on disease onset or survival in several SOD1 mutant mouse models, suggesting no benefit from elevating HSP70 (Liu et al 2005). These conflicting results from various studies into the role of HSP70 in ALS suggest we still do not know exactly how it functions to protect the neuron from stress.

HSP70 is expressed in stressed motor neurons making it a good marker for stressed neurons and further studies should be performed to look at its potential as a therapeutic target. As HSP70 is expressed at areas of stress and is expressed in motor neurons, it may be used as a biomarker of motor neuron stress. This model allows visualisation of areas of stress in the zebrafish embryos by tagging the HSP70 promoter to a fluorescent molecule. By tagging the HSP70 promoter to a Ds-Red fluorescent molecule, it is possible to visualise where the HSP70 protein is being expressed.

Ds-Red is a 28kda fluorescent protein which is taken from the oral disc of the coral species *Discosoma genus.* It has an emission wavelength of 583nm or 602nm and is a particularly useful fluorescent probe due to its ability to resist extreme pH changes and photo bleaching and its ability to be used in co-localisation studies with GFP (Baird et al 2000). By looking at the number of normal neurons in comparison to the number of stressed neurons, it becomes possible to quantify the level of stress. This could have key implications on the testing of therapeutic agents as the stress levels in the neurons will be quantifiable after drug treatment and drug effect can be measured. This has the potential to be developed for use in large scale drug studies which could rapidly identify new therapeutic targets for ALS treatment.

1.10 Hypothesis and aims

We hypothesis that mutant Sod1 in the zebrafish, leads to increased cellular dysfunction and an ALS phenotype. We hypothesise that the mutant Sod1 model can be utilised as a tool to further understand the cellular mechanisms involved in ALS. Furthermore we hypothesise that the Hsp7-DsRed readout can be utilised as a readout of stress, and be used to develop and implement a high-throughput drug screen to identify neuroprotective compounds in an *in vivo* model.

Aims:

1. To investigate the cellular events occurring at different embryonic and adult stages to identify the cell types showing the hsp70-DsRed expression and identify the dysfunction.
2. To develop and validate a high-throughput drug screen using the zebrafish stress readout, and to identify modifiers of neuronal stress by screening a compound library.
3. To take the hits from the primary screen into secondary screens to identify compounds having a genuine positive effect in reducing neuronal stress caused by mutant Sod1 as a potential therapeutic.

Methods

2.1 Animals

The transgenic lines G93Ros10, G93Ros10, G85Ros6 and WTos4 were initially developed at the Ohio State University, Columbus, OH and were imported to the University of Sheffield, Sheffield, UK, in 2010. These *sod1* mutant zebrafish lines were generated according to the protocols previously outlined in (Ramesh et al 2010). The transgenic lines utilized for this study included the Tg(sod1:sod1WT;hsp70:DsRed)os4-Sh4 (Sh-Sheffield line), the line expressing the highest level of WTSod1 (x3.3 as compared to non-transgenic lines), referred to as WTos4-Sh4 line; Tg(sod1:sod1G93R;hsp70:DsRed)os10-Sh1, referred to as G93Ros10-Sh1 (high expresser with Sod1 expression increased x3 and comparable to WTos4); Tg(sod1:sod1G93R;hsp70:DsRed)os6-Sh2, referred to as G93Ros6-Sh2 (moderate expresser with Sod1 expression increased x2.5); and Tg(sod1:sod1G85R;hsp70:DsRed)os6-Sh3 line, referred to as G85Ros6-Sh3 (low expresser with Sod1 expression increasedx1.5). When both G93R and G85R lines are discussed, they are referred to as MUTsod1 lines. All other lines used in this thesis were internally sourced from the University of Sheffield CDBG aquarium.

All zebrafish that were imported to the facility were kept in quarantine and the embryos obtained were bleached at 24hpf and then transferred to the University of Sheffield, MRC zebrafish facility. Adult and larvae zebrafish (*Danio rerio*) were maintained at 28.5°C and bred according to established procedures (Westerfield & ZFIN. 2000). Animal protocols were undertaken in line with a Home Office approved project licence. The care and maintenance of animals were performed under the Home Office project licence as per the animals (scientific procedures) act of 1981 (ASPA) (http://www.homeoffice.gov.uk/publications/science-research-statistics/animals/transposition_of_eudirective/aspa_amendment_regulations).

2.2 Zebrafish crossing

Paired matings were set up with a divider between a male and female zebrafish the day prior to collection, to prevent mating. For timed matings, the divider was removed the following morning or at specified time to allow the fish to mate and lay eggs. Later the same day the fish were removed from the tank and the water drained from the pair mating tank through a fine sieve to filter out the fertilised eggs. The eggs were placed into a petri dish, topped up with embryo medium (E3 – NaCL-5.03mM, KCl-0.17mM, $CaCl_2$.$2H_2O$-0.33mM, $MgSO_4$.$7H_20$-0.33mM) and placed in an incubator at 28°C until the appropriate stage of development was reached.

2.3 Dechorinating method

The removal of the chorion can be performed at any stage after 24hpf. Fine forceps are used to pull the chorion apart and release the embryo using a 5X light microscope for guidance. After removing the embryos from the chorion a sterile embryo medium change is performed to remove chorion debris from the plate to avoid fungal contamination and allow maximum embryonic survival.

2.4 Adult tissue collection, fixing and sectioning

The adult zebrafish were terminally anaesthetized in Tricaine and decapitated as per the project licence procedure list. Muscle and spinal cord were dissected from the zebrafish using fine micro dissection tools under a microscope and fixed in freshly made 4% paraformaldehyde (PFA) overnight at 4ºC. The spinal cord was taken whole from the body before removal of the vertebrae from the spinal cord by fine dissection. The tissues were embedded in Optimal cutting temperature compound (O.C.T) (Tissue-Tek) and snap frozen in isopentane (-80°C). Orientation of the embedded tissue

was confirmed under a light microscope. Serial cryostat sections (20 μm) of the tissue performed on a Leica CM3050S cryostat set at -20°C for both the objective temperature and chamber temperature. The protocol was updated later to embed the tissue in fish gelatin rather than O.C.T solution. For 50ml of the embedding solution (27.5ml of fish gelatin (Sigma, Cat: G7765), 7.5g sucrose and the remaining volume was dH_2O) was gently heated and stored on a roller until the solution was completely dissolved. The sectioning was performed as before with an objective temperature of -33°C and a chamber temperature of -26°C. The sections were collected on superfrost plus slides (ColePalmer) and stored at -80ºC until later processing. The muscle sections were taken as lateral sections to give the best NMJ structures for imaging, whereas spinal cord sections were taken as cross-sections.

2.5 Immunostaining of muscle samples

Muscle staining in adult fish was performed using synaptic vesicle 2 (SV2-a presynaptic marker), α-bungarotoxin (BTX-a post synaptic neuromuscular junction marker) and DsRed (stress response marker). The samples were washed 5x10mins in phosphate buffer containing 1% bovine serum albumin, 1% DMSO and 0.5% Triton-X100 (PBDT). The samples were blocked using PBDT with 5% normal goat serum (NGS) for 20 min and then incubated for 30min in PBDT containing 2% NGS along with alexa 488 conjugated α-bungarotoxin (Molecular Probes, 1:100, Cat No: B14322) at room temperature (RT). Following this the samples were washed for 15 minutes with 6 changes in PBDT (6 x 15min) (phosphate buffer containing 1% bovine serum albumin, 1%DMSO and 0.5% Triton-X100). The samples were then incubated with primary antibody solution containing mouse monoclonal anti-SV2 antibody (Developmental studies hybridoma bank, 1:50) and rabbit anti-DsRed antibody (1:100, Clontech, Cat No: 632393) in blocking solution for 24 hours at 4^0C. The following day the samples were washed 6x20 minutes in PBDT and incubated with the secondary antibody solution containing goat anti-mouse 633 and goat anti-rabbit 568 (1:200) in blocking solution containing 2%NGS and

incubated for 24 hours at 4°C overnight (ON). The samples were then washed 6 times with 30mins washes in PBDT and the slides were mounted with coverslip using Vectashield Hardest with DAPI (Vector Labs) and imaged using confocal microscopy (TCS SP5 2, Leica). Quantitative analysis of confocal images was performed on image stacks of 16-20 μm thickness (0.5-1μm /section) obtained and processed using Image J Software (National Institutes of Health). For quantitation of the fluorescence intensity of individual neurons, an outline around the fluorescent cells was drawn and the average fluorescence intensity measured. A minimum of 50 DsRed positive neurons from multiple larval samples were pooled for analysis in quantifying the average DsRed fluorescence of G93Ros6-sh2 and WTos4-sh4 lines. Image analysis for NMJ analysis was performed using NIH ImageJ software and quantitative analysis of the NMJ was performed using a colocalization analysis plugin (Costes et al 2004, Li et al 2004).

2.6 Spinal cord staining

Spinal cord staining in adult fish was performed using choline acetyltransferase (CHAT- a presynaptic neuronal marker) and DsRed (Stress response marker). The sample slides were washed in phosphate buffer containing 1% bovine serum albumin, 1%DMSO and 0.5% Triton-X100 (PBDT) for 5x10mins before blocking in PBDT with 10% normal donkey serum in PBDT for 60 min. This was followed by a 3 day incubation at 4°C in goat polyclonal anti-ChAT antibody (1:100, Chemicon International, Cat: AB143) and rabbit anti-DsRed antibody (1:100, Clontech). The samples were gently washed 6x15mins in PBDT and incubated in alexa 633 donkey anti-goat (Invitrogen, Cat No A21082, 1:250) and alexa 568 donkey anti-rabbit (Invitrogen, Cat No: A10042 1:250) in blocking solution containing 5% NDS in PBDT at 4°C overnight (ON). The samples were then washed for 6x30mins with PBDT and mounted with coverslip using Vectashield Hardest with DAPI (Vector Labs) and imaged using confocal microscopy (TCS SP5 2, Leica).

2.7 Zebrafish drug screening – initial screen

The G93Ros10-sh1 line was used to identify drugs that inhibit neuronal stress as this showed the brightest fluorescence and a stable measurable increase in fluorescence over several days. 24hpf embryos were obtained by timed matings and were dechorinated. The embryos were put in plates (25-50 embryos/plate) containing the appropriate concentration of the test compound in embryo medium. The stock solutions of the drugs were made using DMSO as a solvent at a final concentration of 10mM. For the assay, the final concentration of drugs was 10µM leading to a final well DMSO percentage of 1:1000 or 0.1%. Zebrafish embryos can tolerate up to 2% DMSO so at 0.1% DMSO embryos are generally healthy and grow normally. The drug-containing media was changed daily and maintained for 5 days. At 5dpf, the embryos were sorted for DsRed expression by fluorescence using a standard fluorescent microscope to determine expression in the brain and spinal cord. Transgenic and non-transgenic embryos were then sorted and separated. The non-transgenic samples were used to set minimal threshold for fluorescence as these are non-transgenic and show background fluorescence. The transgenic embryos were put into tubes with 3 embryos/tube before sonication in 100µl phosphate buffer saline (PBS) for 5 seconds and 25% amplitude (Vibracell, Sonics and materials). After sonication, the transgenic samples were centrifuged at 1300RCF for 10 minutes (CWS ALC PK120 centrifuge, T536 Rotor). The supernatant (75µl) was pipetted to 96 well fluorescent clear bottom plates (96 well black, µClear, Greiner Bio One, Cat No: 655096) and the well fluorescence measured using a FLUOstar Omega (415-0153) plate reader (BMG Labtech, Offenburg, Germany) at the excitation wavelengths 560 and 544 and emission wavelengths 645 and 590 respectively. The fluorescence of all transgenic samples (control and treated), were subtracted by the average fluorescence of transgenic negative samples to remove the effects of background fluorescence. The negative controls used in drug studies contained only solvent (DMSO) alone at the highest concentration used for the test compounds (Spectrum library is at 5mM and 400nl is added to each test well, 400nl of DMSO in 200µl =0.2% DMSO per well). The treatment effect was

measured and analysed by t-test and compared to vehicle treated samples. To allow for a comparison between different experiments, the percent inhibition of the fluorescence signal by test compounds as compared to vehicle in each study was used for standardization. Riluzole (10µM), a drug used clinically for treatment of ALS (Bensimon et al 1994), was used as a positive control for validation of the assay. The other compounds tested were Apomorphine-S, Epigallocatechin gallate (EGCG) and Tricaine and they were studied at 10µM, 20 µM and 610 µM doses respectively.

2.8 Genotyping embryos at 2dpf using the InCell microscopy system

G93Ros10 (male) x Ab embryos were collected and manually dechorinated at 24hpf. At 48hpf individual embryos were loaded into 96 well plates (96 well black, µClear, Greiner Bio One, Cat No: 655096) in 50µl of E3 media. The plates were scanned on the INCell analyser 2200 plate reader (GE healthcare) to determine TG's from NTG's based upon fluorescence at the DsRed wavelength (543 excitation and 604 emission) in the hindbrain and SC. The InCell analyser is a fast, sensitive modular lamp based system allowing high-throughput imaging to be performed in multiple wavelengths, multiple plate types and different conditions. The 96 well plates containing the embryos were loaded into the Incell before the protocol for genotyping was designed on the InCell analyser software. The wavelengths selected were both from Polychroic QUAD2 for brightfield (0.03s exposure) and DsRed (2.500s exposure) wavelengths to identify any damage to the embryos, the presence of developmental abnormality and to confirm expression of the DsRed. The 2X Nikon, Plan Apo, CFI/60 lens was chosen as it took a whole well image. The camera used was the large chip CCD camera which uses a CoolSNAP K4 2048x2048 pixel array (7.40µm square pixel). This camera has the advantage of delivering high resolution images in low light applications with a large field of view. For the genotyping process, binning was set at 4x4 to ensure even the faintest DsRed expression was detectable. The image processing was performed using 2-D deconvolution as

this provided both the speed and quality of image required for genotyping large numbers of embryos rapidly as well as reducing the blurring effect caused by the objective lens. Flat field correction was also applied to each well due to the curvature of lenses as this corrects for the focus at the edge of wells. Laser autofocus at 1% power was used to focus on each well for optimum imaging. The laser-based HWAF (Hardware autofocus) uses a 785nm laser to focus onto a target while the z-axis is moved to determine the exact location of the target.

2.9 Genotyping embryos at 6dpf using the InCell microscopy system

At 6dpf, individual embryos were loaded into 96 well plates (96 well black, µClear, Greiner Bio One, Cat No: 655096) in 200µl of E3 media and anaesthetised using Tricaine (MS-222 at 4.2ml/100ml E3 media). The plates were scanned on the INCell plate reader (GE healthcare) to look at the fluorescence in the DsRed wavelength and a brightfield image to look at general zebrafish morphology and structure. The settings on the InCell were kept identical to the 48h protocol except the exposures for brightfield and DsRed were reduced to 0.03s and 0.400s respectively due to the increased DsRed signal of older larvae. The larvae were imaged at this stage to investigate any abnormalities in the development of the fish such as organ malformation and death. It also allowed the confirmation of DsRed fluorescence expression at the end of the assay to ensure no NTG fish had been included in the assay.

2.10 Printing of the spectrum library

The spectrum library is stored in deep well storage plates within the SPOD system (Roylan) to prevent library deterioration. The SPOD system is a specialised drug storage system to extend the lifespan of compound libraries by controlling environmental conditions (pressure of 0.5PSI, Oxygen level <10%, Relative humidity <5%).The classical method of drug storage was to utilize a freeze thaw cycle exposing the drugs to repeated oxidation and water exposure. Using the SPOD system the drugs are kept in the dark to prevent UV exposure and damage to the drugs and in a low oxygen high nitrogen environment which prevents oxidation of the drugs. The compounds are also kept under a positive pressure that forces moisture out of the storage pods preventing hydrolysis of the libraries. To utilise the library using the Echo550 liquid handling system, the plates were imprinted onto low dead volume (LDV) 384 well plates (Echo™ Qualified 384 well polypropylene microplate, clear, flat bottom, Cat #P-05525) using the Thermo Scientific Platemate Plus (Matrix Technologies Corp, Thermo Scientific) a robotics liquid handling system that imprints from 4x96 well plates into quadrants on the 384 well source plate. The system was set to dispense 12µl of drug from each 96 well deep storage plate into the 384 well LDV library plate. Between each dispense a tip wash of 5 cycles was performed using filtered water and the tips were changed for each plate to ensure that no cross contamination of compounds occurred during the transfer.

2.11 Loading of drugs into plates using the Echo550 liquid handling system

Zebrafish dosing plates were generated using 96 well plates (96 well black, µClear, Greiner Bio One, Cat No: 655096) loaded with 20µl of E3 media which had the drugs added from the library using the Echo 550 liquid handling system. The Echo 550 liquid handling system is a state of the art fluidics system that can dispense very low volumes of compound libraries

into destination plates rapidly and accurately. It is a powerful tool in high-throughput screening due to its tipless transfer of solution with transfers of solutions as low as 2.5nl. This allows for assay miniaturisation and reduces cross contamination and costs. It also allows library management due to its ability to measure DMSO concentration, hydration level and total well volume allowing easy management of the library health over time. The Echo system works by using acoustic energy to disrupt the well meniscus and transfer 2.5nl droplets from a source plate to a destination plate. The system allows for the transfer of 200 droplets per second (500nl). Using the Echo plate reformat software (Echo550 liquid handling control software) protocols designed to dispense the desired volume of drug from a source plate (Echo™ 384 LDV plates) into a destination plate (96 well black, µClear, Greiner Bio One, Cat No: 655096). Before usage the Echo550 system is calibrated to ensure that the dispensing process is uniform and stable throughout the experimental procedure. 20µl aliquots of embryo medium are added to the destination wells (WellMate, Thermo Scientific, Matrix) so that the Echo system dispenses into a larger volume of embryo media meaning the drug does not degrade due to exposure to the environment. This volume must remain low so that the forces in the plate do not allow the solution to drop out during the inversion of the plate which occurs at the beginning of the dispensing process. The destination plate (96 well plate) is taken into the Echo550 system and inverted while a drug source plate (385 LDV plate) is brought into the machine and manoeuvred close to the destination plate so that the dispensing distance is as low as possible. An anti-static bar removes any static energy from the plate at the beginning of the process to avoid any interference with the transfer of compounds between the plates. Once the dispensing process has been completed the plates are backfilled up to 150µl again using the WellMate system. Once the drug dosing process has been completed, the fish are then added to the well in 50µl to make a final well volume of 200µl at the desired final concentration

2.12 High-throughput drug screening readout

At 6dpf the fish were terminally anaesthetised using Tricaine (4.2ml per 100ml) and imaged using the InCell for fluorescence and brightfield to identify death and malformation before being loaded into 96 well V bottom plates (V bottom, Clear, Greiner Bio One, Cat No: 651101) in 50µl of media. The wells were then individually sonicated at 25% for 5 seconds using the Vibracell sonication system (Sonics and Materials, Inc) before being centrifuged at 1300G for 15 minutes (CWS ALC PK120 Centrifuge, T536 Bucket). 20µl of the supernatant was then loaded on to 384 well plates (384 well, µClear, Greiner Bio One, Cat No: 781096) before the fluorescence was measured using the OmegaStar plate reader system at the excitation wavelengths 560 and 544 and emission wavelengths 645 and 590 respectively.

2.13 Pherastar

Pherastar analysis was performed in 384 well plates (µClear, Greiner Bio One, Cat No: 781096). The Pherastar FS system (BMG Labtech, Offenburg, Germany) was set to a 15x15 well-scan with 3mm width using the bottom optic. The optic module 520-20, 590-20 was used with the gain set at 1018.

2.14 Spectrum library

The spectrum library was sourced from Microsource Discovery systems Inc. (Gaylordsville, CT, 06755, U.S.A.). The Spectrum library is a preselected library of compounds with a wide and diverse range biological activities and structural subtypes designed for use in screening and assay development. The spectrum library provides information on drugs, biochemical profiles and molecular structures. All compounds in the library are provided at >95% purity. The libraries were then stored under negative pressure, in the dark with a low oxygen/high nitrogen environment to prevent degeneration of the

library by oxidation, hydrolysis and UV using the Roylan Development SPOD system.

2.15 Zebrafish behavioural analysis

Zebrafish were recorded using the tracking equipment and related software included in the Viewpoint analysis suite (Viewpoint Lab Sciences, Inc). Tracking was performed to identify compounds which were increasing zebrafish behaviour (hypermobility) or were leading to a sedative/anaesthetic effect (immobility or hypomobility). By controlling the light and dark settings within the zebrabox system we can also identify behavioural changes in response to the presence or absence of light. Using the zebrabox attachment, 96 well plates (96 well µClear, Griener Bio One) containing one embryo per well, the larvae were imaged at 6dpf using the tracking software. The plate size information was added to the system and it used the locations and size of the top left, top right and bottom right wells to automatically draw areas of measurement around each of the 96 wells. Tracking was performed for 20mins while the lighting controls were changed at the ten minute stage. Ten minutes of movement were measured in bright conditions followed by a separate ten minute measurement in total darkness. The detection threshold colour was set as transparent with the maximum threshold set at 120. The movement detection parameters for small/fast behaviour were set at 6.0 whereas the inactive/small was set at 3.0. This allows the user to investigate the data more thoroughly and identify fish spending more time in rapid movement phases and fish which are more sedentary.

2.16 Statistics used in high throughput screening plate screening

The statistical test used to determine hits in the screen was the strictly standardised median difference (SSMD) (Zhang 2011). SSMD works by measuring the effect size by comparing it to any two groups with random

values. SSMD expressed most simply is a measure of the fold change of the drug effect but this is penalised based upon the variability of the fold change. This means that each compound gets an effect which is representative of the difference between the compound and the negative control.

$$\mathrm{SSMD}^* = \frac{X_i - \tilde{X}_N}{1.4826\tilde{s}_N\sqrt{2(n_N - 1)/K}}$$

X_i = measured value for a tested well

X_N = Sample median

n_N = Sample size

s_N = Median absolute deviation

K = n_N – 2.48

The SSMD result for each individual well corresponds to a β-Value as depicted in Table 2.1. This method is suitable for high-throughput hit selection as it allows the grading of hits based upon strength of effect compared to the negative control. This is advantageous over other methods such as the z-score which just gives a yes/no answer. Table 2.1 shows the grading system from extremely strong to an extremly weak effect for both inhibiton of fluoresence (negative SSMD) and activation of fluoresence (positive SSMD).

The SSMD* measurement assumes that the tested plate is primarily composed of inactive test compounds. Thus, the majority of compounds in the plate containing test compounds would have SSMD score of around 0, while a true hit would have an SSMD score significantly above or below 0. Compounds with a SSMD* score of below 0 are inhibitors, while those showing SSMD* above 0 are activators. The threshold for a hit in this screen was set at +0.5 or +1 for moderate and strong hits

Effect subtype	Thresholds for negative SSMD	Thresholds for positive SSMD
Extremely strong	$\beta < -5$	$\beta > 5$
Very strong	$-5 < \beta < -3$	$5 > \beta > 3$
Strong	$-3 < \beta < -2$	$3 > \beta > 2$
Fairly strong	$-2 < \beta < -1.645$	$2 > \beta > 1.645$
Moderate	$-1.645 < \beta < -1.28$	$1.645 > \beta > 1.28$
Fairly moderate	$-1.28 < \beta < -1$	$1.28 > \beta > 1$
Fairly weak	$-1 < \beta < -0.75$	$1 > \beta > 0.75$
Weak	$-0.75 < \beta < -0.5$	$0.75 > \beta > 0.5$
Very weak	$-0.5 < \beta < -0.25$	$0.5 > \beta > 0.25$
Extremely weak	$-0.25 < \beta < 0$	$0.25 > \beta > 0$
No effect	$\beta = 0$	

Table 2.1: β value scoring system for SSMD with positive and negative hits

2.17 Quality control statistical analysis

Quality control is essential in hit selection as it statistically confirms the validity and integrity of hit compounds from the screen. Quality control of each plate tested with test compounds was performed using the β-numbers of positive and negative controls in each plate. The sensitivity of an assay shows how many hit compounds are being detected and needs to be maintained as high as possible to ensure hits are not missed by the screen.

The specificity of an assay informs of how many true negative compounds in the screen are showing up as true negatives and must remain as high as possible so that false hits do not occur among the negative controls. To perform the QC experiments the positive control and negative control data for all the plates in each replicate was used and the following equations were used to calculate the sensitivity and specificity.

Sensitivity = (true positives/(True positives + false negatives)) x 100

Specificity = (true negatives/(True negatives + false positives)) x 100

2.18 Electrophysiology

Whole cell voltage clamp recordings were conducted in 4 dpf larvae as previously described (Drapeau et al 1999). The fish were perfused with Evans physiological saline containing the neuromuscular blocker D-tubocurarine (10µM), the sodium channel blocker tetrodotoxin (TTX; to synaptically isolate neurons), kynurenic acid (2.5mM, to block spontaneous glutamatergic currents), and bicuculline (25µM), to block spontaneous gamma-aminobutyric acidergic [GABAergic] currents). Cells were voltage clamped at -75mV, a potential at which the chloride conducting glycine receptors generate inward currents. Sulforhodamine (0.1%) was included in the electrode solution to visually identify the cell type. The frequency of glycinergic miniature postsynaptic currents (mPSCs) was determined by averaging the number of events in a 300-second period. To examine the rise time, decay, and amplitude of mPSCs, the first 50 mPSCs were selected from each recording and averaged across each experimental condition.

Chapter 3: Cellular changes in a zebrafish model of ALS and the identification of drug effect in this model

ALS is a progressive neurodegenerative disease with poorly understood disease mechanism and pathways. An important step in furthering our understanding of the disease would be to elucidate exact cell types affected during the disease course and to understand at what stages they become affected. Knowing the exact cell types involved and the pathways they are associated with means that more targeted therapeutic approaches can be developed that have a direct role at the affected cell. Zebrafish are an excellent model for elucidating the cell types involved. The zebrafish is advantageous because it is optically clear during development, amenable to genetic manipulation and it has a fully developed central nervous system which is well characterised. Using transgenic zebrafish lines, immunolabelling and in situ hybridisation we have tracked the progression of the disease between multiple cell types during the disease course and have begun to identify how ALS progression occurs and which cells may show the strongest susceptibility to mutant Sod1 toxicity. Identifying the cell types affected also raised the hypothesis that the hsp70-DsRed expression system could be used as the readout for therapeutic effect. The idea behind this would be that inhibition of the DsRed fluorescence could be a sign that Sod1 mediated cellular toxicity was lowered and therefore the heat shock pathway activation was lowered. The flipside of this argument is that compounds inducing a large increase in fluorescence could be over-activating the heat shock pathway which is a cellular repair pathway in an effort to counter the Sod1 toxicity. The cellular toxicity was investigated in the zebrafish embryos to identify the cells first affected by Sod1 toxicity.

3.1 Investigating the Hsp70-DsRed response in G93Ros10 zebrafish embryos

Utilising the model previously described by Ramesh *et al* (2010), experiments were designed to identify what cellular changes were occurring in the G93Ros10 Sod1 mutant model of ALS. Our interest in this field was to extrapolate and identify a timeline of the cellular disease progression based upon the cells expressing the hsp70-DsRed stress response pathway. Using DsRed fluorescence arising from the hsp70-DsRed gene expression particular structures and cell types were observed which were commonly switched on in the mutant fish (Fig 3.1). Identification of which cell types were primarily affected in zebrafish embryos and which cell types were affected in adult fish were used to identify a timeline of the propagation of neuronal stress between cell types in this model. The original findings of Ramesh *et al* (2010) showed that heat shocked G93Ros10 zebrafish containing the hsp70-DsRed construct expressed the DsRed fluorescence throughout the fish (Fig 3.1). This was to be expected and showed that the construct is expressed throughout the G93Ros10 zebrafish and that the hsp70 gene is activated in the presence of a heatshock stimulus. The interesting finding was that when the zebrafish were left to develop in the absence of a heatshock, the DsRed expression was still seen in specific zebrafish anatomical structures. Upon further inspection, the majority of the DsRed fluorescence was seen in the spinal cord, hind brain, eyes and the neuromast cells (zebrafish neuronal cells found on the surface of developing embryos). This suggested that the cells affected were predominantly from the central nervous system and were most likely of a neuronal subtype based upon what is known about ALS and the cell types present in these areas. When studied at a higher magnification, it became more apparent that the cells showing the largest DsRed fluorescence were neuronal based upon their morphology and location (fig3.1). It is important to note that heatshock of the zebrafish does not lead to any changes in survival and the fish have an uncompromised lifespan.

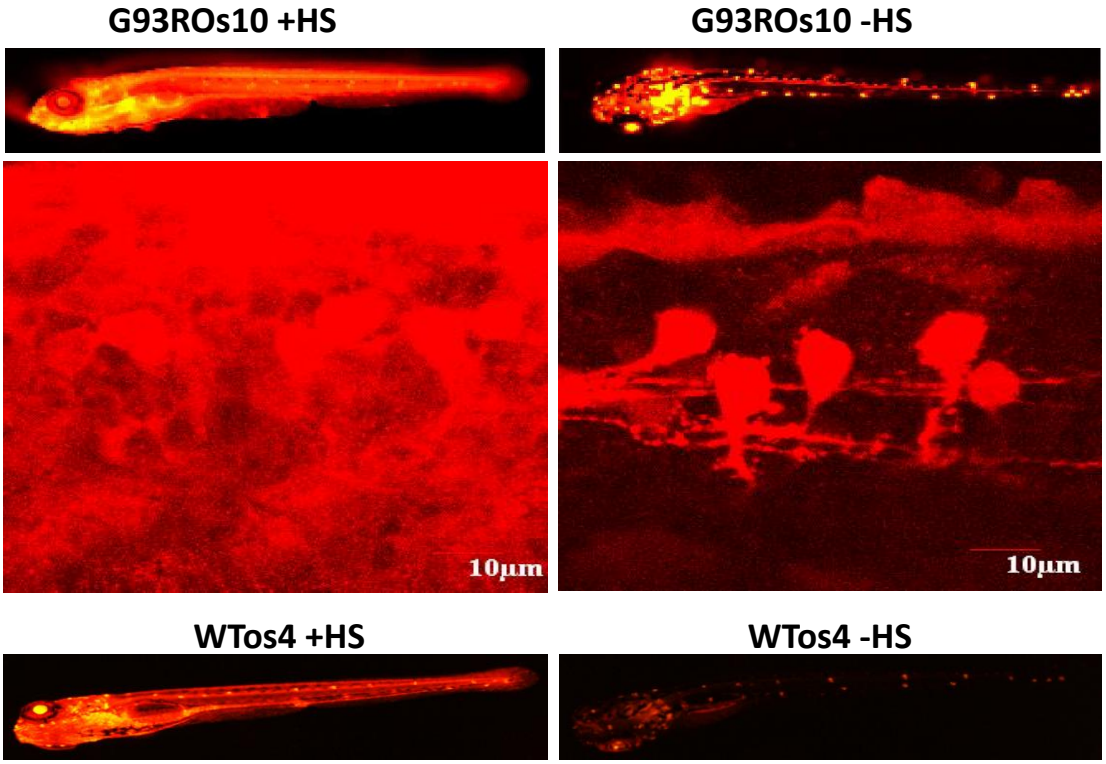

Fig 3.1: G93Ros10 Zebrafish in the presence of heatshock (+HS, Left) and in the absence of heatshock (-HS, Right). Top images show the whole zebrafish embryo at 4dpf. The magnified images are of the spinal cord of zebrafish embryos at 4dpf. Note in the absence of heatshock the DsRed expression is seen in certain cell types, especially the hindbrain and spinal cord. The images below show the expression pattern in the WT overexpression line (WTos4). The HS+ fish shows expression throughout the fish and the HS- WTos4 line shows the lower DsRed expression seen in this line.

3.2 Investigating the Hsp70-DsRed stress response in Sod1 mutant zebrafish

Green fluorescent protein (GFP) transgenic lines and immunostaining were used to identify the cell types showing co-localization with the hsp70-DsRed mediated fluorescence. This was to identify the specific cell types showing hsp70-DsRed activation as a result of Sod1 mediated toxicity. The initial experiments were focused on investigating the expression of motor neuron markers as these cells are classically what would be expected to show pathophysiological changes in a motor neuron disease model.

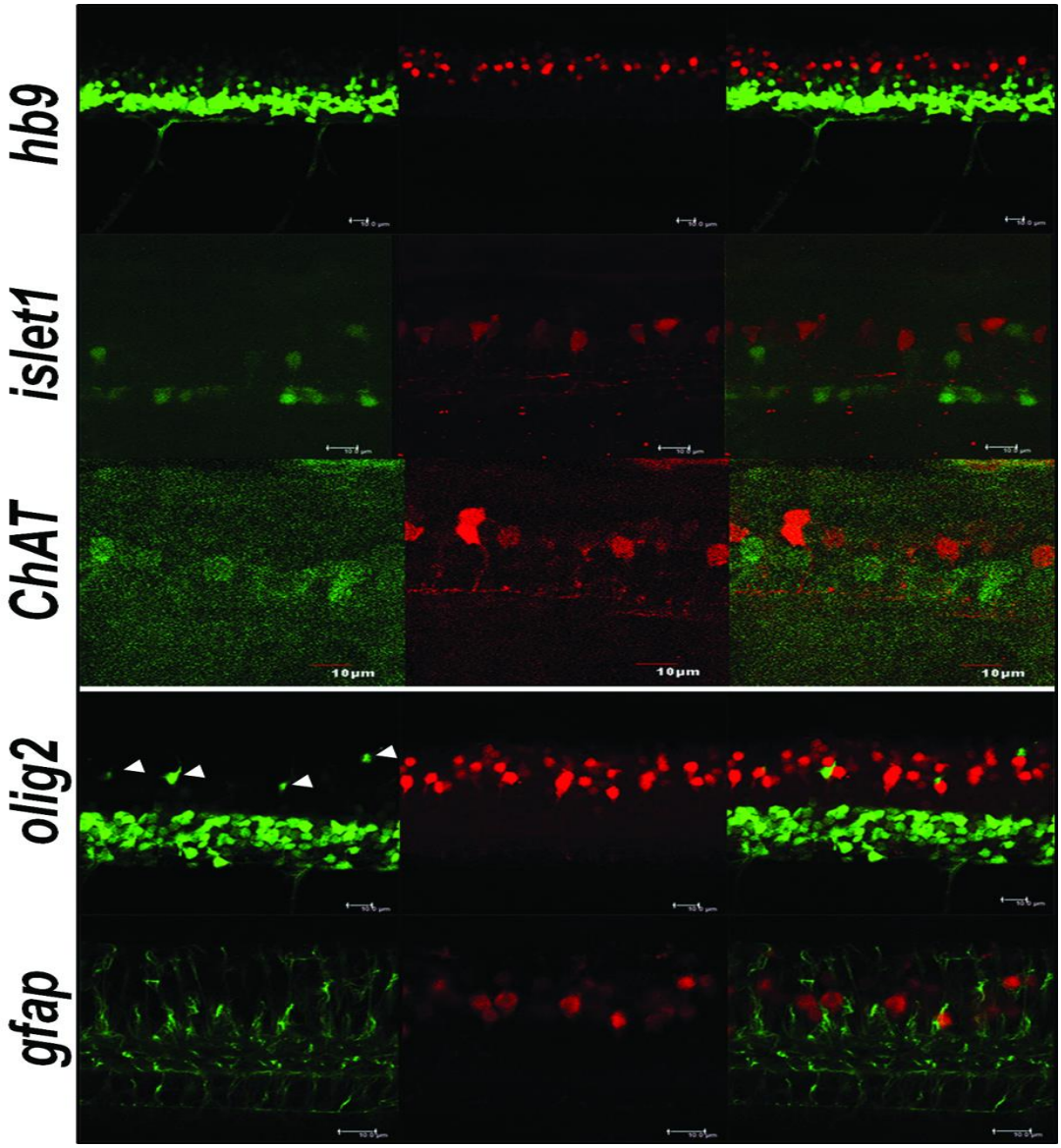

Fig 3.2: Staining G93Ros10 zebrafish spinal cords for motor neuron markers at 72hpf. Hb9 and islet 1 are markers of differentiating motor neurons and ChAT is a marker of mature motor neurons. Olig 2 is a marker for migrating oligodendroctes and GFAP is a marker of astrocytes and radial glial cells. The first column is the GFP marker (Green), the middle column is the DsRed (Red) and the final column is a merged image. Images were taken at 72hpf as this is when many of the neuronal markers are easily detectable. All scale bars show 10µM.

Crossing our mutant Sod1 zebrafish with zebrafish carrying fluorescent markers for different cell types allows the identification of individual cell types that are involved in the mutant Sod1 stress process. Following crossing of our G93Ros10 line with the islet-1-GFP fish which is a marker of motor neuron differentiation we did not see co-localization with the DsRed stress

response suggesting that it is not the early motor neurons that are stressed (Fig 3.2). To confirm this, a crossing of our G93Ros10 mutant line with the hb9-GFP fish (Fig 3.2) (marker of neuronal differentiation) was carried out and again we did not see co-localization with the DsRed stress response suggesting that it is not the early motor neurons that are stressed and that the motor neurons were not expressing a stress response during the neuronal differentiation process. The next step was to determine if it was mature motor neurons that were showing the stress response at the early stages. This was carried out by staining for the mature motor neuron marker ChAT (Choline acetyl transferase) to identify if fully mature motor neurons showed hsp70-DsRed activation. Again it was found that the ChAT positive neurons were not affected at these early stages and did not co-localize with the DsRed signal. From this it is proposed that the motor neurons were not the first cell type affected by the G93R Sod1 mutation and that a different cell type must be stressed prior to motor neurons. The cells expressing the DsRed signal showed neuronal morphology, but to confirm this an investigation of other cell types present in the spinal cord was undertaken. The G93Ros10-Sh1 zebrafish was crossed with the olig2-GFP (Oligodendrocyte marker) and GFAP-GFP (Astrocyte marker) fish to identify any non-neuronal cells which expressed the DsRed fluorescence. The immunostaining showed that the GFAP and Olig2 positive non-neuronal cell types were not showing an upregulation of the hsp70-DsRed response and that a different cell type was expressing the stress response. Based upon the morphology of the cells showing the stress response (fig 3.1, -HS) we further investigated different neuronal subtypes. Staining for these markers could only be performed in the high-expressor line as DsRed expression in the other mutant lines was too low to detect. Staining was not performed in the WTos4 line as the data from the electrophysiology showed no neuronal dysfunction in this line (Fig 3.4).

3.3 Inhibitory interneurons show the stress response prior to motor neurons in the mutant Sod1 zebrafish

These data indicated that it was possible that spinal interneurons were affected first. The hypothesis behind this was that if the interneurons show the stress response and become deregulated, then when this stress and damage builds up to a certain threshold, the cellular mechanisms cannot cope and they lose the ability to correctly input and regulate the motor neurons and this disregulation leads to the stress response in the motor neurons at later stages. Interneurons have also been implicated in ALS as previously discussed in the introduction. In order to test this, investigation of the expression of DsRed fluorescence in these cells was undertaken.

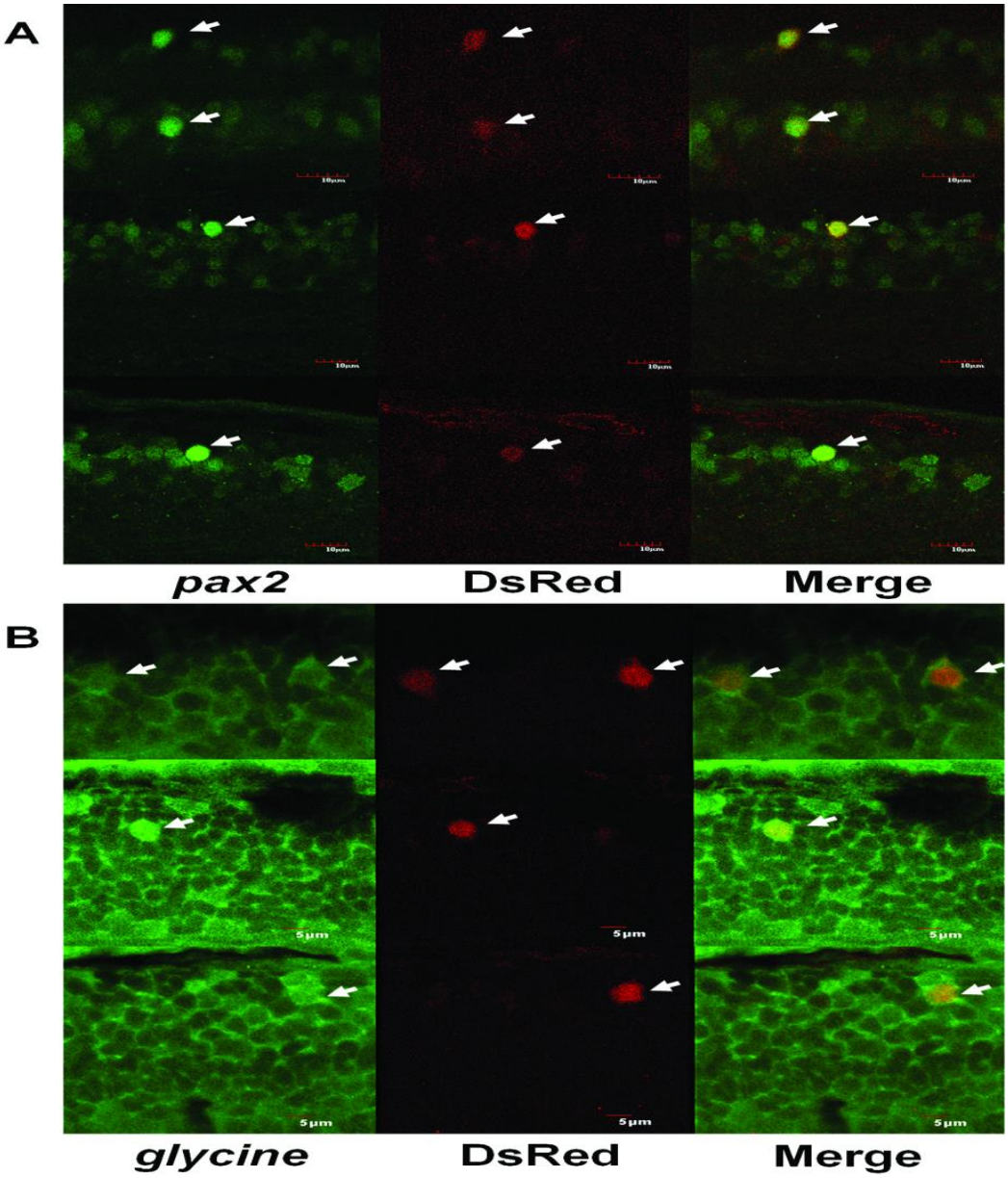

Fig 3.3: Whole mount immunostaining for DsRed, pax2 and glycine in the g93ros10 zebrafish at 48hpf. White arrows indicate co-localization between the marker and DsRed fluorescence. A shows staining for neuronal marker pax2, DsRed and a merge image. B shows glycine staining mainly for inhibitory interneurons, DsRed and a merged image. Scale bars in A show 10µM, Scale bars in B show 5µM.

In order to show that the stressed cells were of a neuronal subtype, staining for the inter-neuron marker, pax2, was carried out. This showed that the DsRed co-localized very well with the pax2 marker as shown in fig 3.3 part A. This indicated that the stressed cells in the early stages are of an interneuron nature. Immunostaining for the glycine antibody which is a marker for

inhibitory interneurons was then undertaken. It was found that a majority of cells stained positive for glycine which indicates that at these early stages it is the inhibitory interneurons that are showing the stress response, not the motor neurons, and that potentially some form of propagation mechanism is occurring by which the stress transfers from one cell type to another over time. As the glycinergic interneurons had been identified as the key cell population showing the stress response, they were further probed using electrophysiology to understand the dysregulation occurring at the cellular level. Staining was not performed in WTos4 zebrafish as the antibody had large background and masked the DsRed signal. This work has been taken further with InSitu hybridization techniques and the data is available in McGown et al, 2013.

3.4 mutant Sod1 zebrafish have impaired glycine interneuron activity

The electrophysiological profiles of the glycine positive stressed interneurons were investigated to determine what was happening to these affected interneurons. In collaboration with Jonathan McDearmid from Leicester University, individual neurons from 4dpf G93Ros10 mutant zebrafish were whole cell voltage clamped and the current measured as per the protocol previously used (Drapeau et al 1999).

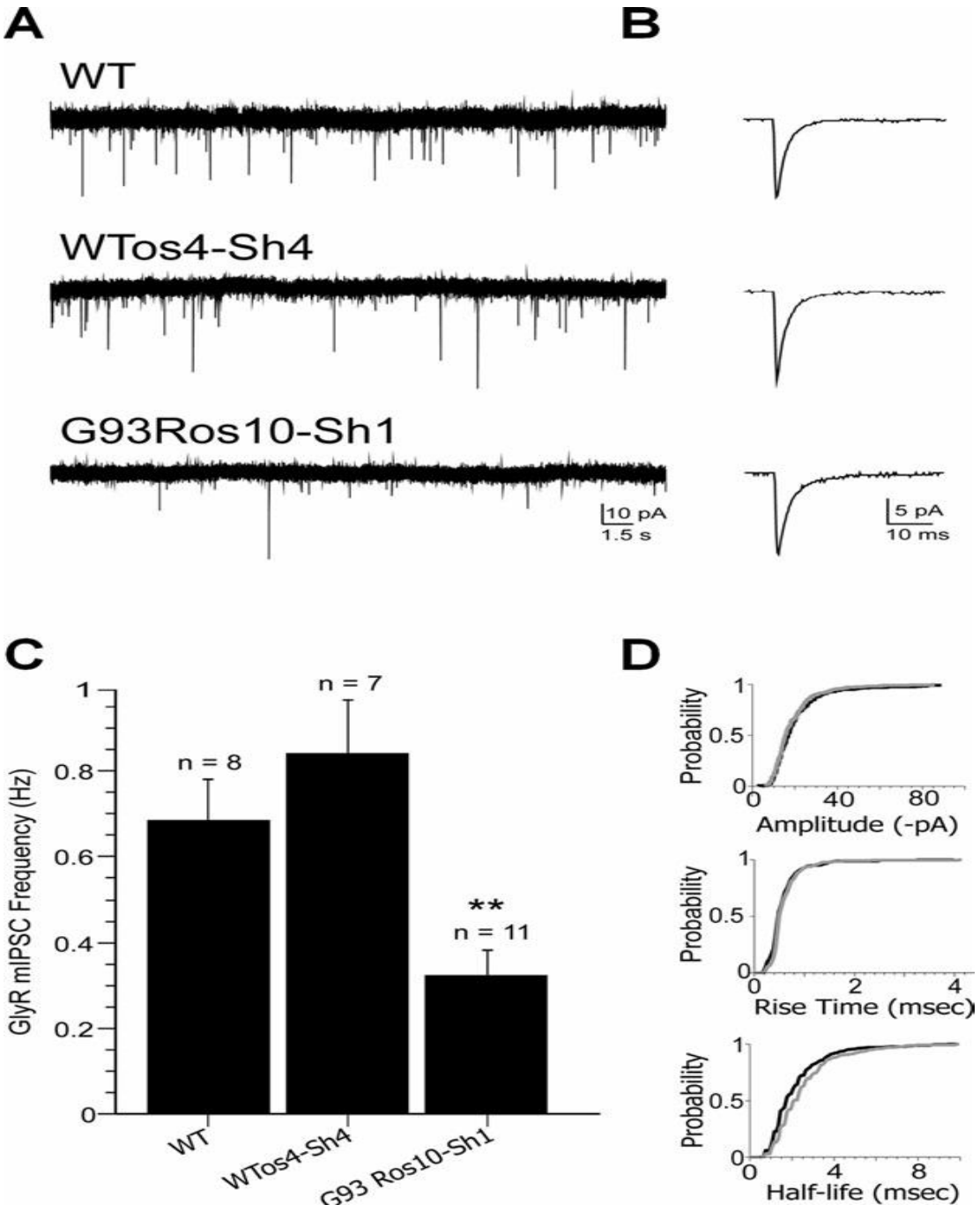

Fig 3.4: Reduced glycinergic transmissions onto motor neurons of Sod1 zebrafish larvae. (A) Representative traces depicting voltage clamp (holding potential 5 275mV) recordings of spontaneous glycinergic miniature postsynaptic currents (mPSCs) in motor neurons of wild-type (WT), WT Sod1 over-expressor (WTos4-Sh4), and Sod1 mutant (G93Ros10-Sh1) fish at 4 days post-fertilization. Downward deflections represent occasional quantal release of glycine from presynaptic terminals. (B) Average of 30 consecutive glycinergic mPSCs from each experimental condition. (C) Bar chart depicting mean mPSC frequency for each experimental condition. GlyR 5 glycine receptor; mIPSC 5 miniature inhibitory postsynaptic current. **WT vs. G93R $p < 0.001$. (D) Cumulative probability plots of mPSC amplitude, rise time, and half-life ($p < 0.05$) in WT (black lines) and G93Ros10-Sh1 (grey lines) motor neurons.

Fig 3.4 A shows representative traces of the potential of the impulses from glycinergic inhibitory interneurons from G93Ros10 mutant zebrafish, WTos4 overexpressing WT Sod1 and wild type fish. The traces show a reduced frequency and strength of spontaneous presynaptic potentials in the G93Ros10 mutants when compared to the WT and WT overexpressing zebrafish models. Fig C shows the mean frequency of mPSC (Hz) for each of the models which confirm that the frequency of glycine currents is reduced in the mutant Sod1 model when compared to the WT. This shows that the DsRed positive glycinergic interneurons have abnormal behaviour in the model and that interneuron dysfunction is occurring at the embryonic stages. Based upon these findings at the embryo stages, the disease progression in the adults was probed to see how the disease pathology changed over time.

3.5 Investigating the stress response of motor neurons in the spinal cord of mutant and wild type zebrafish

Based upon these findings, the next stage was to investigate which of the neuronal cell subtypes were affected at each stage and identify which cells were particularly susceptible to neuronal stress in the Sod1 mutant model. In adult spinal cord, ChAT (Choline acetyltransferase) immunolabelling was carried out to identify spinal cord motor neurons and co-localize these with DsRed fluorescence (stress marker) in the spinal cord. The high expressor mutant line (G93Ros10-Sh1) shows highly elevated levels of DsRed expression in the spinal cord which co-localize largely with the ChAT staining indicating that the mature motor neurons in the high expressing mutant Sod1 model are undergoing a large stress response (Fig 3.5 A-D). In the G93Ros10-Sh1 line, all motor neurons showed the stress response, indicating how widespread the stress response is in the spinal cord. Many neurons also appear to show the DsRed signal but no ChAT staining, suggesting that a strong DsRed signal indicates complete neuronal dysfunction and thus the cells no longer express the ChAT signal and are most likely undergoing apoptosis. In the G85Ros6-Sh3 line, a lower expressing mutant line, the neuronal stress is still seen in the spinal cord, but the overall levels are significantly lower than the high-expressor line (Fig 3.5

E-H). A study of the co-localization of the stress response with the motor neurons showed some motor neurons exhibit a significant upregulation of the heat shock response, whereas others showed no co-localization. This can be seen in fig 3.5 (H) which identifies the presence of ChAT positive motor neurons showing the stress response alongside ChAT positive motor neurons showing no DsRed co-localization. This suggests that certain motor neuron subtypes are more susceptible to cellular stress than others or that the toxicity from the Sod1 has not reached a sufficient level to activate the response. In the wild-type expressor line very little DsRed expression was seen, with no co-localization with the ChAT staining, showing that the motor neurons are unstressed and that mutant Sod1 mediated toxicity, but not wt-Sod1, is leading to an activation of the hsp70-DsRed response in ChAT positive motor neurons in adult zebrafish (Fig 3.5 I-L).

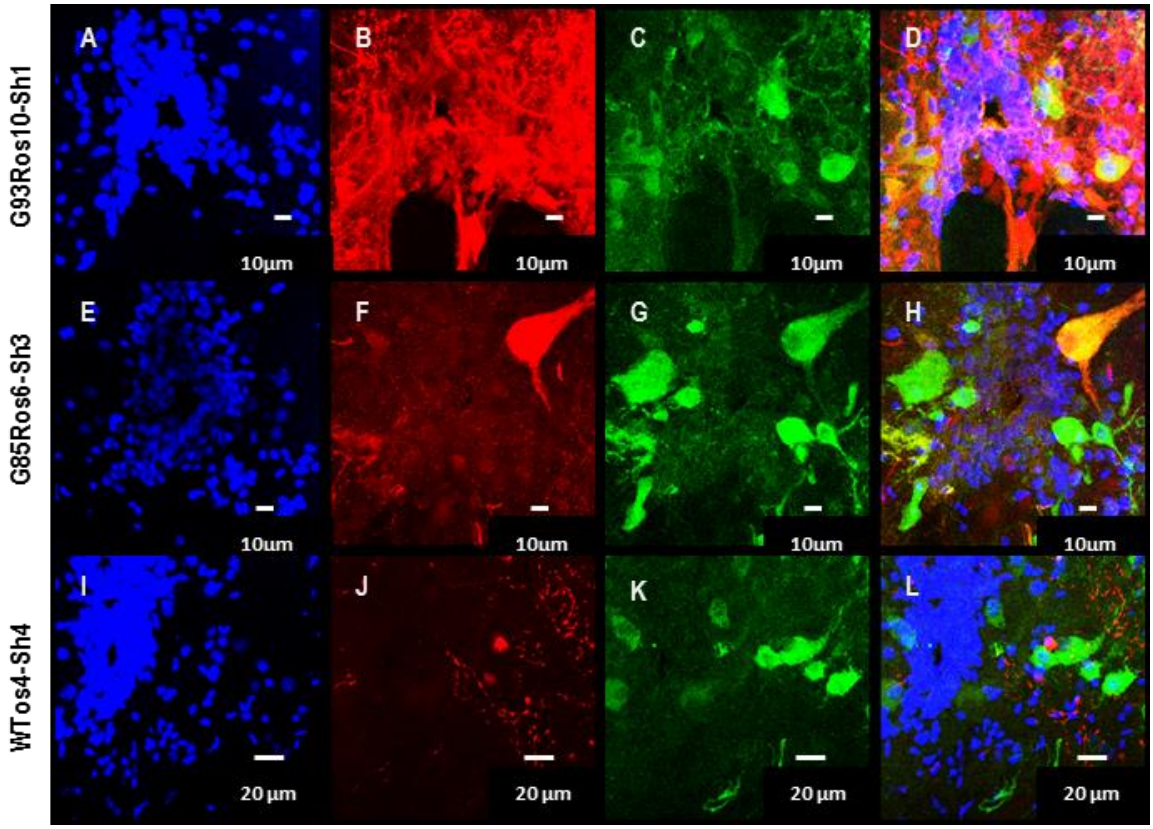

Fig 3.5: Symptomatic adult mutant Sod1 zebrafish show induction of HSR in the large spinal motor neurons: Spinal cord cross sections from 1-1.5 year old symptomatic adults stained with DAPI (A,E,I),DsRed antibody (B,F,J) and ChAT antibody (C,G,K) show robust induction of HSR (B,F) and co-localization of DsRed with ChAT in the high expressor (3X) G93Ros10-Sh1 line (A,B,C,D), and the moderate expressor (2X) G85Ros6-Sh3 line (E,F,G,H) . High expressor (3X) WTos4-Sh4 line shows little DsRed staining and the DsRed label does not co-localize with the large ChAT positive motor neurons (I,J,K,L).

3.6 Mutant Sod1 leads to abnormal NMJ morphology

Based upon the stress seen in the 1-1.5y old Sod1 mutant fish, it was decided to look at the muscle tissue to investigate whether changes were seen in the NMJ innervation of the muscle alongside the stress response seen in the spinal cord ChAT positive motor neuron cell bodies. Problems at the level of the NMJ would be expected if death and dysregulation was occurring in the motor neurons. The fish chosen for this analysis were selected at the ages which showed defects in the swimming tunnel test (Ramesh et al 2010). The reasons for looking at the NMJ's are that they are the key boundary between the muscle and the neurons and are the site of

innervation to the muscle. As paralysis and denervation is a key pathology of ALS sufferers, this area is an important region to investigate. Sections from body muscle samples from 1-1.5y old fish were stained using SV2 to demonstrate presynaptic neurons, α-bungarotoxin to stain post synaptic NMJ's and DsRed as a marker of neuronal stress. From this any defects in the pre- or post- synaptic components can be identified using the DsRed fluorescence. The staining showed that in the high expressor mutant line (fig 3.6 B) neuronal stress could be seen co-localizing with the SV2 marker and the bungarotoxin indicating that the fish showed a large stress response throughout the NMJ. This stress response also appears to coincide with an absence of complete NMJ's with only punctate and sparse co-localization between SV2 and bungarotoxin. This is also seen in the lower expressing mutant (Fig 3.6 C) to a lesser degree with small levels of pre- and post-synaptic markers present along with DsRed expression suggesting disruption of normal NMJ morphology. The arrows show the presence of a stressed and unstressed NMJ where an almost complete loss of co-localization is observed in the presence of the stress response. In the WT expressor (fig 3.6 A) line normal pre- and post- synaptic expression is seen with no DsRed expression, which again shows that the hsp7-DsRed fluorescence is a direct result of the mutant Sod1 toxicity.

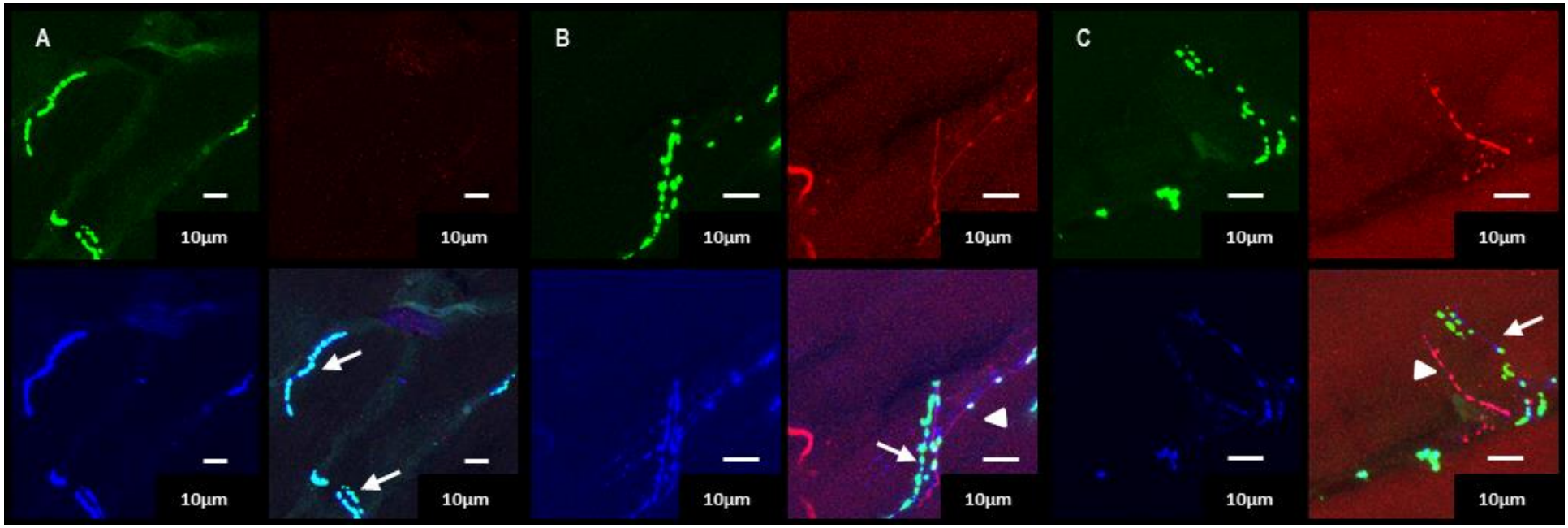

Fig 3.6: Immunostaining of NMJ in mutant Sod1 adult zebrafish body muscle. Muscle sections labeled with synaptic vescicle-2 (SV2) antibody (blue), α-bungarotoxin (green), and DsRed (red) in high expressor WTos4-Sh4 (A), G85Ros6-Sh3 (B), and G93Ros10-Sh1 (C). Normal NMJs' are indicated by arrows. The arrowheads in B and C show denervation occurring in the samples.

After showing that defects in innervation can be seen in the mutant lines, the size of the NMJ in stressed and unstressed axons in the low expressor mutant line was investigated to determine whether the stressed NMJ's that were present had an altered morphology. From the imaging in figure 3.7 it can be seen that stressed neurons result in aberrant NMJ's which leads to denervation of muscle. This provided an appropriate control for us to quantify changes in the morphology of the NMJ within the same specimen in the presence of stressed versus non-stressed axons. Using the Image J co-localization software, the NMJ volume was measured in stressed and unstressed axons. The stressed axons showed reduced NMJ volume in comparison to the unstressed axons which suggests that the Sod1 mutation is leading to neuronal problems which eventually leads to muscle innervation problems and supports the data found in the previous swim tunnel testing when the mutant fish failed to continue swimming for as long as the WT fish (Ramesh et al 2010).

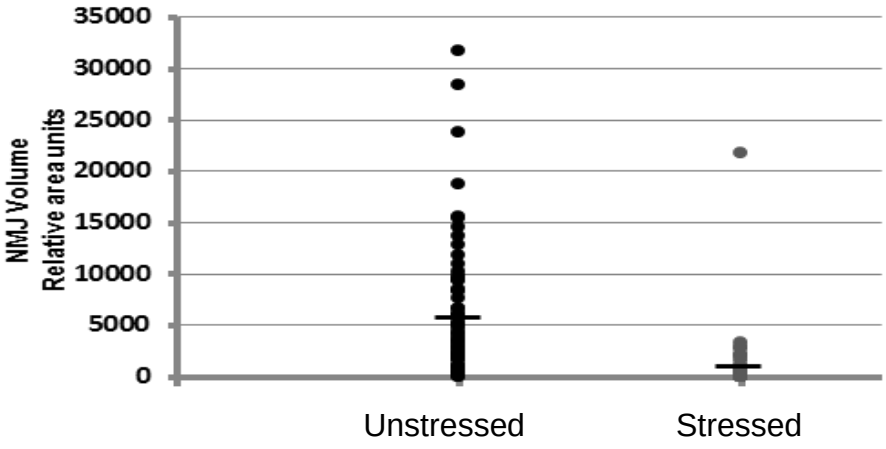

Fig 3.7: Stressed motor axons in mutant Sod1 fish show reduction in NMJ Volume. A measurement of NMJ volume in stressed versus non-stressed motor axons of low expressor G85Ros6-Sh3 line was carried out. Muscle sections were immunostained with antibodies to DsRed, SV2 and labeled α-bungarotoxin. 113 NMJs from multiple sections were measured for NMJ volume from confocal stacks in SV2 positive-DsRed negative axons and SV2 positive-DsRed positive axons using co-localization software from NIH Image J and analyzed by unpaired t-test. Significant reduction in NMJ volume was observed in stressed motor axons as compared to the non-stressed axons. The mean is represented as a line over the distribution. Each dot represents the volume of an individual NMJ. $p<0.00001$. Representative images of stressed and unstressed NMJ's are in A and C of Fig 3.6.

3.7 Riluzole reduces the Hsp70-DsRed response in a dose dependent manner

Knowing that the DsRed upregulation was a direct result of neuronal stress caused by the mutant Sod1 expression and that the major cell type affected in the embryos was inhibitory interneurons, it was hypothesized that measuring the DsRed expression levels would allow us to determine a baseline stress level in the mutant zebrafish which could then be utilized as a way of measuring drug effect. Using this baseline DsRed readout allows an investigation of test compounds for their efficacy in reducing neuronal stress by looking for compounds which showed reduced DsRed fluorescence, as this could arise due to reduced neuronal stress and lead to the identification of lead molecules for further analysis. It also allows the identification of compounds that activate the stress response as potential candidates for neuronal protection via upregulation of the cellular repair pathways. Riluzole was the first compound tested, as it is the available neuroprotective treatment for human ALS patients and thus adds the most validity to the model's use in showing drug effect. The effect of this drug is measured as its ability to reduce the neuronal stress, which can be quantified as a reduction in DsRed expression correlating with a reduction in HSP70 expression. The embryos were chronically immersed in a drug solution from 24hpf to 5days of age with daily drug changes in the plate. Drug effect can be seen to act in a dose dependent manner as increasing dose of Riluzole causes a progressive reduction in DsRed fluorescence.

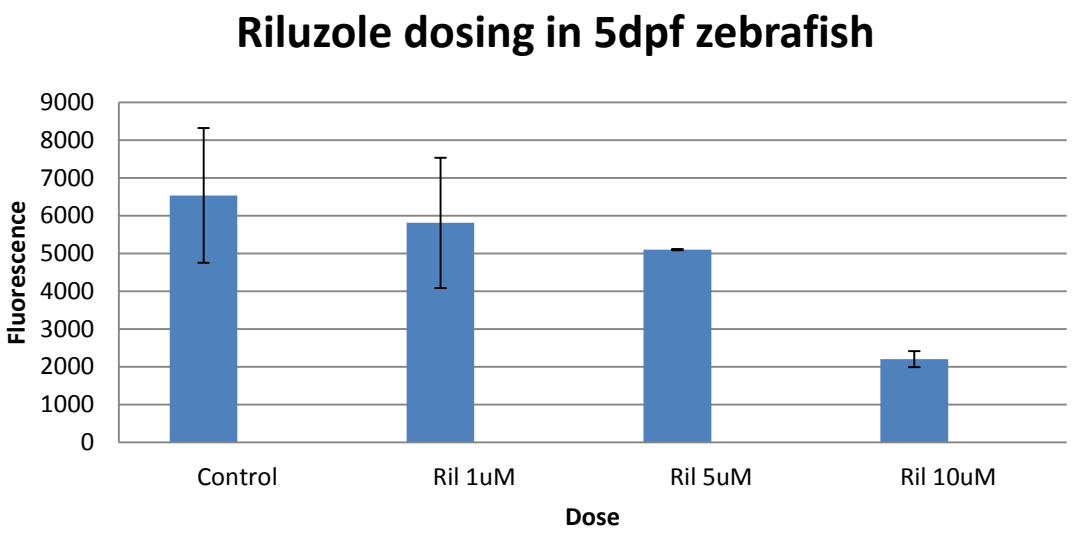

Fig 3.8: Measurement of DsRed Fluorescence in 5dpf G93Ros10 zebrafish. Zebrafish DsRed expression was measured after 4days exposure by immersion in Riluzole. The DMSO control was used as baseline readout of neuronal stress and the reduction in stress was measured by increasing dose. The higher doses of Riluzole (10uM) showed a reduction of 70% in comparison to the Control dose. This can be used as readout for drug effect. The error bars represent the SD. N= 14 fish per group

The results show Riluzole has the ability to reduce neuronal stress in a dose dependent manner. At 1µM Riluzole has no significant effect when compared to the control zebrafish with fluorescence readings around the 6000 region. At 5µM a slight reduction in fluorescence was seen, but this was not found to be significant. At 10µM we saw a reduction of over 60% in fluorescence. This suggests that at 10µM the Riluzole is reducing the neuronal stress significantly when compared to the control zebrafish. This was a major step in validating our assay as it shows that Riluzole, the current treatment for human ALS, was showing a positive effect in our mutant Sod1 zebrafish model. This gave the model more strength and highlighted the ability of Riluzole to function as a positive control of drug effect when screening further compounds or for designing a high-throughput screen. To confirm that this was a positive effect of the drug, Riluzole was also tested in the wild type overexpression line, WTos4. As Fig 3.9 shows Riluzole at 10µM shows a significant reduction in fluorescence, but the reduction is around 20%, less than the 60% reduction in the mutant Sod1 line. This suggests that the toxicity from WT overexpression is less than the mutant Sod1 toxicity.

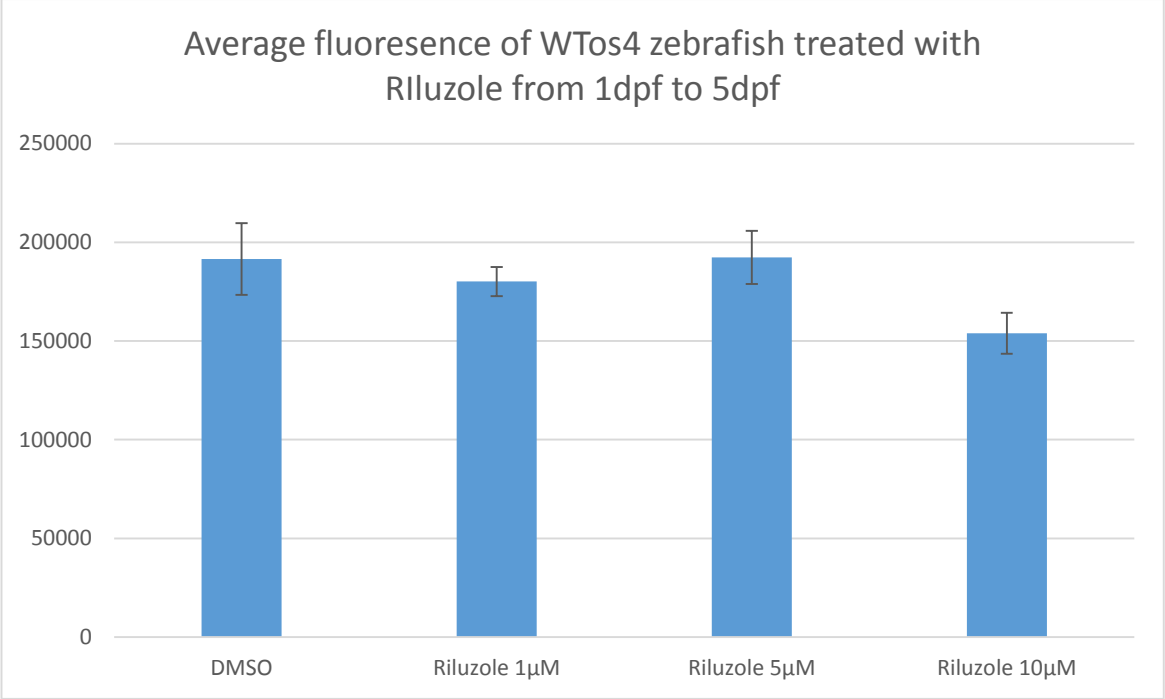

Fig 3.9: Measurement of DsRed Fluorescence in 5dpf WTos4 zebrafish. Zebrafish DsRed expression was measured after 4days exposure by immersion in Riluzole. The DMSO control was used as baseline readout of neuronal stress and the reduction in stress was measured by increasing dose. The higher doses of Riluzole (10uM) showed a reduction of 20% in comparison to the Control dose. The error bars represent the SD. N= 14 fish per group

3.8 Riluzole and other neuroprotective compounds reduce the neuronal stress in mutant Sod1 zebrafish

Further validation studies were undertaken with compounds that had been shown to be neuroprotective in ALS (Apomorphine S)(Mead et al 2013) and with a general neuroprotective effect (EGCG Epigallocatechin gallate)(Yu et al 2010) to investigate their effect on DsRed expression in the G93Ros10 model.

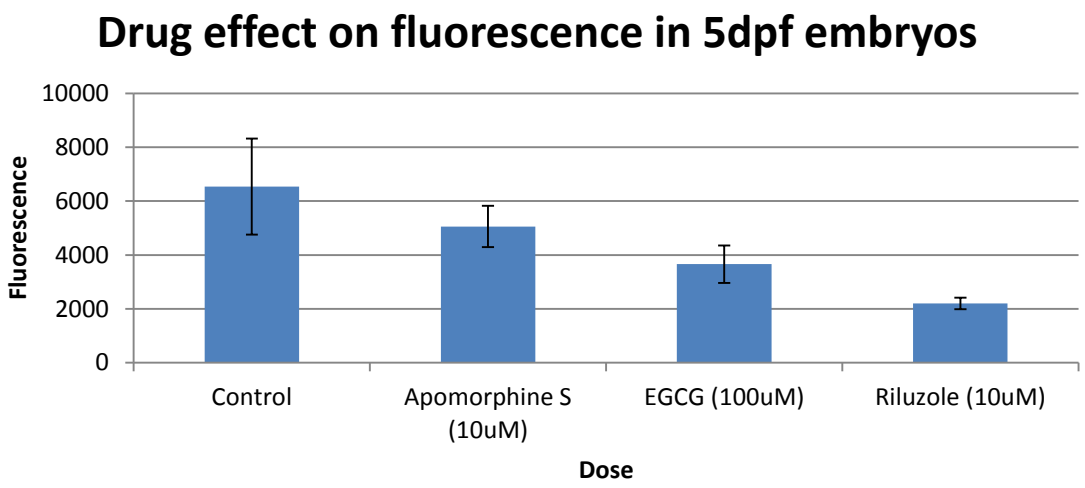

Fig 3.10: Effect of drug treatment in a 5dpf zebrafish model. Zebrafish DsRed expression was measured after 4days chronic exposure to various compounds known to show neuroprotection in other models of ALS. The DMSO control was used as the baseline readout of neuronal stress and the reduction in stress was measured for each compound. The higher doses of Riluzole (10uM) showed a reduction of 70% in comparison to the Control dose. This can be used as the readout for drug effect. The error bars represent the SD. N= 10 fish per group.

ApoS at 10µM and EGCG at 100µM both showed a significant reduction in fluorescence which was lower than the effect of Riluzole. Both compounds led to a significant reduction in the fluorescence compared to the control treated fish. These data suggest that drug effect is measurable and that the size of effect can be measured for individual compounds. This highlights that the sensitivity possible with this model means it is ideal for the development of high-throughput screening assays where large numbers of compounds could be screened and compounds with strong and weak effects would be detectable and distinguishable.

3.9 Comparison of different enantiomer's of Apomorphine for drug effect in a zebrafish screening model for ALS

The zebrafish DsRed fluorescence model was used to determine drug effect with the *R* and *S* enantiomers of the NRF2 activator molecule Apomorphine. The ability to distinguish the difference between these structurally similar

compounds is a good measure of the sensitivity of the model in expressing the difference in drug effect.

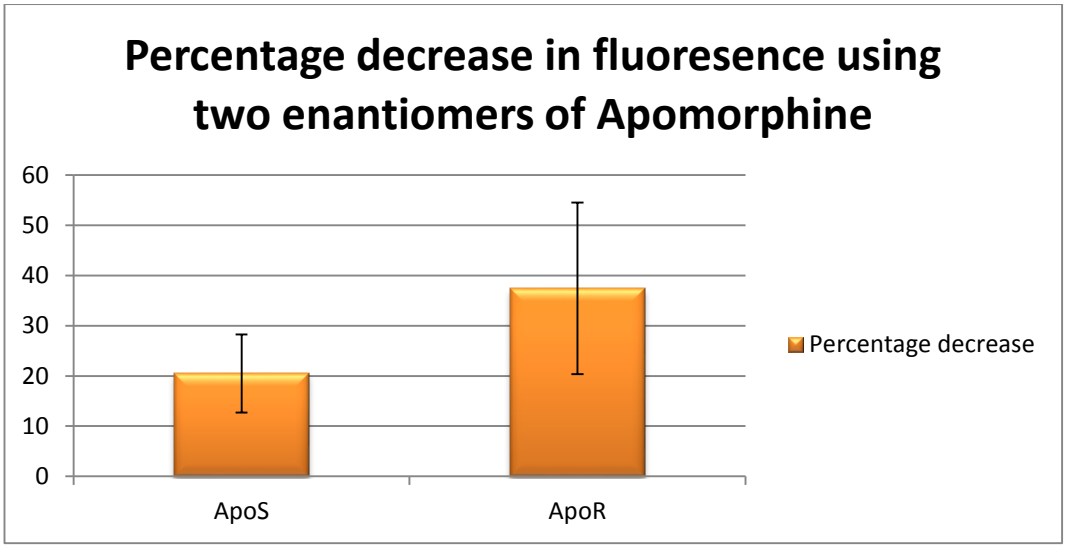

Fig 3.11: Comparison of the ability to reduce neuronal stress with the R and S enantiomer's of the compound Apomorphine. DsRed expression was measure after 4days of immersion in 10µM solution of the Apomorphine compound. Both drugs managed to induce a reduction in neuronal stress with *R*-Apomorphine (ApoR) causing a reduction of over 35%, whereas S-Apomorphine (ApoS) caused a reduction of over 20% compared to the DMSO control. There is no significant difference between ApoS and ApoR.

The effects of the two enantiomers of Apomorphine showed that the different enantiomers had different efficacies in reducing the neuronal stress. ApoS reduced the neuronal stress by 20% whereas the R enantiomer led to a reduction of over 35% showing that the different structures have different abilities to lower the neuronal stress. This was further evidence that this assay has the capability to distinguish drug effect even between different enantiomers of compounds and that it is possible to utilize this model for high-throughput screening. ApoS has been highlighted recently as a potential treatment for ALS (Mead et al 2013) whereas ApoR was identified primarily as a treatment for Parkinson's disease as it is a potent dopamine agonist unlike ApoS (Kempster et al 1990). This suggests that both of these compounds have the ability to cross the BBB and have neuroprotective properties.

3.10 Discussion

The aim of the project was to identify the different stage and cell populations which were more susceptible to Sod1 mediated neuronal stress. By investigating the cell types affected, we could begin to generate a timeline of the propagation of cellular stress in the Sod1 mutant model. When heatshocked, the G93Ros10 zebrafish carrying the hsp70-DsRed lead to complete expression of the fluorescence throughout the fish which is what would be expected due to the activation of the hsp70 response. When the G93Ros10 zebrafish were raised in the absence of any heatshock the hsp70-DsRed activation was still seen in specific anatomical structures, particularly in the spinal cord and hindbrain. This was not seen in the WTos4 zebrafish carrying WT Sod1 alongside the hsp70-DsRed gene where very little activation of the DsRed was seen and expression was not confined to a particular cell type. This strongly supports the hypothesis that the mutant Sod1 is leading to the cellular stress. In Sod1 mediated ALS the disease pathways mainly occur due to the loss of motor neurons in the spinal cord and the mutant zebrafish model strongly supports this as the hsp70 pathway, a cellular repair pathway, is highly upregulated in these cells suggesting cellular problems are occurring. Mutant Sod1 is causing many of the cellular problems such as excitotoxicity, mitochondrial defects, aggregation and oxidative stress and these are leading to an upregulation of the hsp70 pathway in an attempt by the cell to rectify the problems. Hsp70 activation is a common cellular response to an insult and in many cases has the ability to repair the cell via the unfolded protein response and protein stabilization and targeting proteins to the ubiquitination and proteolysis pathways (Mayer 2013). Based upon findings from the G93Ros10 zebrafish, this activation of the hsp70 response is not enough to protect the cell types affected and possibly a stronger response is needed to protect the cells. This identified a potential therapeutic pathway to investigate by up-regulation of the hsp70 response to a higher level to maximize the protective pathways within the cell so that the cell may protect itself from the toxic insult from mutant Sod1. In the spinal cord of 1.5y old G93Ros10 mutant zebrafish, the stress response is seen throughout the spinal cord with particularly strong expression in the

ChAT positive motor neurons. This is in contrast to the WTos4 zebrafish expressing WT Sod1, where very little hsp70-DsRed activation and no co-localization with the ChAT motor neuron staining is observed. This is further evidence that in ALS, a disease leading to the death of motor neurons, the mutant Sod1 is leading to the cellular problems and death, the same phenotype seen in the zebrafish. In the G93Ros10 the hsp70-DsRed response is strongest in the ChAT positive motor neurons which suggest that the motor neurons are particularly sensitive to the Sod1 toxicity compared to other cell types. The motor neurons may be more susceptible to the cellular insults such as oxidative stress than other cell types (Bosco et al 2010). Further support for the hypothesis that mutant Sod1 leads to cellular stress and hsp70 activation, is given by the G85Ros6 Sod1 mutant transgenic line. This line has a lower mutant Sod1 copy number than the G93Ros10 line and this leads to reduced Sod1 toxicity. This translates to less DsRed fluorescence in the spinal cord as lower levels of mutant Sod1 lead to a slower disease course and less DsRed fluorescence. The lower copy number also allows the identification of individual ChAT positive neurons that are showing the stress response as well as neurons not showing the stress response. This is very useful in investigating the timeline of disease progression as the slower disease course allows the imaging of the disease progression over time and the identification of the different cell types being affected.

Stress and loss of motor neurons is a key pathological feature in ALS and as these input to neuromuscular junctions immunostaining was performed to look at the pre and post synapse alongside the hsp70-DsRed fluorescence. We found that in the WTos4 WT Sod1 expressing line no stress was seen and fully functional NMJ's were formed. In the G93Ros10 mutant Sod1 line a drastic stress response was seen in the majority of NMJ's still expressing the pre- and post- synaptic markers. The NMJ's still expressing the markers and stress response appeared smaller and more punctate in nature suggesting defects at the neuron-muscle boundary. NMJ defects have been highlighted in ALS and are the major cause of the paralysis at late stage disease due to the loss of innervation to the muscle. In a zebrafish mutant FUS model and a FUS knockout model the NMJ's showed reduced and aberrant patterning

showing defective NMJ formation (Armstrong & Drapeau 2013). In G93A Sod1 mutant mice a timeline of NMJ defects was generated which showed clinical weakness at 80 days and death by 130 days. This is in contrast to what is happening at the NMJ level where they found 40% denervation at 47 days and 60% loss by 80 days (Fischer et al 2004). These data, alongside our findings, suggest that stress in the motor neurons and the dysfunction that result means the NMJ's become dysfunctional. Mutant Sod1 is causing motor neuron problems and stress which propagates to the end plates and eventually affects the neuron muscle boundary leading to weakness and paralysis after total loss of innervation. Upon further investigation using the lower mutant Sod1 expressor line (G85Ros6), it appeared that certain neurons may be more susceptible to the stress response than others or that some neurons may have some protection from the Sod1 toxicity. This selective vulnerability has been seen in mice with G93A Sod1 mutations, where fast fatigable motor neurons appeared to be selectively affected first, long before symptom onset, whereas the slow motor neurons appeared to be resistant to the Sod1 toxicity (Pun et al 2006). Again this leads to a hypothesis that ALS is a progressive disease with a propagation of the stress from the most vulnerable neurons to Sod1 toxicity to other more resistant neurons over the disease duration. It also suggests that this neuronal stress is not something that occurs at a late stage and just appears at symptom onset, but that neuronal pathophysiological changes could be happening from a young age and only when the stress has reached a critical level in certain neuronal subtypes and the dysregulation is large enough a clinical phenotype occurs. Based upon the literature the NMJ morphology was investigated in the G93Ros10 mutant Sod1 model to investigate the effect of mutant Sod1. In the mutant sod1 zebrafish the NMJ's were found to have a lower volume when compared to the WT Sod1 line. These data provide further evidence that mutant Sod1 mediated toxicity is causing problems in the spinal cord and at the NMJ which correlates with the clinical pathways seen in human ALS patients. This zebrafish Sod1 model highlights the disease progression and closely mimics what is seen in both mouse models and human patients with ALS. It highlights the potential of this model for further modeling the disease pathways and for potential therapeutic

development with the utilization of the stress response readout as a measure of drug effect.

To investigate the cell progression fully, the cellular subtypes affected in the embryos were examined to identify the cells affected by the hsp70-DsRed expression. Identifying the cellular changes at embryo stages would be a much more usable way to develop a screen over a number of days rather than months, allowing the screening of large numbers of compounds rapidly. The initial experiments focused on identifying the cell types affected at the embryo stage to find where the stress is localised. Initially ChAT immunostaining was performed on the embryos to look at the motor neuron co-localization with the stress response. The G93Ros10 zebrafish hsp70-DsRed response did not co-localise with the ChAT staining which leads to the hypothesis that at the early stages of ALS it is not the motor neurons that show the Sod1 toxicity but other cell types. The G93Ros10 zebrafish was crossed with transgenic lines with motor neuron reporter fluorescent markers to identify co-localization with other motor neuron markers or markers of neuron progenitors. No co-localization was seen with Hb9 or islet-1 markers for motor neurons with the DsRed, which suggests again that at the early embryo stages of the Sod1 mutant fish it is not the motor neurons showing the stress response, but another cell type. G93Ros10 zebrafish were crossed with transgenic lines for oligodendrocytes and astrocytes to identify if these supporting cells were expressing the DsRed response. None of these cells show the stress response in our model which suggests that it is not these supporting cells that are having the stress response in the early stages. This is in contrast to the literature which highlights the possible role of astrocytes as a toxic mechanism in ALS. Astrocytes are the largest cell population in the CNS and in ALS patients, reactive astrogliosis is seen around the neurons (Nagy et al 1994, Schiffer & Fiano 2004). This is also seen in mice, where astrocyte activation is observed in the grey matter of the spinal cord where low activity is normally seen (Barbeito et al 2004). This astrogliosis is seen as early as 5 weeks of age in the spinal cord (Wong et al 1995). Data from mouse studies also suggest that astrocytes are essential for ALS pathogenesis as expression of mutant Sod1 in only astrocytes or neurons did not lead to disease (Gong et al 2000, Pramatarova et al 2001). These data,

alongside our findings, suggest that ALS is not caused by astrocytes but that mutant Sod1 toxicity leads to activation of astrocytes, which in turn accelerates the degeneration of the neurons. The G93Ros10 model infers that astrocytes are not stressed directly by the Sod1 toxicity as the astrocytes are not directly expressing the DsRed fluorescence but are most likely in an activated state due to stress in neighbouring cell types. A future experiment would be to stain these cells with GFAP markers and examine whether astrocytes were in an activated state when surrounding the stressed DsRed expressing motor neurons. Another avenue of research is into therapeutics that target the astrocytes in ALS. Compounds that protect the motor neurons and reduce the astrogliosis have the potential to prevent the neuronal degeneration and thus therapeutics targeting astrocytes are an interesting avenue of research.

Based upon the findings from imaging of the stress response, the morphology of the stressed cells appeared to be neurons and this was further supported by the lack of a stress response in the supporting cells. As the stressed neurons were not mature motor neurons, further investigation was needed of other cell types to identify the stressed cells. To elucidate the cell types affected, staining was done for interneurons which have been implicated in ALS. The glycine positive inhibitory interneurons were found to be highly expressing the DsRed fluorescence suggesting that interneurons are primarily affected long before the motor neurons and that loss of interneuron function may lead to the later problems in motor neurons. Normal interneurons function in a regulatory role throughout the brain and CNS and interneurons are strongly involved in the spinal reflex arc. Evidence from ALS models has supported our findings that interneurons may be a particularly sensitive neuronal population to Sod1 toxicity. In histological studies, cortical and spinal interneuron numbers were found to be drastically reduced, with increased loss as the disease progressed (Nihei et al 1993, Stephens et al 2001). Neurophysiological studies using transcrainal magnetic stimulation showed sporadic ALS patients had higher cortical excitability compared to healthy controls (Yokota et al 1996). This has also been shown in spinal interneurons in the mouse which identified defects in the interneuron control of the motor neurons, particularly from the glycine interneurons and Renshaw

cells (Chang & Martin 2011, Jiang et al 2009, Mazzocchio & Rossi 2010). Interneurons are a cell population with a pivotal role in the CNS and thus normal function is essential for survival. The interneuron susceptibility to neuronal stress has been identified as a possible early causative factor for disease progression in ALS. This highlights the possible therapeutic target of providing drugs earlier to patients so that these cell populations are exposed to the drug earlier to try and slow disease progression and protect these vital cell types. This also provides evidence as to why Riluzole has such a modest effect in patients and that possibly the damage is already done by the time clinical symptoms present, meaning that Riluzole can only have a small role in delaying the disease. A future experiment would be to treat zebrafish and/or mice with Riluzole from very early stages to see if the effects over a long period might give a better survival. Further work must look into elucidating some of the model weaknesses to ensure all the effects seen are a real disease progression that can be mapped using the DsRed readout. As with all models there are strengths and weaknesses that are limitations to the data they produce. One such limitation in zebrafish is the regenerative capacity which may mask any neuronal loss making it difficult to model a disease of degeneration. Further work into understanding how much regenerative capacity the zebrafish CNS possesses at different stages and which areas are more affected will help to give further support and strength to this model system. Further understanding of the exact cell types involved and the brain structures in a zebrafish compared to a human will also help to strengthen this model as a useful tool for modelling human disease.

The DsRed response in the G93Ros10 model produces a readout of neuronal stress based upon the DsRed fluorescence. As this stress response was a direct response of toxicity cause by the presence of mutant Sod1, a hypothesis was formed in which compounds could be screened in the model and drug effect quantified as a significant change in DsRed fluorescence. Reduction in DsRed fluorescence was highlighted as a positive screen readout as this may implicate reduced hsp70 activation suggesting that cells are being protected by the compounds with reduced activation of the heat shock response. Conversely, an increase in fluorescence may also be a positive screen readout as the heat shock response is designed to protect

cells and thus a large increase could be neuroprotective. The first compound screened in the model as a validation of the screen was Riluzole, the only approved treatment for ALS in patients. A dose response experiment was performed in G93Ros10 zebrafish embryos from 24h-5dpf. The zebrafish were chronically treated with the drug throughout the screen, before overall fluorescence was measured. Riluzole showed a positive reduction in fluorescence in a dose dependant manner. These data showed that using this readout of DsRed fluorescence a positive reduction in fluorescence could be seen using a known neuroprotective compound and thus this model had the potential for use in therapeutic identification and optimisation with Riluzole being employed as a positive control in further screening. The positive effect of Riluzole also adds further support that the zebrafish model is truly modelling the human disease, as treatments that are effective in humans show a positive role in the zebrafish.

To provide further validation of the potential to test therapeutics using the mutant Sod1 model, known neuroprotective compounds were screened in the model to show a reduction in hsp70 activation. Apomorphine was selected as it is a known neuro-therapeutic that has been historically used in the treatment of Parkinson's disease and is a potent dopamine agonist (Millan et al 2002). Apomorphine has also been recently highlighted as an activator of the NRF2-ARE pathway with a potential therapeutic role in ALS via reduction of oxidative stress as NRF2-ARE activation leads to expression of antioxidant enzymes (Mead et al 2013). Epigallocatechin gallate (EGCG) was selected as a validation for the screen as it is a known antioxidant compound which is found in green tea. EGCG has also been highlighted as a potential treatment for multiple cancers as well as a neuroprotective compound in SMA, Alzheimer's and Parkinson's diseases due to its ability to reduce ion accumulation, implicating a possible role in preventing aggregation (Wang et al 2012). EGCG and Apomorphine both showed a neuroprotective effect compared to the DMSO control, although this was not as strong as the effect of Riluzole. This is supporting evidence for the ability of this screen to show drug effect using the zebrafish hsp70-DsRed readout. Apomorphine that had recently been shown to have an effect in ALS via the NRF2-ARE pathway was shown to be effective in reducing the neuronal

stress. Also Epigallocatechin gallate, a known antioxidant compound, which is a pathway heavily implicated in ALS pathogenesis, showed effects in the model suggesting that compounds mediating different pathways can all be detected in the assay. As a further validation for the screen, the *S* and *R* enantiomers of Apomorphine were screened in the model to explore the sensitivity of the model and show if the assay has the ability to pick up the difference in effect between enantiomers of the same compound. Both the *S* and *R* enantiomers of Apomorphine showed reduction in fluorescence with the *S* enantiomer reaching a reduction of 20% whereas the *R* enantiomer had a reduction over 40%. Apomorphine *R* is a CNS penetrant, non-selective dopamine D_1/D_2 agonist with a more potent effect on D_2 receptors (Millan et al 2002). It was originally highlighted for use as an emetic and is administered as a treatment for Parkinson's disease during off episodes (Quinn 1995). Apomorphine *S,* unlike the *R* enantiomer, is not a dopamine agonist and does not activate the dopamine receptors at 25 times the concentration required by Apomorphine *R* (Saari & King 1973). Both the *S* and *R* enantiomers have a known antioxidant activity and both have been shown to directly scavenge reactive oxygen species (Gassen et al 1996). This suggests that the reduction in DsRed fluorescence that is seen is due to the antioxidant capabilities of these compounds as both have an effect. It appears that in this assay, the dopaminergic agonist activity may also be beneficial to the fish as we see a stronger reduction with the Apomorphine *R*. This highlights the need to further understand and characterise the potential role of dopaminergic neurons and how they input and regulate motor neurons.

In conclusion, we have begun the elucidation of the pathway of neurodegeneration in the G93Ros10 zebrafish. We have identified the early stress response of glycine inhibitory interneurons at the embryonic stages which appear to propagate and lead to degeneration of motor neurons at the adult stages. The next steps in this project are to further understand the cellular processes involved and to generate a complete timeline of the stress response from embryonic stages to adulthood. It is also key to understand how the stress response appears to transfer from one cellular subtype to another. One possible hypothesis is to look at the prion like process of Sod1

toxicity and aggregation. Sod1 aggregation is commonly seen in mutants and both native and mutant Sod1 easily form aggregates that are resistant to proteloytic degradation (Grad et al 2011, Hasegawa et al 2011).There is a potential for neuron to neuron propagation where mutant Sod1 is secreted by affected motor neurons and taken up by normal motor neurons (Urushitani et al 2006). In G93A SOD1 mice immunised with antibodies specific for misfolded SOD1 the mice had lower levels of mutant SOD1 in the spinal cord and showed a modest extension in lifespan (Urushitani et al 2007). Glia cells have also shown an ability to propagate a toxic effect to the neurons. Human mutant SOD1 expressing astrocytes were inserted into mice and death of wild type motor neurons was seen (Papadeas et al 2011). Also siRNA knockdown of SOD1 in astrocytes significantly reduced the stress of adjacent motor neurons (Haidet-Phillips et al 2011). Based upon clinical investigation of propagation and data from models it is possible to make the conclusion that ALS progression has a prion like process. This has big implications on the future of therapeutic targets for disease attenuation. The ability to show drug effect as a change in the basal DsRed fluorescence has also been shown using the G93Ros10 model. This has highlighted the possibility of scaling up this assay to screen a drug library. The next chapter is focused on the improvement of this low throughput assay to design and validate a high-throughput screen utilising the G93Ros10 model and to screen a compound library for potential hit compounds.

Chapter 4: Screen optimization and high throughput development

4.1 Library selection

One of the first considerations when designing a high-throughput screen is to ensure the user selecting the correct library for generating the data they desire. Selecting the correct library is imperative in ensuring the most informative data output is obtained from the screen. There are many commercially available libraries which provide different types of information such as pathways & enzymes involved as well libraries of known chemical structures and subtypes that identify compounds that are efficacious in an assay. Choosing the correct library for the purpose of the screen can lead to the identification of new disease mechanisms and pathways or the identification of potential new therapeutic areas. To this end the Spectrum library (Microsource Inc) was chosen for this assay, as it provides us with the ability to identify possible future therapeutics and pathways involved in the disease, with the added advantage that the library consists of mainly of small drug-like molecules which are predicted to be blood brain barrier (BBB) penetrant.

The Spectrum library is made up of:

US Drug Collection: 1040 drugs that have reached clinical trial stages in the USA. A small percentage of these compounds are on patent for the treatment of various diseases in the US. The majority of the drugs in this section are synthetic or semi-synthetic, with pharmacological and toxicological profiles available.

The **International Drug Collection**: 240 drugs that are marketed in Europe and/or Asia but have not been introduced in the US. The majority of the drugs in this section are synthetic or semi-synthetic, with pharmacological and toxicological profiles available.

The **Natural Products Collection:** 800 compounds, which are a unique collection of pure natural products and their derivatives. These compounds generally have unknown biological activity.

As is shown in the components of the Spectrum library there is a diverse collection of compounds from multiple sources to improve the ability to identify a larger range of compounds showing effect. Another advantage of choosing the Spectrum library is that it is optimized for medical research, as many of the drugs are FDA approved, having been shown to be safe and efficient for human treatment which means any future clinical trials would be rapidly accelerated. Also drugs that achieved FDA-approved status have literature available on potential pathways and mechanisms involved in animal and human models facilitating the understanding of drug effects. The FDA approved drugs within the Spectrum library have shown efficacy in different diseases and therefore human toxicity, safety and dosage data are already available. The Spectrum library is dissolved within DMSO at 5mM concentration and stored in deep well plates within the multipod system (Roylan Dev) under positive pressure in an environment of high nitrogen and low oxygen, to prevent oxidation and hydrolysis of compounds in the plates until use. The system uses positive pressure to drive out moisture which prevents hydrolysis of the drugs and the drugs are kept in the dark to prevent UV damage to any light sensitive compounds within the library. The Echo liquid handling system (Labcyte) was used to dispense compounds from the Spectrum library into destination plates containing 20µl of E3 media. The Echo 550 liquid handling system is a pharmaceutical grade, state of the art, tipless liquid handling system that transfer drugs using acoustic energy to dispense droplets of drug in 2.5nl volumes. Once the compounds have been transferred, the plates are backfilled with 130µl of E3 so a final volume of 150µl was attained. Zebrafish are then added to the plates in 50µl to obtain a final plate volume of 200µl per well and a final drug concentration of 10µM. 400nl of 5mM library compound in 200µl of E3 leads to a final DMSO concentration in the well of 0.2% for the Spectrum library compounds and controls. This concentration of DMSO is well within the safe limits of tolerance for zebrafish with studies showing an LD_0 (maximal concentration with no effect on embryo survival) of 1.25% DMSO in embryos dosed from the 4 cell stage (1hpf) to 4hpf (Lahnsteiner 2008).

4.2 High-throughput screen readout

Optimization of the readout was performed to maximize sensitivity, so that drug effect was detectable even if the effect size was relatively small, to gain the maximum data from each experiment and which could potentially allow the recovery of the fish to raise to adulthood. In the original screen, embryos were grouped prior to sonication and fluorescence analysis. This was a relatively crude method which required large numbers of embryos for each drug and excluded the possibility of rescuing the fish after the screen. In order to optimize the methods, we tested three potential screen readouts for use on individual embryos. These were:

- The Omega plate reader system which had the limitation of culling the fish as sonication is required.
- The Pherastar plate reader system which can carry out 30x30 well scanning for fluorescence, thus keeping the fish alive.
- The InCell system which captures fluorescent images of the fish for use with analysis software to segment the key structures and look at fluorescence in the spinal cord and hindbrain.

Pherastar

The Pherastar system (Pherastar Plus, BMG Labtech) is a high-throughput microplate reader with the ability to measure fluorescent intensity, polarization, and FRET. The aim of selecting the Pherastar was to measure the fluorescence of the zebrafish using a 30x30 well scanning mode and be able to quantify the fluorescence along the spinal cord. This had the advantage of being able to keep the zebrafish alive after the assay for raising, further treatments and behavioral analysis. The Pherastar is a far more sensitive readout than the sonication assay, but certain limitations reduced its applicability in a high-throughput screen. Firstly the Pherastar system uses a 30x30 well scanning system which is ideal for square wells such as 384 well plates. In a circular 96 well plate the Pherastar misses the

edges of wells so any fish which does not lie central in the well may be missed or risks being inaccurately calculated. Another limitation when using the Pherastar system is the speed of the assays. To perform a 30x30 points per well scan in 384 well plates takes a relatively long period of time, which severely limited the numbers of plates which could be analyzed per day, slowing down the screening process and limiting the throughput. Another problem when using the Pherastar system for this analysis is common across all platforms of readout when using live animals. If the animal moves during the assay, the data for that well is completely lost. We found that even under anesthesia with Tricaine, any small involuntary movement in the zebrafish or incorrect orientation completely invalidated the data from that well. Fig 4.5 shows that it is possible to see the difference between Riluzole treated and DMSO treated G93Ros10 zebrafish, but even with 30x30 point scanning the clarity is not high enough to distinguish changes in distinct anatomical features. Based upon these four key areas of concern, we opted not to use the Pherastar system for our analysis in the primary screen as there was a risk of losing wells to mis-placed or moving fish, meaning more repeats and the time constraints on using the system, thus reducing the throughput of the assay.

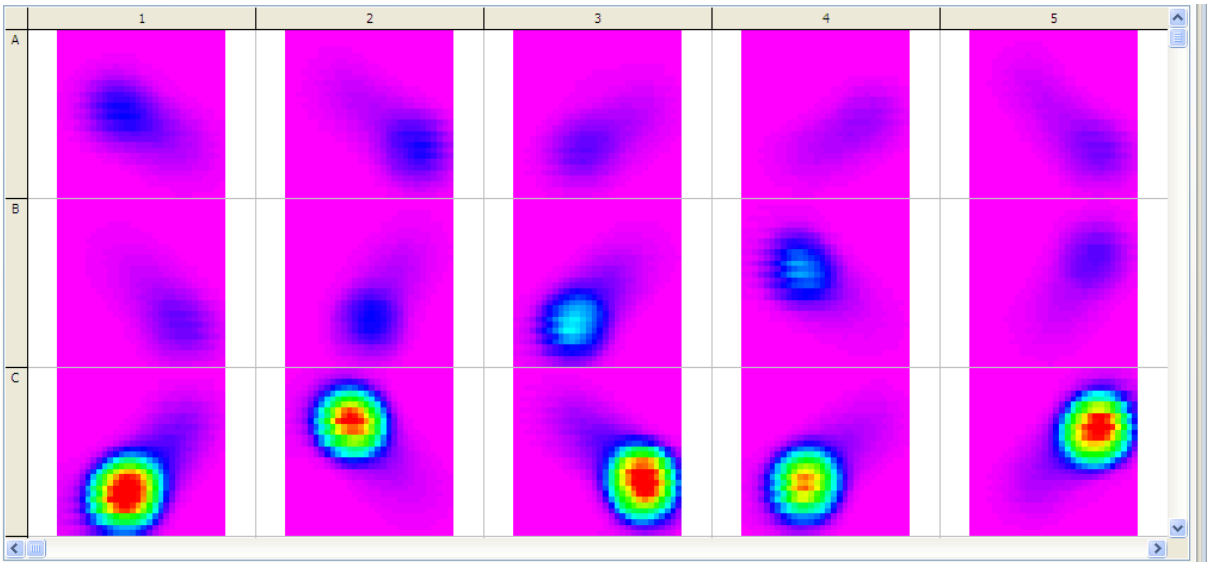

Fig 4.1: Pherastar readout of G93Ros10xAb zebrafish dosed with Riluzole at 10µM (A +B), and DMSO (C) scanned in a 30x30 point well scan for DsRed fluorescence.

InCell analyzer 2000

The InCell analyzer 2000 is an automated, modular lamp based microscope that can rapidly image plates in multiple wavelengths. By taking fluorescent images of the zebrafish it was postulated that quantification of the reduction in fluorescence would be detectable by analyzing the images. GE healthcare provides a plug-in which links the InCell microscope system to a computer program which automatically segregates the zebrafish image into anatomical structures such as spinal cord, liver and brain. It was hypothesized that the use of this would allow the examination of fluorescence in the zebrafish spinal cord and brain in live embryos whilst keeping the embryos alive for further experiments or tissue collection. The InCell system is already utilized at the end stage of the assay to ensure the embryos are morphologically well (Brightfield image) and are expressing the DsRed protein (DsRed image) and it was hypothesized that the system could be used to measure changes in fluorescence within the spinal cord and hindbrain of the zebrafish. Unfortunately this plug in was designed for zebrafish at day 4 and our screen finishes at day 6 so the results were variable and segregation was not always correct when confirmed by eye (Fig 4.2). This meant at 6dpf the software was not accurately segmenting the fish and therefore was not suitable for use in high-throughput analysis. Another major problem encountered when using the InCell as the screen readout was that the zebrafish is not always positioned in the correct orientation for imaging of the spinal cord and if the fish moves during the imaging or rests at an angle, then imaging becomes impossible and the data from the well is lost (Fig 4.3). If imaging is not possible then the analysis cannot be performed and the data from the well would be lost leading to missed data points and requirement for repetition.

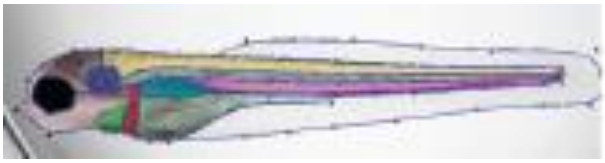

Fig 4.2: Image showing the body segregation software plugin supplied by GE Healthcare for use with the INCELL imaging system. This image is taken using the 2X lens on a MS222 treated 4dpf AB zebrafish. Image taken from the promotional material supplied with the InCell 2000 system.

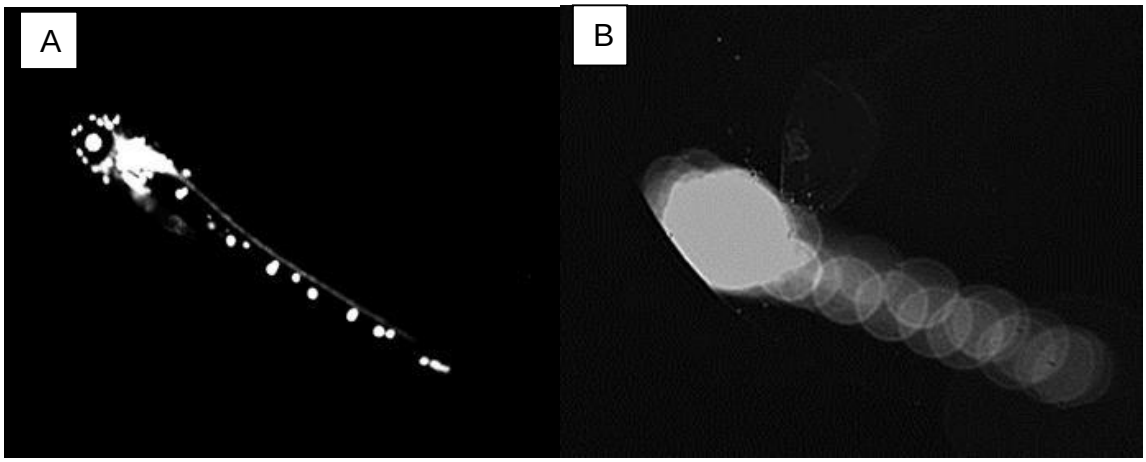

Fig 4.3: Images of G93Ros10 zebrafish taken at 6dpf on the Incell microscope using a 2x lens measuring for DsRed fluorescence. Image A shows a zebrafish in the correct orientation to allow quantification of fluorescence in the spinal cord and hindbrain. Image B is a zebrafish that is out of focus due to movement or proximity to the edge of the well.

FLUOstar Omega

The FLUOstar Omega (BMG Labtech) microplate reader is a high-throughput multi-mode plate reader with the capability to measure absorbance and fluorescence intensity. This system does not have the sensitivity of the Pherastar system, so keeping the zebrafish alive for the assay was not possible. This required the use of the original screen format of sonication and centrifugation before measuring the supernatant on the FLUOstar Omega plate reader. In the original screen, three embryos per dose were sonicated in 100µl and overall fluorescence measured. This was scaled this down to one embryo per well in 50µL to reduce the number of fish needed for

screening the library per drug. This means throughput is increased and the number of animals used for experiments is lowered which links in with the 3R's principles. 96 well V-bottom plates were evaluated for the sonication step as this allowed the easy sonication and formation a pellet when the centrifugation step was performed. We found that this method was perfectly suited to the screening, as it was possible to replicate the findings from the original screen. The downside to this screen was the inability to keep the zebrafish alive after the screen due to the need to sonicate. This updated screen showed that Riluzole caused a reduction in fluorescence of 56.4% compared to the control. This demonstrated that a 96 well plate format using the automated liquid handling to load drugs onto the plates can accurately detect drug effect in both our negative and positive controls and therefore have the ability to screen for hit compounds using this assay.

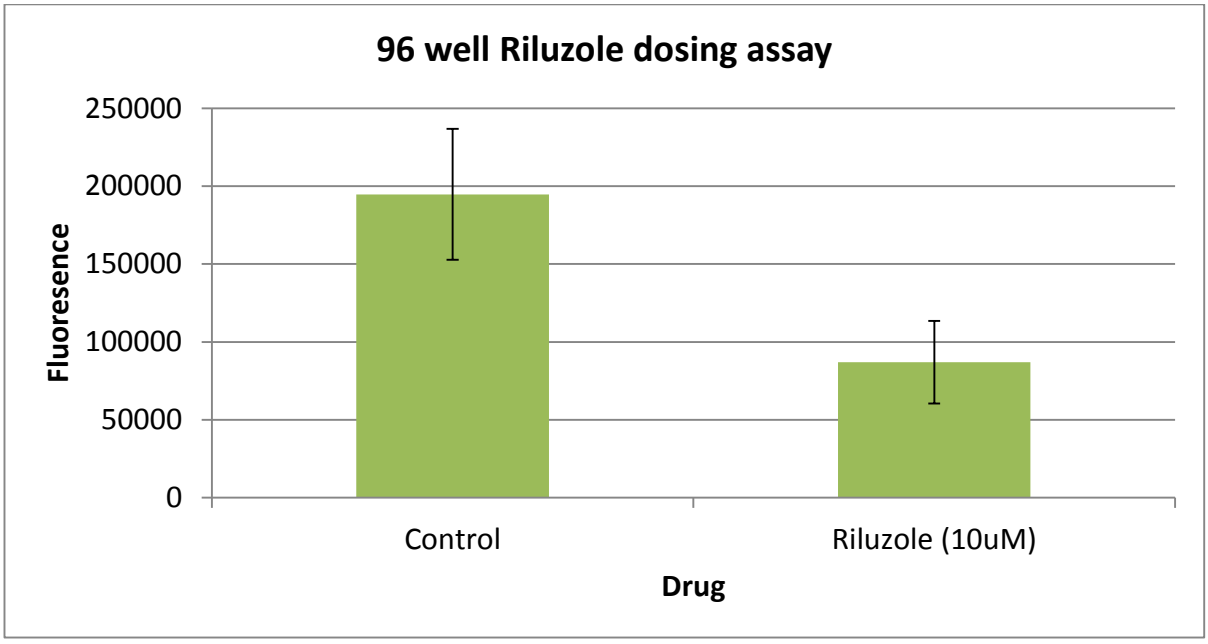

Fig 4.4: Graph of G93Ros10 zebrafish dosed in 96 well plates with DMSO control and Riluzole at 10µM. The error bars show the SD. N= 29 fish per group.

4.3 Plate selection

Selection of the optimal screening plates was a key part of scaling up the high-throughput assay, as ideally the plate should contain the maximum number of drugs possible to screen on one plate to reduce plate to plate variation together with large numbers of controls per plate to provide assay confidence. This would give strong datasets for each plate and reduce variability due to the large numbers of controls. In cell based assays 1564 and 384 well plates are regularly used for screening. The wells of 1564 well plates were too small to fit the embryos so were not taken forward for testing. Another advantage of using large numbers of wells per plate is that this reduces the volumes of drugs needed per well for the screen which reduces costs. Another key consideration was to ensure the plates were compatible with the liquid handling and automated imaging systems available.

The key criteria for plates were:

- Large numbers of wells – allows large numbers of controls per plate
- Low volumes required per well – Reduced library usage
- Compatibility – Allows improved throughput via usage of automated systems

384 well plates

Three hundred and eighty four well plates were investigated due to the attractive properties of these plates. The low volumes required per well mean that very low quantities of the libraries are used for each assay and large numbers of compounds can be screened on each plate, improving assay throughput and the cost effectiveness. Both of these properties make 384 well plates very attractive when designing a high-throughput compound screening using zebrafish. A literature survey of past screens showed that zebrafish were viable in 384 well plates although these did not cover the

timescale (4 days) used in our protocol. (Tran et al 2007). A study on the viability of embryos in 384 well plates was undertaken using microscopy to identify death and malformation in the embryos. The fish were able to survive normally in 100µl volume of E3 media from 48h-6dpf and appeared normal in morphology under the microscope. The next step was to validate the 384 well plate assay using compounds which were identified in the preliminary assays to show drug effects in the zebrafish.

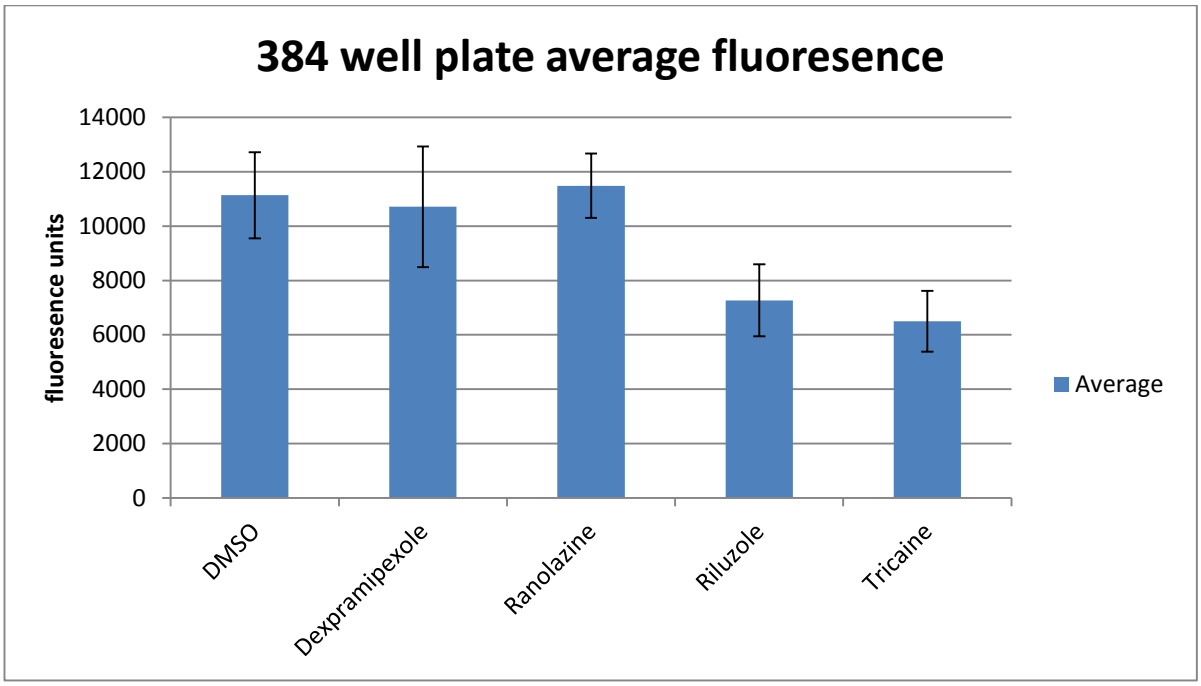

Fig 4.5: 384 well plate average fluorescence of G93Ros10 mutant zebrafish after treatment with various compounds at 10µM (except Tricaine which was dosed at 610µM). Error bars show the SD. n=12 fish per group.

These data show that in 384 well plates a reduction in fluorescence is observed in Riluzole and Tricaine treated zebrafish compared to control (DMSO only) treated zebrafish. The reduction in DsRed fluorescence by these compounds correlates with what was seen in the original validation assay. A reduction of around 40% was seen in Riluzole and Tricaine dosing using the 384 well formats. The problem is that the reduction is not as large as was seen in the original assay when dosing in Petri dishes. There are also much larger error bars, suggesting that conditions in the wells have increased variability compared to conditions where larger volumes are used

such as in petri dishes. It was therefore decided to omit 384 well plates as a viable option for high-throughput screening. Although they have the benefit of large numbers of drugs per plate and the low volumes of drugs required, the 384 well plates have the limitations of high variability and decreased sensitivity compared to the original method. This means that detecting hit compounds would be more difficult as drug effect is lowered. Using these plates to measure changes in fluorescence would be difficult to quantify and detect due to the variability also seen, leading to reduced sensitivity and specificity and bringing the validity of any hits identified in the screen down. This is shown in fig 4.6 which compares the fluorescence of the fish kept in 384 well plates with those in petri dishes meaning any drug effect would be smaller and thus harder to detect.

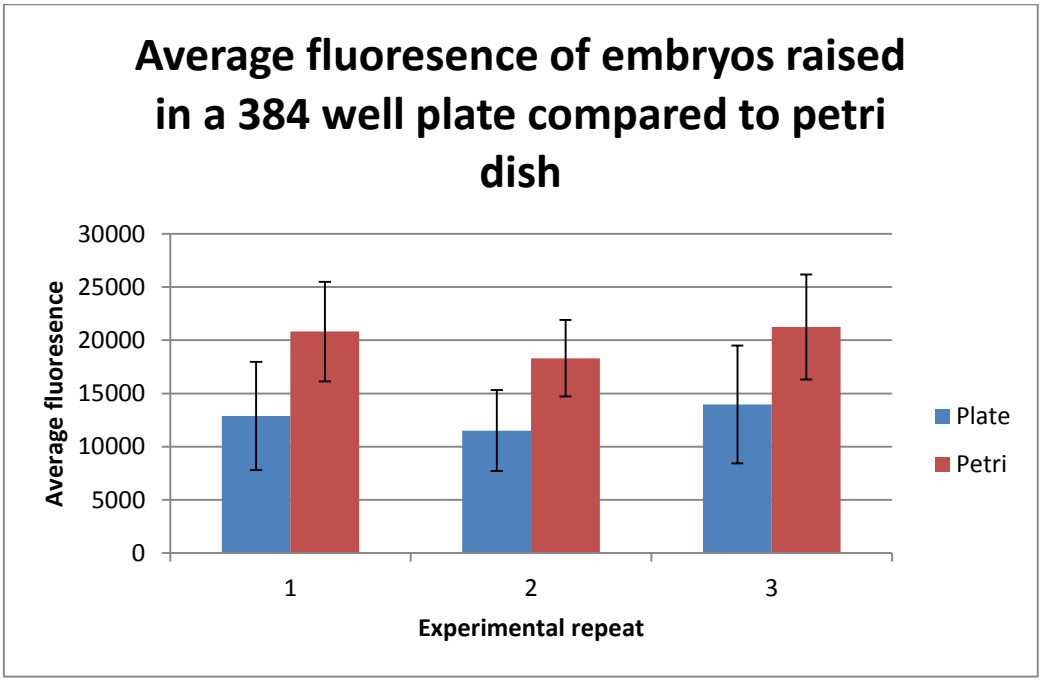

Fig 4.6: Average fluorescence of undosed G93Ros10 zebrafish kept in different conditions from 48phf to 6dpf. N = 12 per group and error bars are SD.

One hypothesis for seeing a reduced change in fluorescence and increased variability between fish is that the wells in a 384 well plate are too small for the fish. In our screen over 4 days in such a small area and volume the fish may have a buildup of toxic conditions and waste, along with reduced oxygen in the well due to a smaller surface to volume area. This may lead to increased toxic environment in the well, such as pH changes, leading to the

induction of stress in the fish which could potentially activate the heat shock response. If this is the case then any drug effect could be masked by hsp70 activation leading to an activation of fluorescence. The wells of the 384 well plates are square which also leads to problems with blurring in the corner of wells.

Twenty four well plates

Twenty four well plates were identified as a possibility to screen zebrafish due to the large well size and the ability to dose multiple fish per well giving multiple readouts per drug. The advantage of using larger volume wells is lower concentrations of toxin build up over the screen and the higher n-numbers possible in each well would give less variable results. The limitation of using 24 well plates was the large volume of drugs needed for each well (µl quantities) which uses larger quantities of the libraries, thus increasing costs and decreasing the life span of the drugs in the library. 24 well plates are also not suitable for use on the robotic handling systems or the echo 550 liquid handling system, thus increasing the potential for human error. When used in preliminary screening, 24 well plates showed drug effect and were suitable for screening but due to the high cost implications, 24 well plates were not used for the screen as it did not fit into the high-throughput screening profile due to their limited compatibility with the hardware available. In the end we chose not to use 24 well plates for screening as they do not fit the properties required for a high-throughput drug screen.

96 well plates

As a compromise between the 24 and the 384 well plates, the use of a 96 well plate format was investigated as this had the potential to provide the consistent and accurate data while being suitable for maintaining a fairly high-throughput approach to screening. The original readout of sonication was maintained as a standard in this experiment to test the applicability of 96

well plates for screening zebrafish. Using 96 well plates for zebrafish compound screens is standard practice in the zebrafish community so that survival in the wells and drug delivery would not be an issue. 96 well plates have the advantage of having enough wells to test many compounds and space to allow a large number of control wells to add statistical validity to the data from every plate. They also have the advantage of relatively low volumes required in each well with 200µl being small enough to reduce unnecessary use of drugs from the library, whilst being high enough for the embryos to develop normally from 48hpf to 6dpf. Another key aspect of 96 well plates is that they are compatible with the robotics and liquid handling systems available *in house* which is a major advantage over 24 well plates due to the ability to rapidly dose, screen and analyze the data accurately when compared to a manual screen thus increasing the screen throughput.

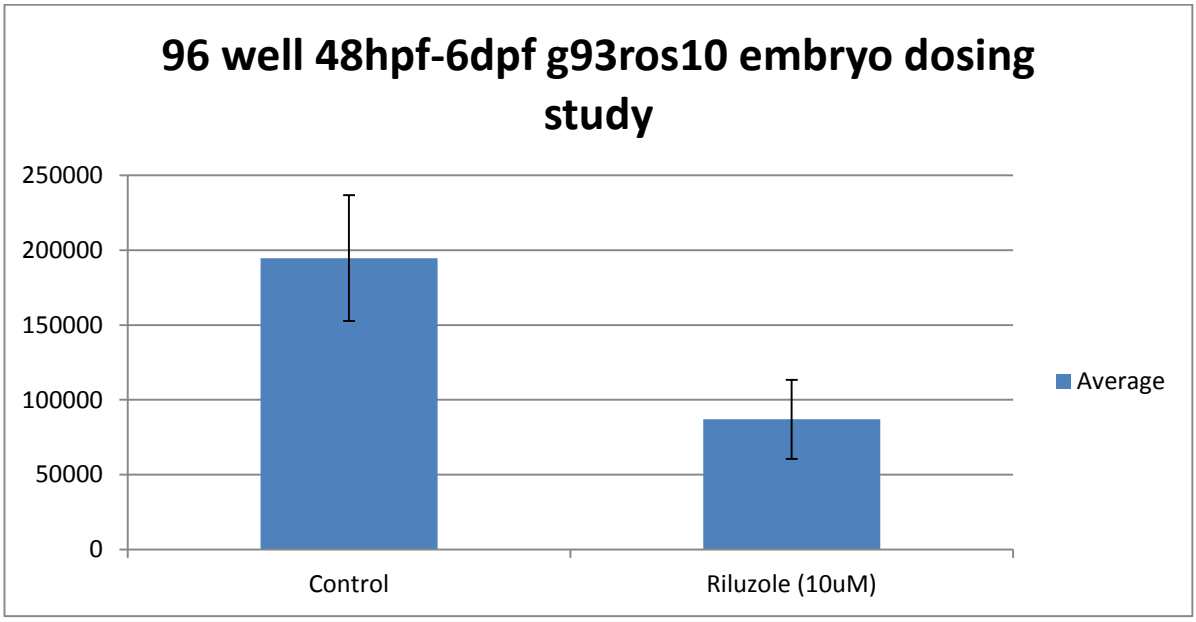

Fig 4.7: Screening of G93Ros10 Sod1 mutant zebrafish in a 96 well plate. The zebrafish were dosed with DMSO and Riluzole (10µM) from 48hpf to 6dpf. N=25 embryos per group.

These data show that 96 well plates are suited for high-throughput compound screening. The screen is able to detect a large difference between the positive and negative control as the Riluzole fluorescence is 44.66% of the total control fluorescence. The SD shows us that the variability between fish is low and smaller than the other plate types. These data show that the 96

well plates are best suited to high-throughput screening when using zebrafish. Based upon the findings from the 3 different plate types, the 96 well plates were chosen for the screen as they offered the optimal balance between cost, readout and the number of embryos to provide the best sensitivity and specificity possible for our assay, while delivering the lowest variability.

When using the 96 well plates a drying effect on the edge wells was observed which occasionally led to embryo death. This is a common effect seen in fan assisted incubators due to a constant circulation of air leading to an evaporation effect particularly to the edge wells. To reduce the drying effect size we introduced a water tray to the incubator and used lids on each plate. To further reduce the risk of losing any of the screening data, a firewall was introduced on each plate in the top and bottom rows (A & H). The rows were filled with E3 but no test compound or fish to act as a barrier. The edge columns (1 and 12) were used for positive and negative controls. The positive and negative controls were placed at both ends with one inside the plate and one outside the plate so any adverse effects from drying would be detectable. To ensure any edge effect on the wells was not having a strong effect on baseline fluorescence, multiple plates were analyzed for average fluorescence.

Plate	Edge DMSO wells average	Inside DMSO wells average	% difference
1	45077	49208	9%
2	79686	76947	3%
3	116091	100494	13%
4	38964	39751	-2%
5	9196	9029	2%

Fig 4.8: Table of 5 replicates showing the average fluorescence of DMSO treated G93Ros10xAB zebrafish based on the edge wells vs the inside wells. N=6 fish per location for each replicate.

As fig 4.8 shows the edge drying has a minimal effect on the average fluorescence of the wells with only small manageable differences between

outside and inside. Any effect this may have on the screen is reduced further due to large numbers of controls on each plate and not having any test compounds situated within edge wells, to eliminate the risk of missing compounds with a weak effect.

Throughout the screening no adverse effect from drying was observed at the edges when the firewall was used. This plate layout incorporated 12 positive controls, 12 negative controls and 48 test compounds on each plate. This has the advantage of testing a relatively large number of drugs per plate, with the strength added from having extensive data from large numbers of controls for each plate.

	1	**2**	**3**	**4**	**5**	**6**	**7**	**8**	**9**	**10**	**11**	**12**
A												
B	Riluzole	Ctrl	1	2	3	4	5	6	7	8	Riluzole	Ctrl
C	Riluzole	Ctrl	9	10	11	12	13	14	15	16	Riluzole	Ctrl
D	Riluzole	Ctrl	17	18	19	20	21	22	23	24	Riluzole	Ctrl
E	Riluzole	Ctrl	25	26	27	28	29	30	31	32	Riluzole	Ctrl
F	Riluzole	Ctrl	33	34	35	36	37	38	39	40	Riluzole	Ctrl
G	Riluzole	Ctrl	41	42	43	44	45	46	47	48	Riluzole	Ctrl
H												

Fig: 4.9: Spectrum zebrafish screen plate layout: A firewall is maintained in rows A and H. Riluzole (+ve control) is maintained in columns 1 and 11 and DMSO (-ve control) is maintained in columns 2 and 12. The numbers from 1-48 show where the test compounds sit on the plate.

4.4 Final screen layout

From the data collected from different plate types, layouts, screen lengths and assays analysed the final screen was brought together. Below is a flow chart of the screening process.

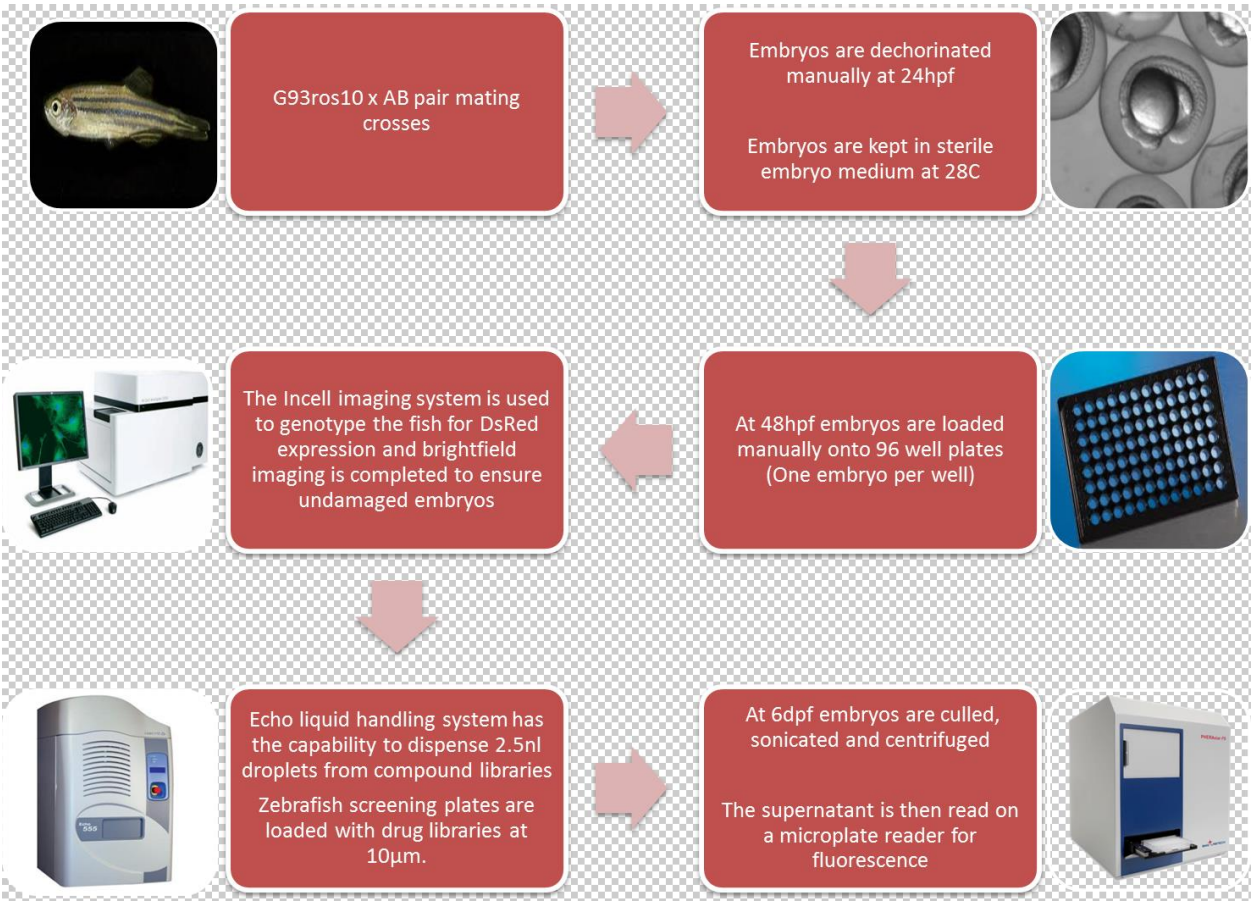

Fig 4.10: Flow chart of the final high-throughput screening protocol. The screen has optimised and utilised many of the high-throughput systems available.

The screen was performed on dechorinated 48hpf G93Ros10 zebrafish that were loaded into 96 well plates before being genotyped on the InCell system based upon DsRed transgene expression. 96 well plates were dosed using a combination of the Platemate system (E3 backfilling) and the Echo 550 system (compound loading) upto a volume of 150µl. the transgenic G93Ros10 zebrafish in 50µl were added to the plate to make the final volume of the well 200µl with a final concentration of 10µM. The zebrafish were then chronically dosed in the well at 28°C until 6dpf at which stage death and genotyping was confirmed again using the InCell system before loading into V bottom plates in 50µl. A single dose was used as this is the only viable way for high-throughput screening to maintain the throughput and to reduce the variability involved with multiple dosing. Riluzole was also shown to be stable and efficacious in the drinking water of a mouse for 1 week so it was

assumed the drug would be stable in the zebrafish media throughout the 4 day assay (Waibel et al 2004). The embryos were then sonicated before centrifugation to form a pellet and supernatant. 20µl of the supernatant was then loaded onto a 384 well plate and a raw value for the DsRed fluorescence measured on the OMEGAstar fluorescent plate reader system.

4.5 Assay statistics

Selecting the optimal statistical analysis for the assay is a key part of assay design as inappropriate statistical methods and poorly implemented statistics can lead to missed hit compounds and false positives. Many cell based high-throughput screening assays utilise a Z-score as the statistical tool for hit selection. Z-score measures the statistical effect for each compound and judges if each compound in the assay has a large enough effect to warrant further investigation. Generally it is utilised alongside the 3-sigma rule which selects hits based upon them being within 3 standard deviations of the mean (Zhang 2011). The problem of the Z-score method comes when the data are not uniformly distributed such as in a high-throughput screen utilising an in-vivo model where variability can be high from plate to plate. Due to this we implemented a statistical test called Strictly Standardised Median Difference (SSMD*). SSMD is applicable for a screen with replicates as it accounts for the inter plate variability thus is far more applicable for a screen using zebrafish with replicates. For more information on SSMD please refer to the materials and methods (Chapter 2 Section 2.16).

4.6 Screening quality control and results

With the high-throughput assay developed, 2000 compounds were screened from the Spectrum library to identify key modulators of Sod1 mediated neuronal stress. Experiments were performed in duplicate to identify double activators and inhibitors and these were taken forward for secondary screening as hits. To ensure that the screening protocol was being

implemented correctly, statistical analysis was used to ensure that specificity and sensitivity were maintained. Data sets were analysed at multiple SSMD threshold values to ensure the statistics were as strong as possible and maintain the best balance of the highest specificity and sensitivity so as to not miss hits and reduce false positives. To do this the plates were analysed based upon an SSMD score of <-0.5 and <-1.0. False positive and false negative numbers were recorded for each plate and analysed to allow the calculation of the sensitivity and specificity of each plate for quality control. False positives were calculated as the number of negative controls that show up as a hit based upon the SSMD threshold. False negatives were calculated as the number of positive controls that do not reach the hit SSMD threshold. Based upon the false positive and false negative rates, it is possible to calculate the sensitivity and specificity. Sensitivity is a measure of how many hits are detected and specificity is a measure of how accurate the assay is. Sensitivity is measured as the percentage of true positives compared to false negatives. The specificity is measured as the percentage of true negatives compared to the false positive.

Replicate 1 Quality control (SSMD cut off of <-0.5)

Plate	True positives	False negative	True negatives	False positive	Sensitivity	Specificity
1	12	0	10	2	100	83.33333333
2	11	1	12	0	91.66666667	100
3	9	2	12	0	81.81818182	100
4	12	0	11	0	100	100
5	6	0	10	1	100	90.90909091
6	4	1	10	1	80	90.90909091
7	5	0	7	4	100	63.63636364
8	10	0	12	0	100	100
9	8	0	11	1	100	91.66666667
10	6	0	9	0	100	100
11	6	0	8	3	100	72.72727273
12	10	0	8	3	100	72.72727273
13	10	2	10	2	83.33333333	83.33333333
14	11	0	9	3	100	75
15	11	0	8	0	100	100
16	12	0	11	0	100	100
17	9	2	6	5	81.81818182	54.54545455
18	5	0	8	2	100	80
19	6	0	8	3	100	72.72727273
20	5	1	9	1	83.33333333	90
21	12	0	9	3	100	75
22	12	0	12	0	100	100

23	12	0	10	1	100	90.90909091
24	12	0	9	3	100	75
25	12	0	11	0	100	100
26	11	0	10	0	100	100
27	9	2	10	2	81.81818182	83.33333333
28	8	4	9	2	66.66666667	81.81818182
29	12	0	11	1	100	91.66666667
30	8	4	10	1	66.66666667	90.90909091
31	11	0	9	2	100	81.81818182
32	12	0	9	3	100	75
33	12	0	9	1	100	90
34	12	0	10	1	100	90.90909091
35	12	0	10	2	100	83.33333333
36	11	0	10	2	100	83.33333333
37	11	0	6	5	100	54.54545455
38	11	0	6	5	100	54.54545455
39	9	3	11	1	75	91.66666667
40	12	0	11	1	100	91.66666667
Average	9.725	0.55	9.525	1.675	94.8030303	85.17424242
SD	2.541829545	1.108244165	1.601081365	1.4743534	9.849662233	13.20546647
SEM	0.417874203	0.182194218	0.263216155	0.242382206	1.619274496	2.170965314

Table 4.1: Table showing the quality control data for all 40 plates in the first replicate based upon an SSMD score of <-0.5 being a hit. The table shows the true positive and negative rates as well as the incidence rate of false positive and negatives to give a sensitivity and specificity percentage.

Table 4.1 shows that with a hit threshold of <-0.5 on the SSMD scale, false negatives very rarely show up in the screen, ensuring a sensitivity of 94.8%. This is an excellent score in an *in vivo* primary screen and suggests that the assay is missing very few hit compounds. The use of this low threshold allows for the possibility of only missing a small percentage of hit compounds showing up as false negatives. This is due to the variability of using an *in vivo* model and the weak effect of certain compounds being under the detection threshold. The specificity of the screen at <-0.5 was 85.2% for the first replicate. Although this manifests as a problem due to the risk of false positives within the assay, upon replication of these assays false positive and negatives will be detected and removed from the hit list. To attempt to increase our specificity we analysed the same data set based upon the SSMD hit threshold being <-1

Replicate 1 Quality control (SSMD cut off of <-1.0)

Plate	True positives	False negative	True negatives	False positive	Sensitivity	Specificity
1	9	3	12	0	75	100
2	5	7	12	0	41.6666667	100
3	6	5	12	0	54.5454545	100
4	12	0	11	0	100	100
5	6	0	11	0	100	100
6	4	1	11	0	80	100
7	3	2	8	3	60	72.7272727
8	10	0	12	0	100	100
9	8	0	11	1	100	91.6666667
10	6	0	9	0	100	100
11	6	0	11	0	100	100
12	8	2	11	0	80	100
13	5	7	11	1	41.6666667	91.6666667
14	10	1	12	0	90.9090909	100
15	110	0	8	0	100	100
16	12	0	11	1	100	91.6666667
17	0	11	11	0	0	100
18	5	0	10	0	100	100
19	5	1	10	0	83.3333333	100
20	5	1	10	1	83.3333333	90.9090909
21	3	9	12	0	25	100
22	10	2	12	0	83.3333333	100

23	12	0	11	0	100	100
24	12	0	12	0	100	100
25	12	0	11	0	100	100
26	10	1	11	0	90.9090909	100
27	8	3	12	0	72.7272727	100
28	6	6	9	2	50	81.8181818
29	12	0	11	1	100	91.6666667
30	6	6	10	1	50	90.9090909
31	0	11	11	0	0	100
32	12	0	11	1	100	91.6666667
33	12	0	10	0	100	100
34	12	0	11	0	100	100
35	12	0	10	2	100	83.3333333
36	11	0	12	0	100	100
37	11	0	10	1	100	90.9090909
38	6	5	12	0	54.5454545	100
39	7	5	11	1	58.3333333	91.6666667
40	12	0	12	0	100	100
Average	10.525	2.225	10.875	0.4	79.3825758	96.5151515
SD	16.72199	3.244012	1.064708	0.715171997	28.3897764	6.32150918
SEM	2.749078	0.533312	0.175037	0.117573552	4.66725049	1.03924971

Table 4.2: Table showing the quality control data for all 40 plates in the first replicate based upon an SSMD score of <-1.0 being a hit. The table shows the true positive and negative rates as well as the incidence rate of false positive and negatives to give a sensitivity and specificity percentage.

Table 4.2 shows that if the hit ratio is shifted to a lower SSMD threshold of <-1.0 then this causes a change in the measured sensitivity and specificity of the assay. At <-1.0 a larger number of false negatives were detected, which leads to a reduced sensitivity at 79.4%. This may miss some of the weaker hits as they are not eliciting a strong enough effect to be detected by this assay. The advantage of analysing the data with the threshold at <-1.0 is that the false positive rate is low in every plate. This means that the specificity of the assay is maintained in the first replicate at 96.5%, so very few false hits are detected.

Replicate 2 Quality control (SSMD cut off of <-0.5)

Plate	True positives	False negative	True negatives	False positive	Sensitivity	Specificity
1	5	0	7	1	100	87.5
2	10	0	11	1	100	91.66666667
3	12	0	12	0	100	100
4	8	0	11	1	100	91.66666667
5	9	0	7	0	100	100
6	11	1	12	0	91.66666667	100
7	11	0	12	0	100	100
8	6	6	11	1	50	91.66666667
9	12	0	11	1	100	91.66666667
10	12	0	12	0	100	100
11	12	0	11	0	100	100
12	11	0	11	1	100	91.66666667
13	12	0	11	0	100	100
14	12	0	10	0	100	100
15	12	0	12	0	100	100
16	12	0	9	2	100	81.81818182
17	11	0	12	0	100	100
18	12	0	8	1	100	88.88888889
19	11	1	6	3	91.66666667	66.66666667
20	12	0	12	0	100	100
21	11	1	12	0	91.66666667	100
22	11	0	12	0	100	100

23	10	2	12	0	83.33333333	100
24	12	0	10	1	100	90.90909091
25	12	0	12	0	100	100
26	10	2	12	0	83.33333333	100
27	12	0	12	0	100	100
28	12	0	10	1	100	90.90909091
29	11	0	12	0	100	100
30	10	1	10	2	90.90909091	83.33333333
31	12	0	11	1	100	91.66666667
32	10	1	8	3	90.90909091	72.72727273
33	12	0	10	2	100	83.33333333
34	12	0	9	3	100	75
35	12	0	10	1	100	90.90909091
36	12	0	9	3	100	75
37	12	0	11	0	100	100
38	11	0	11	1	100	91.66666667
39	12	0	11	0	100	100
40	11	1	12	0	91.66666667	100
Average	11	0.4	10.6	0.75	96.62878788	93.2165404
SD	1.601281538	1.057330941	1.614040955	0.980580676	8.834692314	9.007383942
SEM	0.263249063	0.173824136	0.265346699	0.16120647	1.45241447	1.480804798

Table 4.3: Table showing the quality control data for all 40 plates in the second replicate based upon an SSMD score of <-0.5 being a hit. The table shows the true positive and negative rates as well as the incidence rate of false positive and negatives to give a sensitivity and specificity percentage.

Table 4.3 shows the quality control data for each plate from the second replicate of the screen based upon the SSMD hit threshold being <-0.5. At this threshold it was found that the sensitivity and specificity were maintained at a high level for both assays. The false negative rate for each plate on average was 0.4 fish on average per plate meaning that very few hits were missed and the sensitivity was maintained at 96.6%. The false positive rate on average over the 40 plates was 0.75 fish per plate which means that very few negatives were showing as positives which is reflected in the specificity being maintained at 93.2%.

Replicate 2 Quality control (SSMD cut off of <-1.0)

Plate	True positives	False negative	True negatives	False positive	Sensitivity	Specificity
1	5	0	8	0	100	100
2	7	3	12	0	70	100
3	12	0	12	0	100	100
4	8	0	12	0	100	100
5	9	0	7	0	100	100
6	11	1	12	0	91.6666667	100
7	11	0	12	0	100	100
8	6	6	12	0	50	100
9	12	0	12	0	100	100
10	12	0	12	0	100	100
11	12	0	11	0	100	100
12	11	0	12	0	100	100
13	12	0	11	0	100	100
14	10	2	10	0	83.3333333	100
15	12	0	12	0	100	100
16	12	0	10	1	100	90.9090909
17	11	0	12	0	100	100
18	4	8	8	1	33.3333333	88.8888889
19	11	1	8	1	91.6666667	88.8888889
20	0	12	12	0	0	100
21	11	1	12	0	91.6666667	100
22	0	11	12	0	0	100

23	0	12	12	0	0	100
24	12	0	11	0	100	100
25	6	6	12	0	50	100
26	2	10	12	0	16.6666667	100
27	11	1	12	0	91.6666667	100
28	12	0	11	0	100	100
29	9	2	12	0	81.8181818	100
30	8	3	12	0	72.7272727	100
31	12	0	12	0	100	100
32	5	6	11	0	45.4545455	100
33	12	0	11	1	100	91.6666667
34	12	0	12	0	100	100
35	12	0	11	0	100	100
36	12	0	9	3	100	75
37	12	0	11	0	100	100
38	11	0	12	0	100	100
39	12	0	11	0	100	100
40	9	3	12	0	75	100
Average	9.2	2.2	11.175	0.175	81.125	98.3838384
SD	3.79875	3.719591	1.367642	0.555915313	31.7183031	4.911974
SEM	0.624511	0.611497	0.224839	0.091391915	5.21445692	0.80752355

Table 4.4: Table showing the quality control data for all 40 plates in the second replicate based upon an SSMD score of <-1.0 being a hit. The table shows the true positive and negative rates as well as the incidence rate of false positive and negatives to give a sensitivity and specificity percentage.

Table 4.4 shows the quality control data from all 40 plates from the second replicate based upon the SSMD being <-1.0. It shows that the false negative rate per plate was 2.2 fish which led to an average sensitivity of 81.1%, which suggests the weaker hits would be missed using this threshold. The false positive rate of only 0.175 fish per plate leads to an average specificity of 98.4% suggesting that very few negatives falsely get through the assay.

From this it can be confirmed that the specificity and the sensitivity was highly maintained at both <-0.5 and <-1.0 SSMD. By setting the hit threshold at <-0.5 it introduces a reduction in the specificity due to the low threshold and therefore the risk that some false positives may occur with percentages of 85% and 93% in the replicates. The advantage of having the screen at <-0.5 is the improved sensitivity which at over 94% and 96% in the replicates ensures that very few hits are missed and the hits from the screen analysed at <-0.5 are true hits. When analysed with a threshold of <-1.0, an increased specificity due to the high stringency associated with the higher threshold was observed. This is advantageous to the screen as false hits are not occurring with the specificity maintained at 98% and 95% across the replicates. The downside to having the hit threshold at <-1.0 is the reduction in sensitivity to 79% and 81% across the replicates. This means that weaker hits are being missed, which reduces the accuracy of the screen.

When the duplicates of the screen to detect the number of hits were calculated we looked at multiple SSMD scores to ensure that all hit compounds were being investigated. When the SSMD threshold was set at -0.5 for the β Value, 1.9% of compounds showed as a hit both times. When the SSMD threshold was set at -1.0 only 0.35% showed as double hits, but this was due to the higher stringency requited to be classed as a hits. Both of these show the specificity of the assay and demonstrate that

SSMD as a statistical tool has sorted the compounds into a manageable number to be taken forward for secondary screening.

SSMD Threshold	Number of replicated hits	Number screened	Percentage hits
Below -0.5	38	2000	1.9%
Below -1.0	7	2000	0.35%

Table 4.5: Collated assay statistics for compounds showing fluorescence inhibition in duplicate.

Analysis was also performed on strong activators of fluorescence which had an SSMD threshold of over 1.0. 20 compounds were found to induce a large increase in DsRed fluorescence after a 4 day exposure. The compounds that caused death in both repeats of the screen were also investigated to determine how much of the library had a toxic effect, at 10µM. 142 compounds from the spectrum library were identified as toxic in the replicates and this equates to 7.1% of the library.

SSMD Threshold	Number of replicated hits	Number Screened	Percentage hits
Above 1.0	20	2000	1%
Caused death	142	2000	7.1%

Table 4.6: Collated assay statistics for compounds showing fluorescence activation and compounds causing embryo death.

4.7 Discussion

Optimisation of preliminary assays to high-throughput assays is a well-documented and highly debated area of research. The primary aims of optimisation and scaling up of an assay is to achieve the highest possible return of data in a short time frame, while maintaining low costs and a high quality of data. High-throughput screening is a form of screening that utilises robotics and liquid handling systems to greatly improve the speed

and accuracy of screening via automation and the reduction of human intervention. Zebrafish compound screening has been performed for many years, but speed of assays and readout has always been a major bottleneck in improving the throughput of assays. One of the first considerations in developing the screen was to select a compound library that provided information on classes of compounds and therapeutic targets in Sod1 mutants while also highlighting possible future therapeutics. The Spectrum library from Microsource Inc was selected as it fits both of the criteria. The library contains FDA approved compounds so the toxicity information is known and therefore future potential therapeutic compounds can be identified. As these drugs have reached a stage of FDA approval, there is generally literature available that suggest mechanisms of action and pathways involved which further improves the understanding of the model and the disease pathways. When scaling up the assay, the main aim was to ensure that the consumables used in the screen had compatibility with the liquid handling and high-throughput systems available as well as the assay readout system so that the majority of the screen could easily be streamlined.

Original Assay	**High-throughput Assay**
Ungenotyped fish (50% TG)	Genotyped fish (100% TG)
20-30 fish per dose	3 embryos per drug/dose (3 replicates of 1 fish)
Manual technique throughout assay	Nearly complete automation of assay
Possible 3-4 drugs per week	200-300 drugs screened per week

Table 4.7: Comparison of the original screening assay to the high-throughput assay. The table highlights the major differences provided by using the automation systems.

As fig 4.7 shows, the screen was scaled up so that it was possible to utilise the DsRed stress readout to screen hundreds of compounds per

week rapidly and with high sensitivity and specificity. To reduce costs and the number of fish required per compound, the style of plate was investigated. 24 well, 96 well and 384 well plates were selected as plausible candidates for zebrafish screening based upon the literature and communications within the zebrafish community. 384 well plates were identified as a possible candidate due to the large numbers of fish per plate but were unsuitable for the screen as over the 4 days of the assay the build-up of metabolites and well volume led to increased background stress in the model which masked the size of the effect from the positive control (Riluzole). 24 well plates had the advantage of multiple fish per plate and thus more data points for each drug. The disadvantage of 24 well plates was the incompatibility with the high-throughput systems and the library stock usage associated with large volumes of drugs required per well. 96 well plates represented the ideal middle ground with both the large numbers of fish per plate and the relatively low volume of compound per well. The use of 96 well plates is also supported by other recent screens published in the literature. One such screen was the identification of glucocorticoid signalling in a zebrafish luciferase reporter system in which the fish were dosed in 96 well plates from 4 days – 6days (48h exposure) to identify positive modulators of the pathway, without the negative side effects commonly seen by current pathway modulators with long term exposure (Weger et al 2013). Another recent screen also showed the applicability of 96 well plates in zebrafish screening for neurological disorders in epilepsy where fish were incubated for 90mins in the Spectrum library compounds to identify anti-convulsants (Baxendale et al 2012). This is evidence that the 96 well plates are well tolerated by the fish, as well as a neurological role of compounds within the Spectrum library.

One of the major concerns when scaling up the screen was the lost wells due to un-genotyped fish. The original screen genotyped the fish based upon DsRed fluorescence post screen, manually using a fluorescence microscope, but this would lead to wasted library as compounds would need repeated multiple times until a TG fish was randomly assigned. The

InCell system was chosen for genotyping as it has the capacity to perform automated imaging in fluorescent wavelengths rapidly. Using the G93Ros10 zebrafish on the InCell system it is possible to genotype the fish with >99% accuracy based upon DsRed fluorescence at 48hpf. Genotyping was possible at 24hpf using the InCell but only 34% of fish screened could be confidently genotyped on fluorescence per plate due to a weak signal, thus the throughput of the assay was reduced. Due to this observation, the screen was shifted from dosing at 24h-5dpf to 48h-6dpf. This meant that all the fish used in the screen were genotyped, which increased throughput and protected the library stocks. It also had the advantage that the fish at 48h is further developed than at 24h. At 48h the zebrafish has a developed heart and liver as well as other organs, meaning the drugs are likely to have less of an effect on developmental processes and any positive effect is more likely to represent a real neuroprotective drug effect.

The Echo 550 liquid handling system was selected for loading drugs onto the assay plates as it provides unparalleled accuracy down to volumes of 2.5nl. Previously, less advanced system would be used for high-throughput dosing that dispensed in the microliter range which required serial dilutions of drugs to be performed, which in turn leads to errors and wastage of valuable libraries. These systems also used tips which led to small errors in dispensing and the risk of cross contamination. The Echo 550 system addressed both these problems by using sonic energy to transfer nl volumes of compounds via tipless transfer. The Echo 550 system, when compared to tip based serial dilutions, led to differences in IC_{50} for some compounds by orders of magnitude. The work goes on to highlight how much of a source of error traditional tip based transfer generates and the effect this can have in biological systems and assays (Ekins et al 2013). The most time consuming part of the assay and the major area of future research to take this assay to the highest throughput possible is the development of automated systems for moving zebrafish. Currently, with the systems available, accuracy and speed are not high enough and the systems cannot distinguish fish based upon DsRed

fluorescence. In the literature various systems are being developed for embryo transfer such as in one publication where the system could dechorinate and load a 96 well plate in 8-10mins but at the expense of 2.8% mortality, 1.2% missed wells and embryo malformation was seen in 2x as many embryos compared to manual loading (Mandrell et al 2012). One system commercially available is the EggSorter from Noldus Information technologies. This system has the ability to load a plate within 5 minutes, but only has an accuracy of 96% and is primarily designed for embryos still with the chorion. With the current systems available, the quickest and most accurate way to dispense the fish is by hand using a manual pipette, but future research should focus on developing systems that can transfer the fish rapidly and accurately between plates based upon fluorescence, thus reducing the human input.

The readout was a major consideration, as ensuring the maximum information is gained from each embryo used is essential for identifying the best compounds. Unfortunately due to the limitations of the hardware and software available, it was not possible to keep the embryos alive post assay and still obtain the fluorescence data. The InCell still provided the imaging capabilities to ensure DsRed positive fish were used in the screen at 2dpf and 6dpf as well as ensuring the fish were developmentally normal using the brightfield channel. The sonication readout method was performed as this was shown to be able to detect drug effect in a dose dependent manner and to show different drug effects. In the final screen the embryos were sonicated individually well by well with a clean between each sample, but a future development would be to investigate plate sonication. Currently the sonication method is a manual and relatively slow process and plate sonication would be much quicker and eliminate the risk of sample cross contamination via the probe. Plate sonication would need to be investigated fully to ensure equal sonication throughout the plate as a common problem with water bath based plate sonicators is uneven sonication throughout the plate. Eventually further development and research into imaging of the embryos will allow the successful imaging and

quantification of embryos so that further assays will be possible that ensure the embryos are kept alive and embryo sonication is not essential.

When the dataset was analysed, the numbers of duplicate hits for each of the screens at different SSMD's showed that when the threshold was β<-0.5 there were 38 compounds that showed a reduction in fluorescence both times in the duplicate screens. When the SSMD threshold was set at β<-1.0 this number dropped to 9 compounds. This highlights the sensitivity and specificity of the assay as we identify reasonable numbers of hit compounds which it is possible to work with. We took all 38 compounds through to further testing based upon the -0.5 threshold as it is possible the compounds may work better at different concentrations and the smaller effect might be substantially larger at a different dose. It is important to highlight that these compounds may not all be hits. Based upon the sensitivity and specificity previously discussed, there is a small risk of false positives showing up in the screen. Also some of these compounds may not have any effect in the model and may just be quenching the DsRed fluorescence, so it is important to validate a positive effect in the model via immunostaining and behavioural analysis. The activators showed 20 compounds that showed a strong increase in DsRed fluorescence with a β Value of >1.0. This was equivalent to 1% of the library and highlights a list of potential heat shock promoters. It is important to point out that these compounds may be fluorescent molecules themselves and thus it is the compound leading to the increase in fluorescence rather than the activation on the heat shock response. The interest in compounds that activate the heat shock pathway as being beneficial stems from the idea that upregulation of the unfolded protein response (UPR) and other cell repair pathways is beneficial in protecting the cell and using compounds to induce a large UPR could potentially further protect the cell. This was highlighted in a mouse study using the compound arimoclomol which is currently in phase 2/3 clinical trials. Arimoclomol has been shown to protect motor neurons and improve motor performance and fatigue in treated mice (Kieran et al 2004). In addition, the mice also showed an extension in survival of 22%. Arimoclomol was

shown to be up-regulating the heatshock pathway, particularly hsp70 and hsp90, which strongly suggests that upregulation of the heat shock pathway has the potential to be neuroprotective.

Compounds with a toxic effect also have the risk of activating the DsRed fluorescence just by stressing the cell, so it is important to distinguish between activator compounds having a potentially beneficial effect and those inducing a non-therapeutic increase in DsRed expression. The number of compounds that lead to death in both replicates at 10µM was also investigated as the death could be due to various reasons. In the screen, 142 compounds led to death in both replicates. This could be due to the toxic nature of the drugs but could also be associated with administration at too high a concentration. The screen was performed at 10µM as this was an optimal dosing regime for Riluzole, but other compounds may show a higher efficacy at a lower concentration. A further experiment will be to screen the double death compounds at 1µM to identify drugs that may have a positive effect at lower concentrations.

Many screens have been performed in the zebrafish model with readouts including developmental defects, toxicity/death and mRNA expression evaluated by in situ hybridisation. These are all valid readouts of drug effects, but are time consuming, costly and not compatible with a high-throughput screen. Using this DsRed fluorescence readout, we have designed and implemented a high-throughput compound screen that is easily implemented, rapid and with a clear and concise readout making it a very powerful tool for screening *in vivo* models.

In conclusion we have scaled up, validated and performed a high-throughput pharmacological screen utilising a Sod1 mutant zebrafish to identify modulators of neuronal stress. In this screen we have optimised the consumables used, liquid handling systems, automated systems, readout and statistics to provide a screen which can rapidly identify neuronal modulators. The next stage for this project was to validate these

hits and identify a lead molecule to take forward for secondary screening. To further understand how the lead molecules are working dose responses, behavioural analysis, functional data and adult dosing should be performed.

Chapter 5: Secondary screening and lead molecule validation

Once the primary screen was completed the next step was to design and implement secondary screens to identify the compounds eliciting the following effects:

- having a true effect in this model
- having off-target effects that mask fluorescence such as toxicity
- having an activator effect on the heat shock pathway

Implementing stringent and accurate secondary screening is important in lead identification and validation as it confirms a positive drug response and identifies any false hits. Secondary screens are designed to be more informative than the original screen with the key aims of defining the optimal dose to benefit ratio whilst identifying any side effects such as behavioural changes, developmental changes and toxicity. By performing secondary screens on hits from the primary screen we aim to identify our strongest hits which are having a real effect in this model and take them forward to screening in different models with the aim to potentially identify new therapeutics for the treatment of ALS. Compounds of interest taken forward for secondary screening include those molecules which cause a reduction in fluorescence as this is a possible indicator of reduction of neuronal stress, compounds which show heat shock protein activation as a cellular protection pathway and compounds that were toxic at 10μM as these may have an effect at a lower dose.

5.1 Fluorescent inhibitors secondary screening

The initial aim was to confirm the activity of the inhibitors of DsRed fluorescence identified in the first screen. This was carried out by repetition of experiments to confirm activity and to give confidence in the observed effects. The top 24 inhibitors were studied.

	Run 1	Run 2	Run 3	Run 4	Run 5	Run 6	Run 7	Run 8	Run 9	Run 10	Average
RILUZOLE	-4.91549	-4.75603	-2.97837	-3.02651	0.382654	-2.20735	-3.5621	-3.70252	-1.0889	-0.81433	-2.6669
2,4-DICHLOROPHENOXYBUTYRIC ACID, METHYL ESTER	0.301766	-0.48856	-1.52289	-0.76337	-1.87351	-2.26309	-4.04613	-3.36519	-0.15665	-1.49511	-1.56727
MYCOPHENOLIC ACID	1.952136	-4.27729	-1.88839	-1.603	Dead	Dead	Dead	Dead	Dead	-1.21671	-1.40665
OXICONAZOLE NITRATE	-4.22414	-4.17407	Dead	-2.24658	Dead	Dead	Dead	Dead	Dead	Dead	-3.54826
PROPANIL	-3.10874	-2.88574	-1.75436	-0.44292	-3.49399	Dead	-1.8199	Dead	-0.62825	Dead	-2.01913
CEFDITORIN PIVOXIL	-5.40116	-4.54497	-2.92175	Dead	2.029808	1.371881	-0.31117	-0.33385	1.0114	-0.63136	-1.08124
2-HYDROXYXANTHONE	Dead	-2.56799	Dead	Dead	-0.10903	-0.35361	-0.8789	-0.20763	-0.88609	-1.02503	-0.86118
PINOSYLVIN	-1.35053	5.757425	0.995229	-1.99932	-0.15948	1.58995	4.579677	-0.13191	0.303948	-2.21885	0.736615
PEFLOXACINE MESYLATE	Dead	Dead	-4.01173	-2.42452	2.160231	2.500586	3.695976	-0.14989	-0.25738	-0.19531	0.164746
SELAMECTIN	-4.9721	-4.21182	-2.01318	-2.95488	Dead	-2.12652	-2.28453	-1.1923	-1.37187	-1.36885	-2.49956
NERIIFOLIN	-4.43636	-2.96354	-0.93938	-0.6043	-3.76204	-3.83945	Dead	Dead	Dead	Dead	-2.75751
ESTRADIOL DIACETATE	-0.75817	-1.54002	1.635735	-0.74719	-0.42544	-0.60167	-0.07215	-0.50127	-0.31897	0.062058	-0.32671
WARFARIN	0.067979	-1.5797	1.79018	1.68619	-1.06779	0.337798	-0.3936	-0.46497	-0.338	-0.19768	-0.01596
11-OXOURSOLIC ACID ACETATE	-1.38635	-0.79591	2.139512	1.148134	Dead	Dead	0.74822	-0.51009	Dead	Dead	0.223918
7-OXOCHOLESTERYL ACETATE	-5.42735	-1.1437	0.390158	-2.60131	-1.13382	-0.05394	3.308407	-0.62201	Dead	Dead	-0.91045
ROCCELLIC ACID	2.623454	2.770581	3.658161	1.084199	-0.44799	-0.90482	2.278614	-0.59476	-0.32255	Dead	1.12721
NONOXYNOL-9	-1.37672	0.156949	-0.90433	0.628181	-0.22737	-1.71317	-0.45559	-0.60291	-0.35105	-1.34442	-0.61904
CHOLESTAN-3beta,5alpha,6beta-TRIOL	-1.03779	-2.58995	0.379759	-3.05078	-0.44404	-1.13754	-0.17234	-0.67495	0.342388	Dead	-0.93169
LORATADINE	-0.01521	-0.37533	2.313215	-0.29849	Dead	Dead	Dead	Dead	Dead	Dead	0.406045
TROXERUTIN	Dead	Dead	Dead	Dead	1.355608	-1.12568	7.627509	0.253874	-0.06951	-0.45916	1.263774
ACRISORCIN	Dead	Dead	Dead	Dead	-1.08058	-3.75646	Dead	-0.93419	0.240614	-0.49162	-1.20445
PRALIDOXIME MESYLATE	Dead	Dead	Dead	Dead	-0.89459	0.080207	-2.46257	-0.17078	-0.30629	Dead	-0.7508
CRESOL	-0.79745	-1.35631	0.861197	1.110389	-2.14163	-1.0192	0.595985	-1.41111	Dead	Dead	-0.51977
RESVERATROL 4'-METHYL ETHER	-0.36609	-2.46246	0.964802	-0.98252	0.589809	-0.85228	0.97808	-0.84651	Dead	Dead	-0.37215

Table 5.1: Table of the top 24 fluorescence inhibitors identified in the high-throughput screen. The data show the SSMD values for ten G93Ros10 zebrafish dosed with the relevant compound from 48hpf to 6dpf. The average fluorescence over the ten runs is shown in the final column. Green shows SSMD <-1.0, Yellow shows SSMD < -0.5, Blue shows SSSMD > 1.0 and Red indicates death of the embryo.

From the fluorescence data, response to stimulus (touch), imaging and measuring the heartbeat under a dissection microscope we identified the compounds which consistently reproduced a strong reduction in fluorescence and did not lead to death or toxicity of the embryo. Riluzole showed a strong reduction in fluorescence in 9/10 assays which shows the robustness of our positive control and our ability to reproducibly detect drug effect. We set our criteria for hit compounds based upon the Riluzole scores and took a hit as any drug which showed effect 9 times out of 10 and had less than one death in order to eliminate drugs which had a strong toxic effect on the embryo. These data show that some of the compounds showed high levels of toxicity when repeated ten times. This is due to the more stringent examination of each fish for a heartbeat and developmental toxicity which was not possible in the original screen of 2000 compounds. A compound having a toxic effect on an embryo may lead to a detrimental effect in the zebrafish, leading to a false reduction in DsRed fluorescence showing as a positive result. Also if the toxicity led to death but the compound preserved the embryo, it may appear as normal with reduced fluorescence. This highlights the importance of secondary screening to carefully identify the real effects of compounds. Based upon our findings and literature searches the compound that satisfied our hit selection criteria was Selamectin. Selamectin was selected as the primary hit compound to take forward as it was the only compound that fitted our hit selection criteria by having a survival rate of over 90%, caused a reduction in fluorescence similar to Riluzole in 90% of samples, looked morphologically normal under inspection, had a normal heart rate compared to control fish and had the ability to respond to a touch stimulus. Furthermore upon performing a literature search, Selamectin fitted the profile for a compound that would be biologically relevant and a potential therapeutic for ALS based upon its proposed mechanisms of action. Other compounds that showed an effect and had good survival were also investigated, but Selamectin was selected for further analysis as it was the strongest lead. Future work will involve investigating the other hits in the assay to identify other therapeutic agents that are efficacious in this model.

5.2 Identification and validation of Selamectin

Once Selamectin had been identified as a candidate lead molecule, a dose response study was performed to identify the optimal dose for reduction of DsRed fluorescence. Zebrafish were treated with concentrations of Selamectin between 0.1 and 10µM. 10µM was the maximum tolerated dose, with toxicity and death seen at higher doses in the fish.

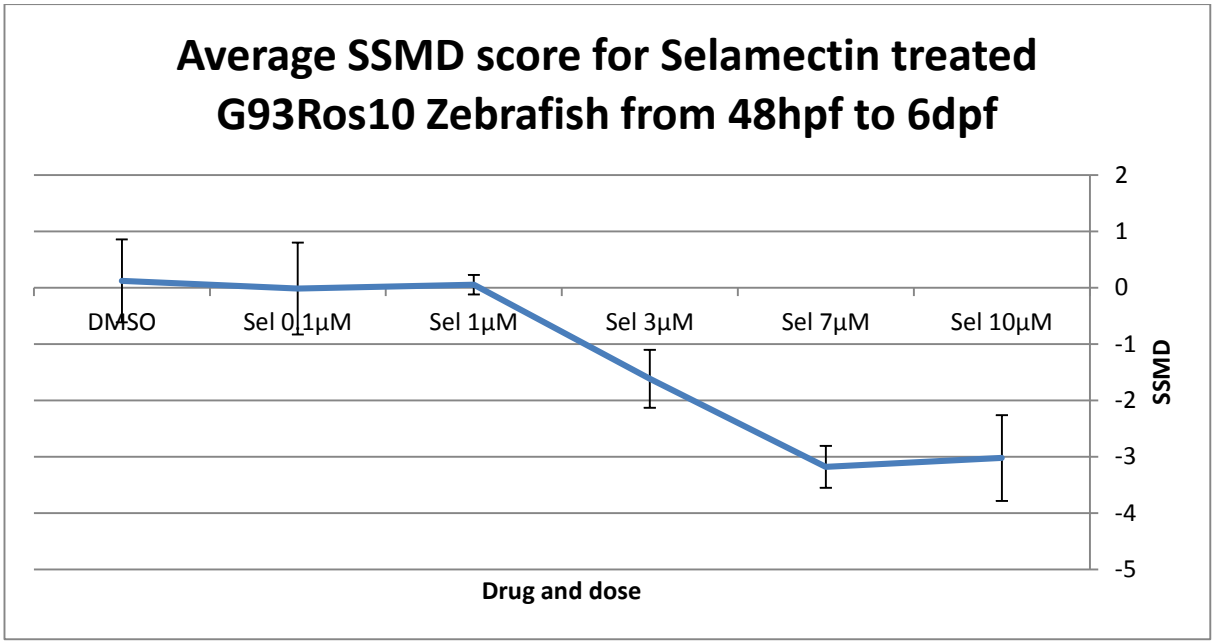

Fig 5.1: Graph of the reduction in average SSMD of DsRed fluorescence in Selamectin treated G93Ros10 zebrafish. N= 17 fish per group. Error bars represent the SD.

Figure 5.1 shows Selamectin led to a reduction in DsRed fluorescence in a dose dependent manner with an IC_{50} between 3-4µM and a maximum reduction in fluorescence seen at 7µM when the compound was incubated 48h-6dpf. When compared to with Riluzole (fig 5.2) it can be seen that Selamectin elicits a reduction in fluorescence to a similar level suggesting both the compounds have similar potencies in reducing the neuronal stress.

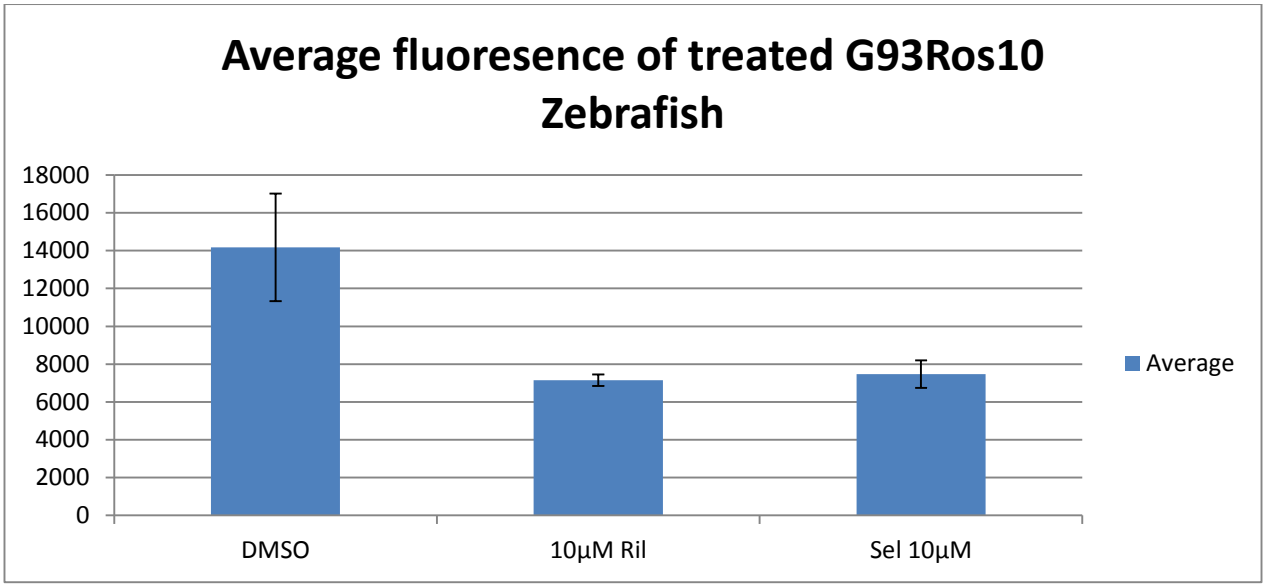

Fig 5.2: G93Ros10 x AB zebrafish fluorescence when dosed with Riluzole or Selamectin from 2dpf-6dpf. Error bars show the SD and n=23 per group.

The data were also analysed using the Pherastar system as it has a more sensitive readout of the fluorescence by performing a 15x15 point well scan and the results showed a large reduction in DsRed expression which further supported the hypothesis that these compounds were reducing neuronal stress. An interesting outcome of screening using the Pherastar was the identification of a strong reduction in fluorescence around the head area of the fish as shown in fig 5.3.This led to the hypothesis that these drugs were acting to reduce the neuronal stress in the CNS with a particularly strong effect in the hindbrain.

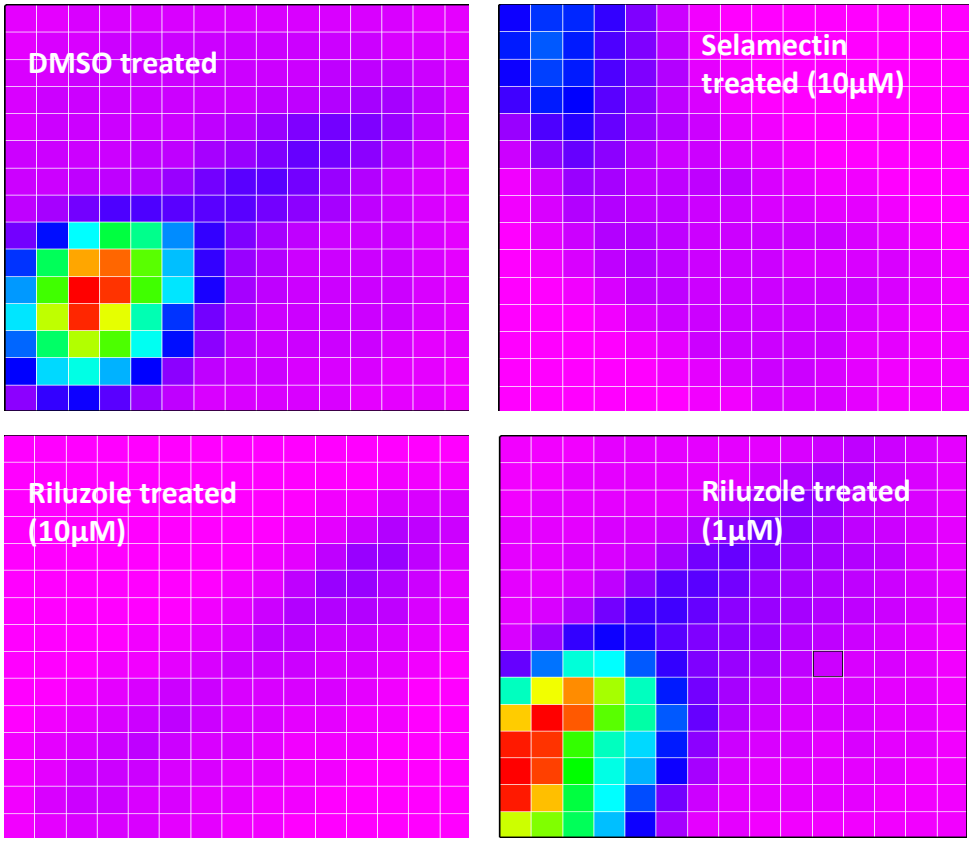

Fig 5.3: Representative Pherastar readout showing G93Ros10 zebrafish scanned for DsRed fluorescence in a 15x15 well scan. The heat map scale runs from pink = low fluorescence to Red = high fluorescence.

When the overall well fluorescence was quantified from the Pherastar readout, it confirmed that the compounds were leading to a large decrease in DsRed fluorescence (fig 5.4). This is in agreement with the OmegaStar sonication method and further validated that our compounds were having a real effect at a cellular level.

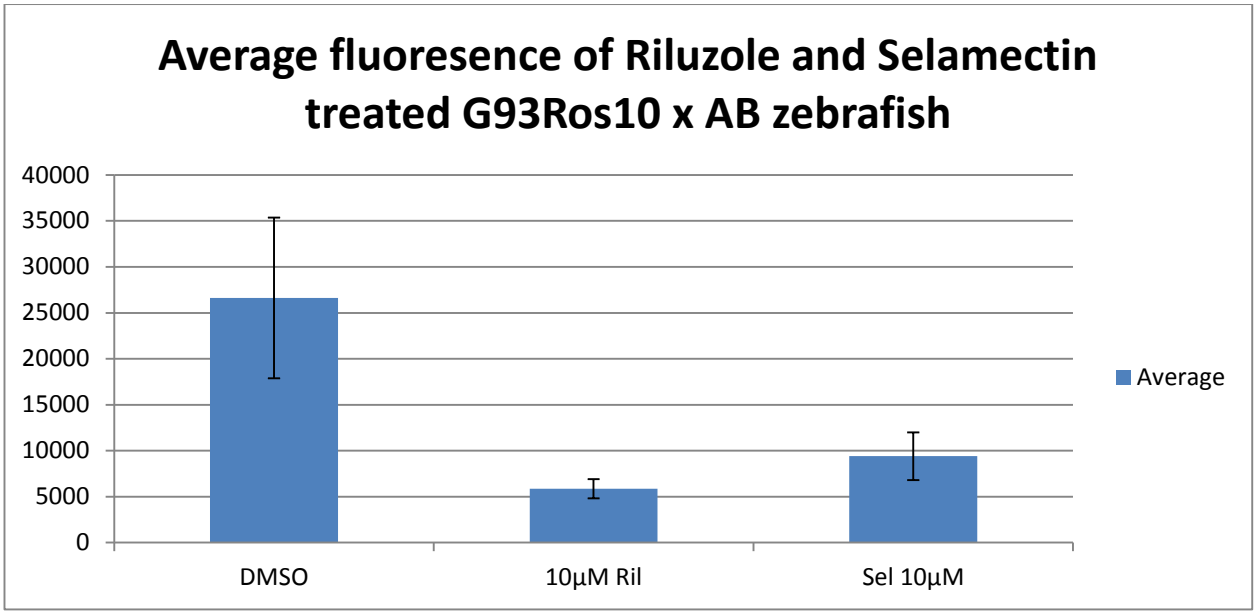

Fig 5.4: Pherastar readout of G93Ros10 zebrafish dosed with Riluzole and Selamectin at 10µM. Error bars show the SD and n= 23 fish per group.

The InCell microscope system was used to take images of the G93Ros10 zebrafish following Riluzole treatment, Selamectin treatment or in control (DMSO) fish. This was to confirm the Pherastar finding that the majority of the DsRed fluorescence reduction was concentrated in the hindbrain, eye and spinal cord regions.

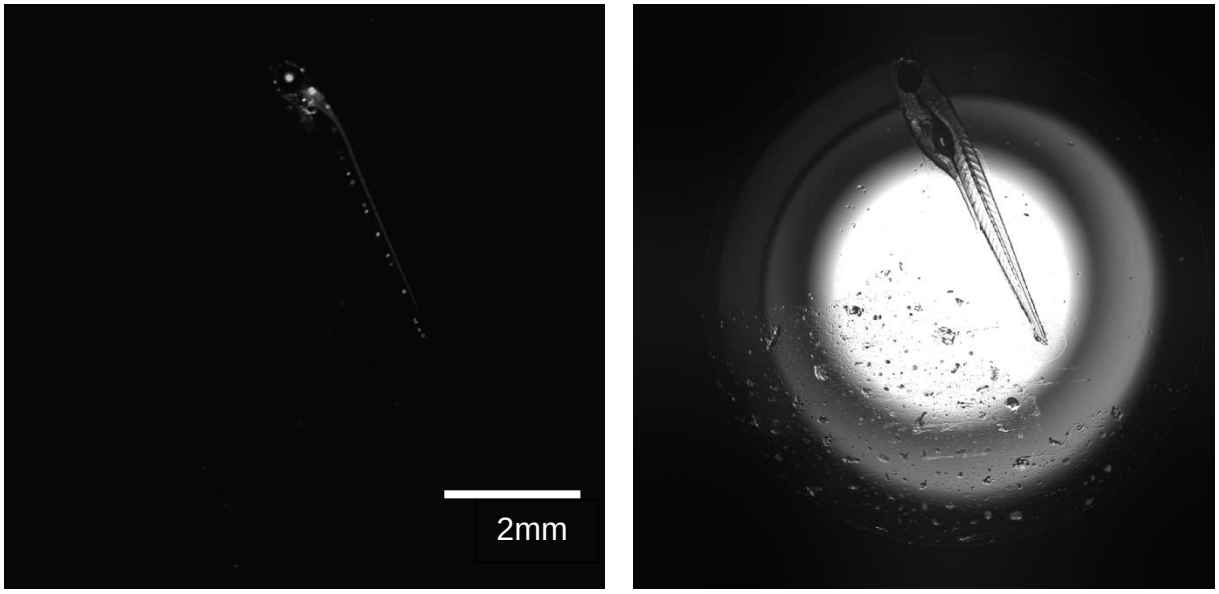

Fig 5.5: Representative image of a DMSO treated G93Ros10 zebrafish imaged using the InCell system. The left image shows the DsRed expression and the right image shows a brightfield image.

Fig 5.5 shows that in the G93Ros10 zebrafish treated with DMSO the majority of the DsRed fluorescence is seen in the eye, hindbrain, spinal cord and the neuromast cells. These are some of the key areas known to be potentially disease relevant as they are affected in ALS mice and patients. This provides supporting evidence that the stress response is accurately highlighting the cells affected by Sod1 toxicity. Based upon the location of the fluorescence in untreated fish (fig 5.3) and the reduction in head fluorescence identified by the Pherastar system when treated with Riluzole and Selamectin, the zebrafish were imaged to identify which anatomical structures and cell types showed the largest reduction in DsRed fluorescence.

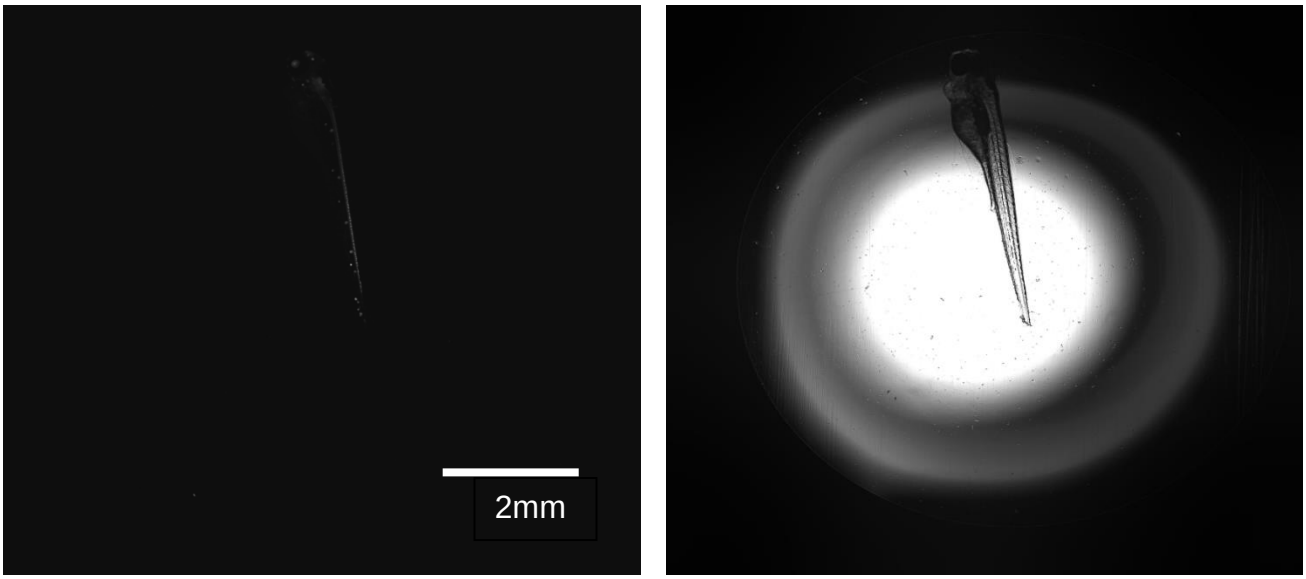

Fig 5.6: Representative image of 6dpf G93Ros10 Zebrafish dosed with Riluzole at 10µM from 48h-6dpf and imaged using the InCell system. The left image shows DsRed expression and the right image shows a brightfield image.

Fig 5.6 shows the reduction in DsRed fluorescence following Riluzole treatment is noticeable upon visual inspection. The major DsRed reduction is seen in the hindbrain, eye and proximal spinal cord which are anatomical areas linked to ALS. This suggests that Riluzole is having a specific effect on the neuronal cells showing Sod1 toxicity in the CNS and is reducing stress in the DsRed expressing cells. To confirm Selamectin was having an effect in similar cell types to Riluzole, the G93Ros10 zebrafish dosed with Selamectin were also imaged using the InCell system.

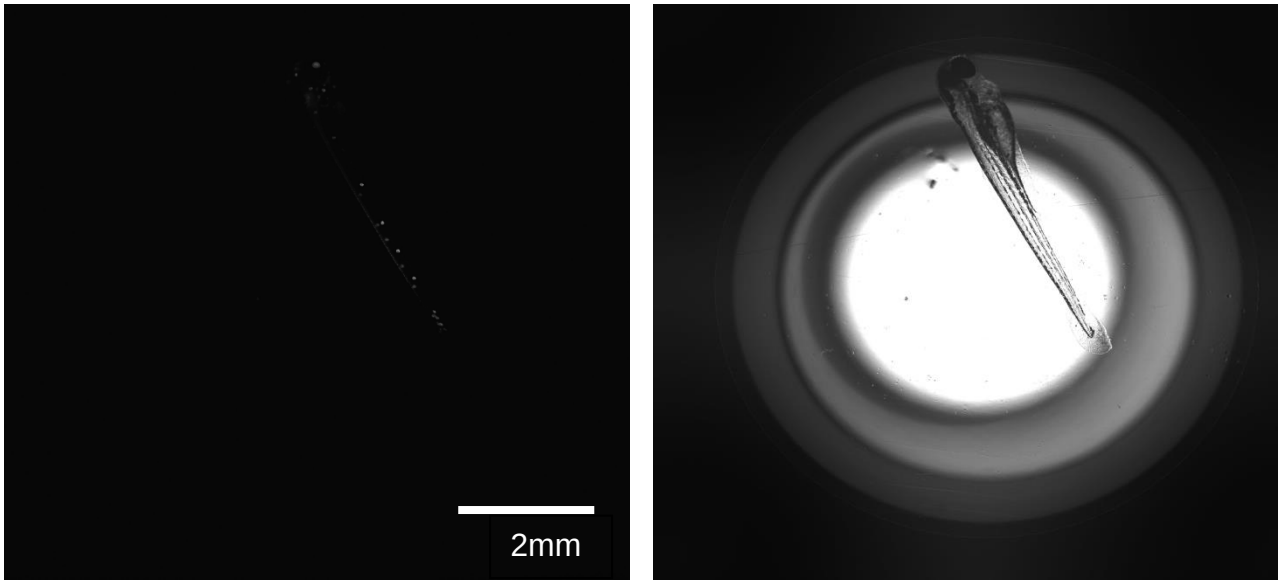

Fig 5.7: Representative image of 6dpf G93Ros10 Zebrafish dosed with Selamectin at 10µM from 48h-6dpf and imaged using the InCell system. The left image shows DsRed expression and the right image shows a brightfield image.

The reduction in fluorescence is apparent in the Selamectin treated G93Ros10 fish (fig 5.7). The reduction in DsRed fluorescence is strongest in the hindbrain, eye and proximal spinal cord. The similarities between Selamectin and Riluzole suggest that both compounds are having a positive role in reducing neuronal stress. As a validation of this a lower concentration of Riluzole was imaged to show that this reduction in DsRed fluorescence is dose specific and not a general side effect of Riluzole treatment.

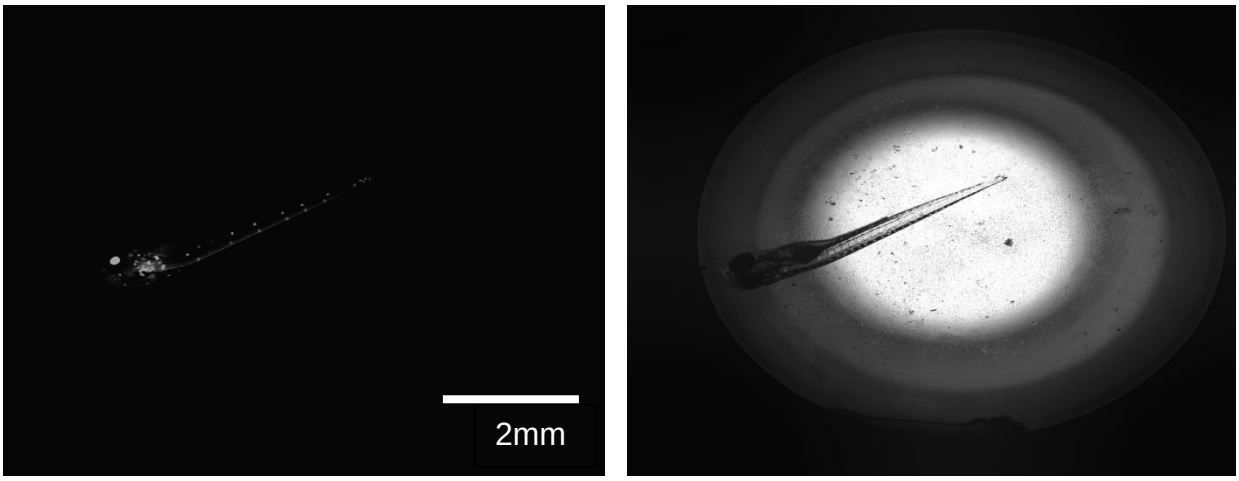

Fig 4.8: Representative image of 6dpf G93Ros10 Zebrafish dosed with Riluzole at 1µM from 48h-6dpf and imaged using the InCell system. The left image shows DsRed expression and the right image shows a brightfield image.

In the 1µM Riluzole treated G93Ros10 zebrafish (fig 5.8), we do not see a reduction in fluorescence such as is seen at 10µM. This suggests that the reduction in fluorescence is dose dependent and supports the findings from earlier screens that Riluzole at 1µM is not effective in reducing neuronal stress.

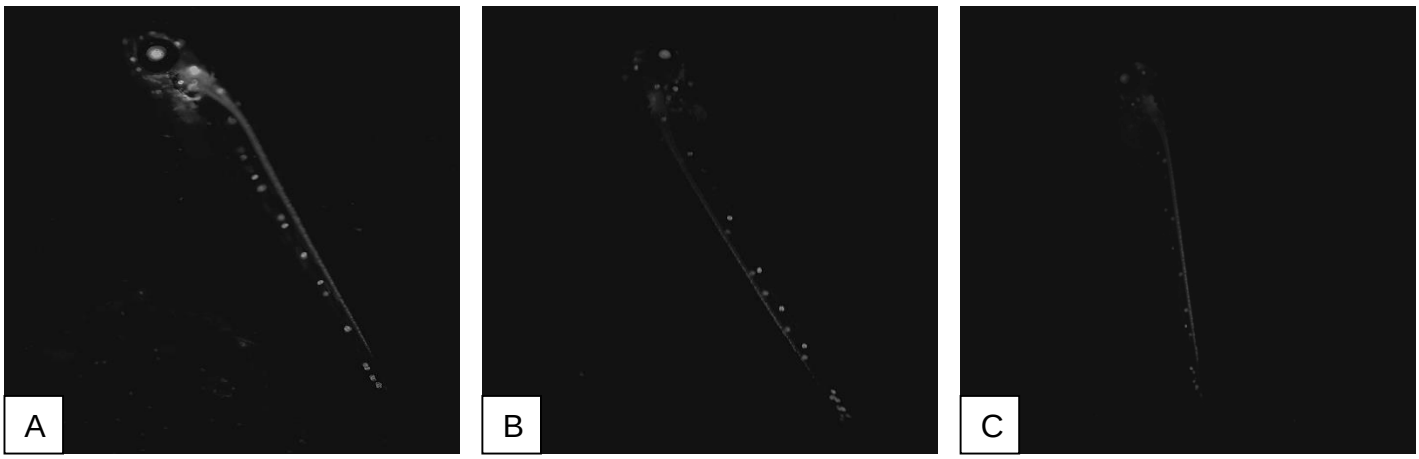

Fig 5.9: Representative images of 6dpf G93Ros10 Zebrafish dosed with DMSO, Selamectin and Riluzole at 10µM from 48h-6dpf and imaged using the InCell system. The images show the DsRed fluorescence for each of compounds. A: DMSO treated, B: Selamectin treated (10µM), C: Riluzole treated (10µM).

From the images, it is apparent that the compounds are leading to a large reduction in fluorescence within distinct anatomical structures. The eye, hindbrain and proximal spinal cord all show large reductions in the DsRed fluorescence when treated with either Riluzole and Selamectin at 10µM. Based upon these findings, Selamectin was taken forward as a candidate molecule for further screening. The DsRed expression is still relatively strong in the tail region with all of the drug treatments. This is most likely caused by the stability of the DsRed protein. At 48h when drug treatment commences the DsRed expression is switched on in the tail region and slightly in the hindbrain which is the basis for one of the main methods for genotyping. As the DsRed is very stable and is already expressed in these regions prior to drug treatment, it persists at 6dpf.

Performing the behavioural analysis gives us data on the behavioural effects of these test compounds. Using the Viewpoint behavioural tracking system it is possible to measure the movement of the zebrafish in 96 well plates whilst controlling the lighting conditions. By altering the thresholds of detection rapid and slow movements can be distinguished, allowing accurate and detailed analysis of the behavioural profiles of the fish. By comparing the level of movement of fish in the DMSO treated control zebrafish, compounds which are having a sedative effect can be identified. Riluzole has a known sedative effect (Doble 1996), so compounds which have a sedative effect are not discarded, but caution should be taken to ensure that the fish can recover. The screen also allows the identification of compounds which lead to a hyperexcitiability state in the fish. This can be identified by large amounts of movement and increased levels of rapid movement in comparison to the DMSO treated zebrafish. By controlling the light cycle within the Viewpoint system we also investigated the behavioural changes in response to light and dark by performing the assay for 10mins in the light followed my 10mins in darkness.

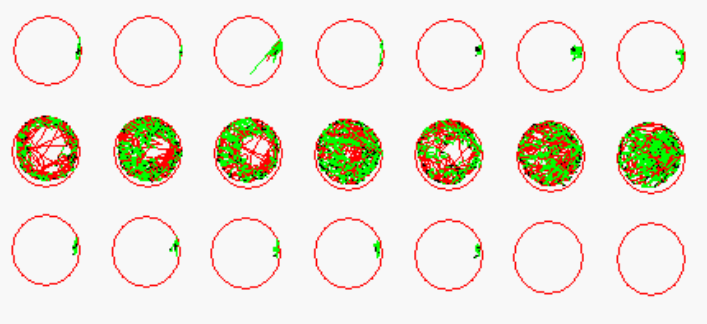

Fig 5.10: Readout from the Viewpoint analysis system showing G93Ros10xAB zebrafish treated with DMSO, Riluzole and Selamectin at 10µM for 10mins in darkness. The green line represents slow movement and the red line represents burst movement.

Fig 5.10 shows the DMSO treated fish continue to move around as would be expected with movement throughout the well in a combination of both slow and burst movement in all areas. The Riluzole treated fish showed little movement and this correlates with previous observations. The Selamectin treated fish also showed no signs of movement which suggests, as with Riluzole, that the drug has a sedative effect at this dose. This may link the drugs with a common mechanism of action or that both have off target effects on neurotransmission that lead to sedation. To ensure that the reduction in fluorescence was not as a direct effect of sedation/lack of movement in the fish, we went back to the original screen results and looked for other compounds with a known sedative effect. These compounds did not cause a reduction in fluorescence as seen in Riluzole and Selamectin which suggests that this is an effect of the drug and not as a result of side effects, such as sedation.

5.3 Selamectin and structurally similar compounds

The next step to investigate the effect of Selamectin was to screen a small panel of structurally similar compounds and other members of the macrocyclic lactone family. The effects of Ivermectin (Sigma-Aldrich, Cat No: 18898), Moxidectin (Sigma-Aldrich, Cat No: 33746) and Eprinomectin

(Sigma-Aldrich, Cat No: 32526) were investigated. Dose responses studies were carried out using these compounds to investigate the pathways involved in the reduction of fluorescence and to determine if this was a Selamectin specific effect or a common effect of macrocyclic lactone compounds. A major issue in the dose responses with other compounds from the macrocyclic lactone family was high levels of toxicity. Even at low doses that are well tolerated in the G93Ros10 zebrafish with Riluzole and Selamectin, high levels of heart oedema and death were observed (Fig 5.11). This was particularly so for ivermectin, with death in all fish at 1µM and above, moxidectin at 1µM and above and eprinomectin at concentrations above 1µM. eprinomectin had no effect at any tolerated concentration which suggests it has a very narrow therapeutic window or no effect. moxidectin caused a reduction of 40% in fluorescence at 0.1µM but had no effect at 0.01µM. Ivermectin at 1µM led to a reduction in fluorescence of over 50% but had no effect at 0.1µM. This data suggests that the other compounds similar to Selamectin may have a positive effect in the model but that they have a small therapeutic window with toxicity seen at higher concentrations. This suggests that in the zebrafish, Selamectin has a much safer toxicity profile and is generally better tolerated.

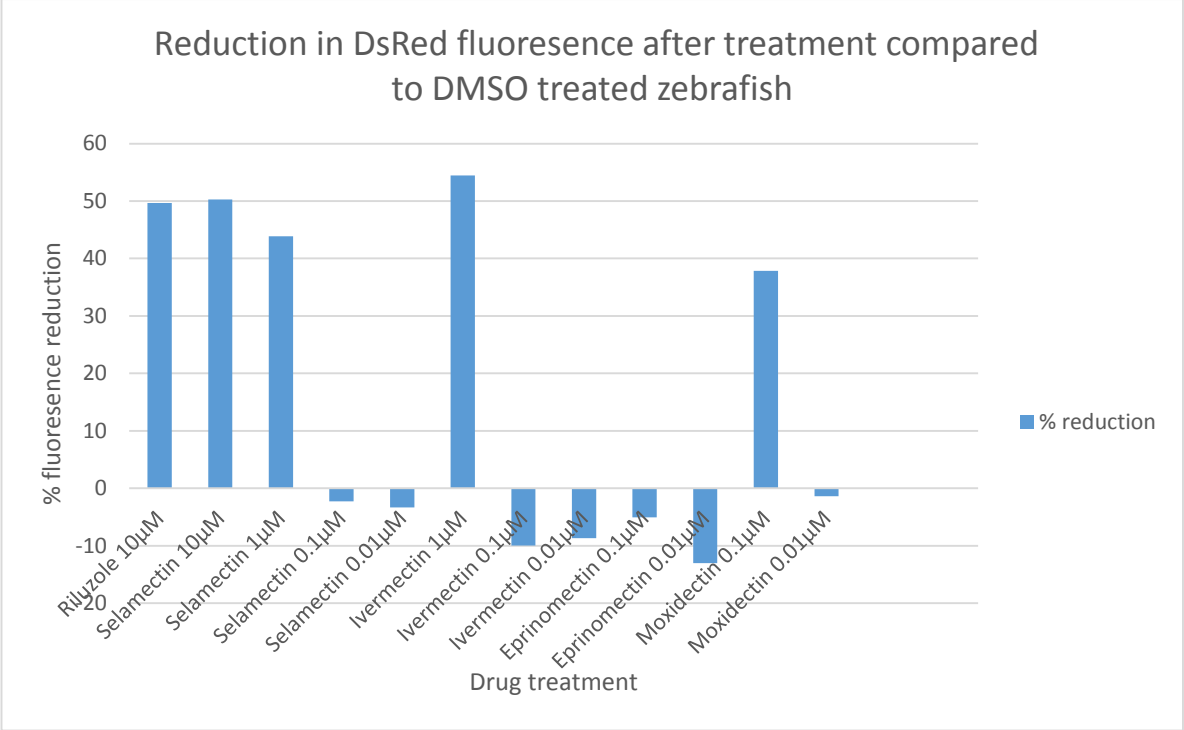

Fig 5.11: Fluorescence reduction after treatment with different concentrations of macrocyclic lactones. N=10 fish per treatment. Treatment was from 48hpf to 6dpf in G93Ros10 zebrafish.

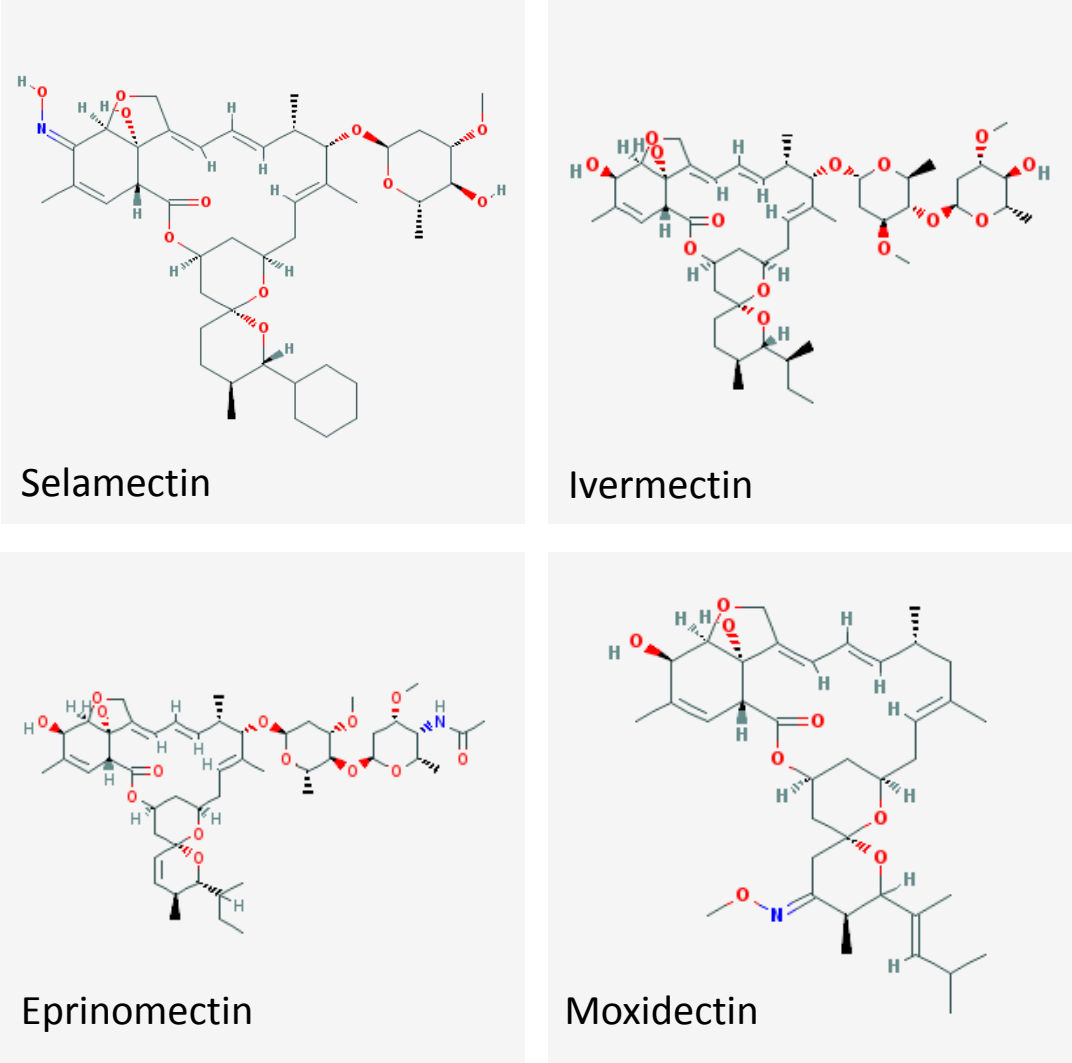

Fig 5.12: Chemical structures of Selamectin, Ivermectin, Eprinomectin and Moxidectin, highlighting the structural similiarities. Images taken from PubChem.

5.4 Combining Riluzole and Selamectin.

As both Riluzole and Selamectin show sedative effects when used at concentrations which elicit a strong reduction in fluorescence, the drugs were given in combination at a lower dose to determine whether it is possible to maintain the reduction in fluorescence whilst showing a reduction in the sedative effects. This would allow chronic drug administration into adulthood as the fish would still have the ability to move and feed throughout the treatment. This method of combination treatment would also allow the identification of any synergistic effects between the drugs which would help to elucidate the pathways involved. To perform this, both compounds were

screened together using a matrix of low and high concentrations. Behavioural analysis and fluorescence measurements were carried out to determine the sedative profile of these combinations and to identify possible synergistic dosing regimes. Figure 5.13 shows combinations of Riluzole between 0-10µM with Selamectin between 1-5µM. These data correlate with the previous dose-response studies where increasing concentrations of either drug results in a greater reduction in fluorescence. This is shown as increasing concentration of Riluzole cause a greater reduction as the concentration increases. The same is seen for Selamectin (Horizontal axis). It is important to point out that a combination of the two lower concentrations of drug leads to a reduction in fluorescence comparable with that of either compound at a higher concentration. With Riluzole at 2µM-4µM and Selamectin at 2-3µM the reduction in fluorescence is around 50% which is comparable to the reduction seen with Selamectin and Riluzole at 10µM (Fig 5.2).

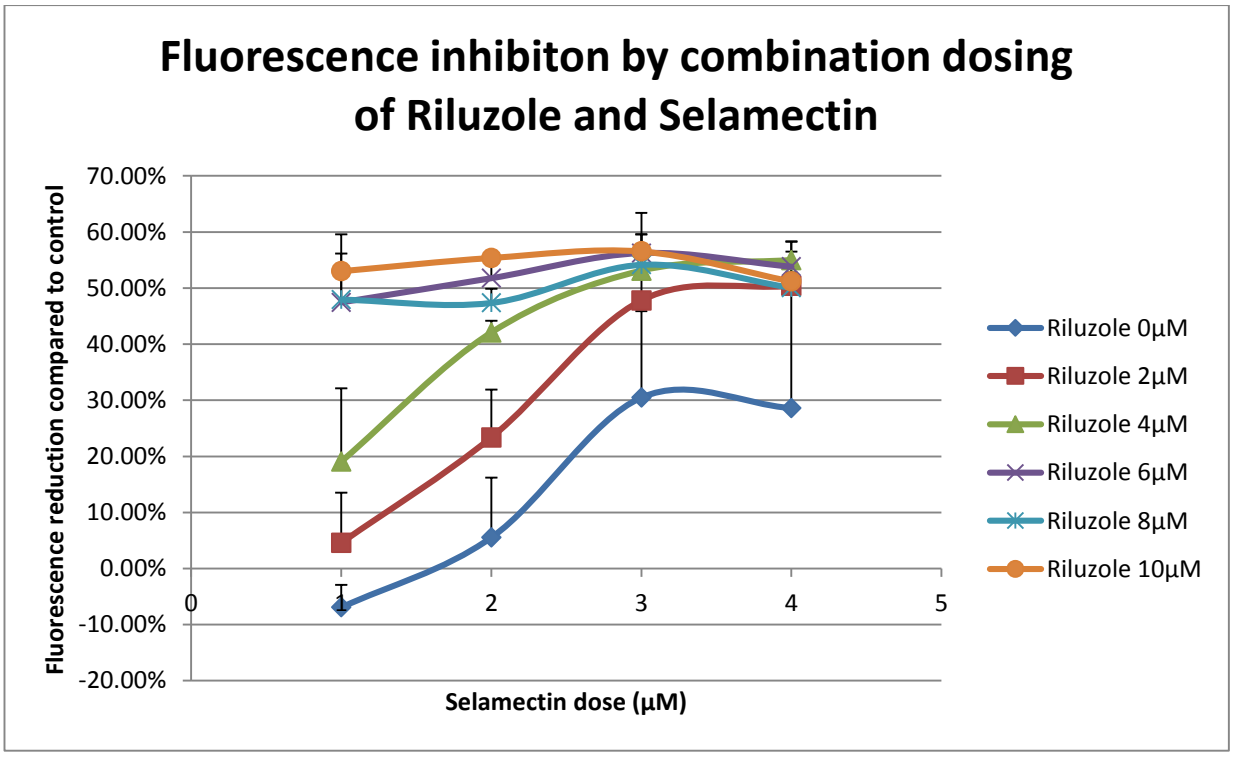

Fig 5.13: Graph of fluorescence inhibition by combinatorial dosing of Riluzole and Selamectin. Error bars show the SEM. N=4 fish per group.

A major advantage of dosing at lower drug concentrations is the potential to reduce any side effects of the individual drugs. By combining two drugs at a lower concentration it may be possible to reduce the anasthetic effect of Riluzole and Selamectin seen at 10µM. In Fig 5.14 the combination dosing regime was focused on the lower doses to indentify the lowest possible combinatorial dose with the strongest effect. A concentration of Selamectin of 1.5µM combined with Riluzole upto 4µM results in a lower reduction in fluoresence than is seen for Riluzole or Selamectin alone (individually) at 10µM. The optimal dose was highlighted as 2.5µM Selamectin in combination with 2-3µM Riluzole as this had the ability to reduce the fluoresence acitvation to a level comparable to the hit compounds individually. Overall the effects appear to be addative rather than synergistic or antagonistic.

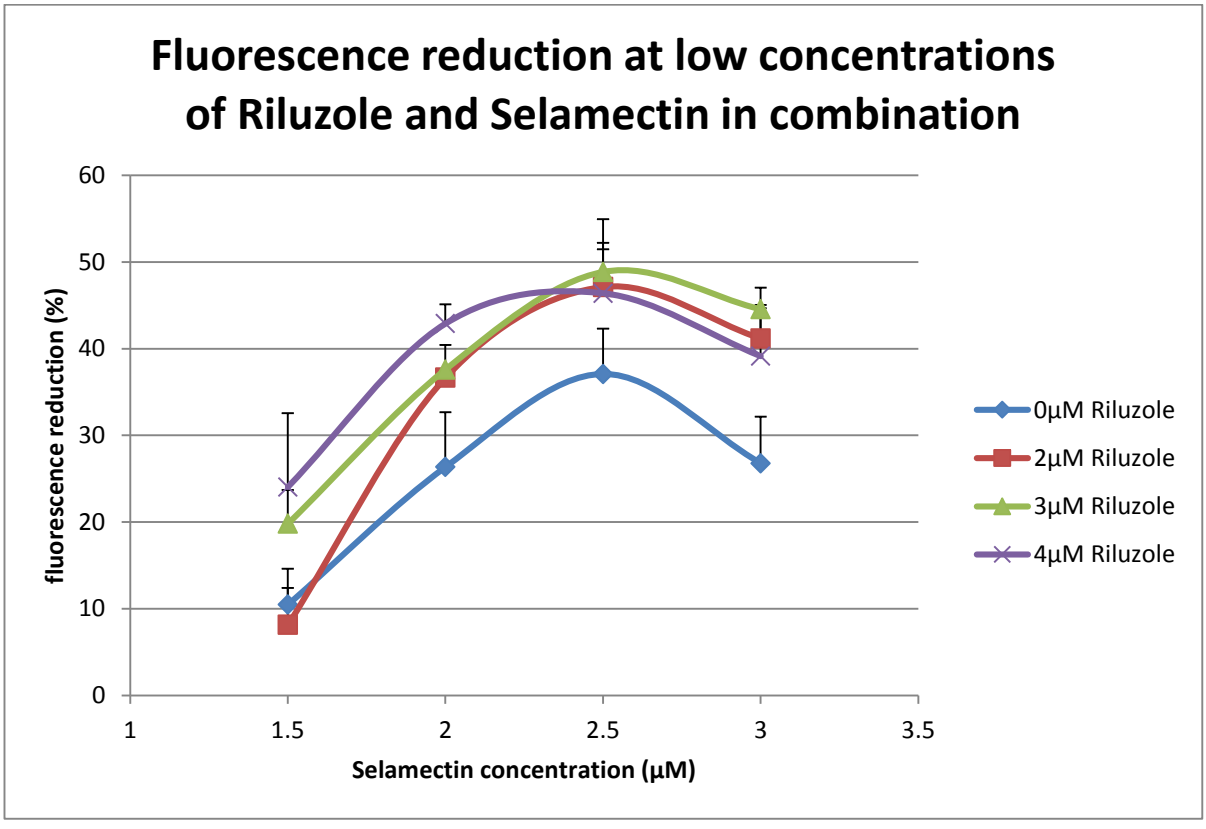

Fig 5.14: Graph of fluorescence inhibition by low concentrations of Riluzole and Selamectin in combination. Error bars show the SEM. N=6 fish per group.

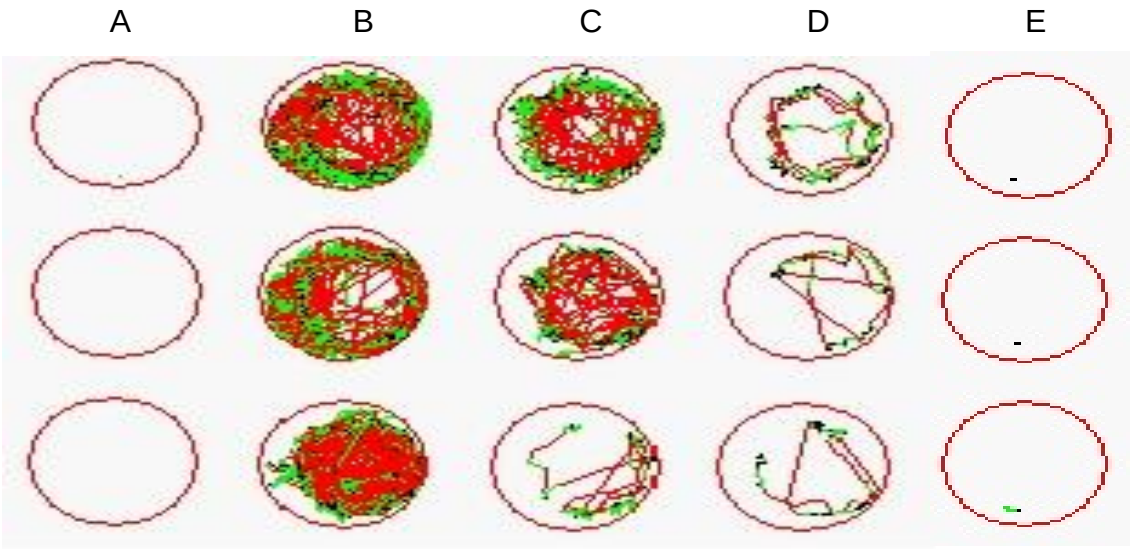

Fig 5.15: Representative image of viewpoint readout for zebrafish treated with different combinations of Riluzole and Selamectin. A- 10µM Selamectin only, B- DMSO control, C- 2.5µM Selamectin only, D- 2µM Riluzole+2.5µM Selamectin, E- 10µM Riluzole only. Green shows slow movement, Red shows fast movements.

Behavioural analysis was performed using the Viewpoint system to measure the movement of the combination dosed zebrafish. In fig 5.15 both the Selamectin at 10µM (A) and Riluzole at 10µM (E) show no movement due to sedation by the drug as was shown in fig 5.10. The DMSO control dosed group (B) show normal movement. Panel C shows that fish treated with Selamectin alone at 2.5µM still has the ability to move with a slight reduction in total movement compared to the DMSO treated (B). When the zebrafish were treated with a combination of 2µM Riluzole and 2.5µM Selamectin (D) the movement of the fish is greatly reduced suggesting an additive sedative effect of the drugs when used together. This may suggest that the compounds work through a similar pathway synergistically or that the compounds both have a sedative effect on different pathways which leads to a cumulative effect. It is important to note that there is still some movement from these fish as shown in D and the sedative effect is not as strong as either hit compound individually at 10µM.

5.5 Double death screening

Compounds that led to death in both of the replicates at 10µM were taken forward to screen at a lower concentrations. At high concentrations the beneficial effect of a drug may have toxic side effects but at lower doses a therapeutic effect may be seen. The double death screening was performed following the same protocol as the main Spectrum screen except all drugs were used at 1µM instead of the original 10µM. This concentration was obtained by using the Echo 550 liquid handling system to dispense 20nl of the library at 5µM into 200µl of E3 zebrafish media to obtain the final desired concentration. One hundred and forty drugs were screened at 1uM (Table 5.2) and from this subset of compounds 16 were found to show a toxic effect and induce death at 1µM. These are most likely highly toxic compounds which continued to cause death even at the lower concentration. From the 140 compounds screened a further 26 also caused a significant activation of the stress response but this is most likely linked to the toxic properties of the compounds which at 1uM may not be strong enough to induce death but do cause an increase in neuronal stress, toxicity and hsp70 activation. The majority of compounds showed a non-significant change in fluorescence suggesting they had no neuroprotective effect in the Sod1 mutant zebrafish model. Six compounds showed a mild inhibition of fluorescence, while 2 compounds showed a strong inhibition of fluorescence. It is important to note that the reduction in fluorescence may be an off-target effect, as a result of toxicity such as in the case of Rotenone which is a known piscicide used to control invasive fish populations (Kurji et al 2006). It is important to highlight these compounds as of interest and further investigation should be undertaken to identify any real hits from this 1µM cohort and take these forward for lead candidate screening.

Drug	SSMD
FLAVOKAWAIN B	2.19659
2,6-DIMETHOXYQUINONE	0.990309
PRISTIMERIN	0.883906
1-BLOBENZYLOXY-CARBONYLAMINOPHENETHYL CHLOROMETHYL KETONE	0.668374
DISULFIRAM	-0.41411
PENTACHLOROPHENOL	-0.36783
ZEARALENONE	2.262879
DEOXYSAPPANONE B 7,3'-DIMETHYL ETHER ACETATE	2.24425
SAPPANONE A 7-METHYL ETHER	0.994796
COLFORSIN	1.22093
HEXESTROL	-0.45221
DYCLONINE HYDROCHLORIDE	-0.18063
SIMVASTATIN	Dead
ESTRADIOL METHYL ETHER	0.695976
ELAIDYLPHOSPHOCHOLINE	0.225611
FLURBIPROFEN	Dead
HEXACHLOROPHENE	-0.07249
CARAPIN	-0.17213
METHOXYCHLOR	-0.02078
4'-METHOXYFLAVONE	0.993865
PEMPIDINE TARTRATE	0.260159
DIENESTROL	0.540018
NIMESULIDE	0.100994
DICLOFENAC SODIUM	-0.19663
beta-DIHYDROGEDUNOL	1.288797
4'-HYDROXYCHALCONE	1.498911
AZELASTINE HYDROCHLORIDE	0.347867
GEMFIBROZIL	-0.11337
DICAMBA	-0.07814
CEDRELONE	-0.71424
PINOSYLVIN METHYL ETHER	0.808345
beta-DIHYDROROTENONE	1.480898
AVOCATIN A	1.457783
IBUPROFEN	-0.2417
MITOXANTHRONE HYDROCHLORIDE	-0.49568
ETHINYL ESTRADIOL	-0.0834
4-ACETOXYPHENOL	1.336889
TETRAC	Dead
THYROXINE	Dead
DIFLUNISAL	-0.09064

CHOL-11-ENIC ACID	-0.00945
CHLOROXINE	-0.45465
HYDROQUINONE	1.00121
BIFONAZOLE	1.055534
BIOCHANIN A	1.731128
TYROTHRICIN	-0.55012
5-NITRO-2-PHENYLPROPYL AMINOBENZOIC ACID [NPPB]	-0.11886
THIMEROSAL	0.006114
MENADIONE	Dead
CAMPTOTHECIN	-0.69368
2,4-DINITROPHENOL	-0.0172
IOPANIC ACID	-0.00506
BRETYLIUM TOSYLATE	2.619769
ISOROTENONE	0.678014
ALEXIDINE HYDROCHLORIDE	-0.26258
HELENINE	0.567623
FENOFIBRATE	0.005063
ALLODEOXYCHOLIC ACID	0.210417
DIFFRATIC ACID	3.296111
PRISTIMEROL	-0.18754
GENTIAN VIOLET	0.032769
FLUFENAMIC ACID	0.067305
SALINOMYCIN, SODIUM	-0.33643
2,4-DICHLOROPHENOXY BUTYRIC ACID	0.848162
AUSTRICINE	2.497006
DIHYDROMUNDULETONE	4.78073
CHLOROACETOXYQUINOLINE	-0.82466
DICHLOROPHENE	-0.42518
2,4-DICHLOROPHENOXYACETIC ACID, METHYL ESTER	0.073228
LASALOCID SODIUM	0.419734
STREPTOMYCIN SULFATE	Dead
DIHYDROROTENONE	Dead
5,7-DIHYDROXY -4-METHYLCOUMARIN	0.512356
MICONAZOLE NITRATE	-0.45384
PHOSALONE	-0.78845
2,4,5-TRICHLOROPHENOXY ACETIC ACID, METHYL ESTER	-0.17483
LOVASTATIN	Dead
CEAROIN	3.400961
SODIUM MECLOFENAMATE	-0.30543
SWIETENOLIDE-3-ACETATE	-0.19976
CHAULMOOGRIC ACID	-0.12596
PURPUROGALLIN	0.178938

IRIGENIN, 7-BENZYL ETHER	0.109866
2-ISOPROPYL -3-METHOXYCINNAMIC ACID	5.197216
CHRYSIN	-0.05914
BITHIONOL	0.682409
TOLFENAMIC ACID	Dead
ARISTOLOCHIC ACID	Dead
PIMPINELLIN	6.305521
MUNDOSERONE	5.359913
NIFLUMIC ACID	-0.07982
MEBENDAZOLE	-0.06668
TETRACHLORO ISOPHTHALONITRILE	-0.35993
STROPHANTHIDINIC ACID LACTONE ACETATE	0.298596
GANGALEOIDIN	3.869896
CETYLPYRIDINIUM CHLORIDE	4.975765
CETRIMONIUM BROMIDE	-0.10047
RESVERATROL	-0.19057
TOTAROL	-0.30679
DIGITONIN	0.668805
TETRAHYDROGAMBOGIC ACID	2.609897
NARASIN	Dead
TRIPTONIDE	Dead
LAPACHOL	1.043109
CENTAUREIN	0.536003
SAPINDOSIDE A	0.456019
CARPROFEN	0.039279
EBSELEN	-0.27125
ABIETIC ACID	-0.19761
CHLORHEXIDINE	-0.6492
DEQUALINIUM CHLORIDE	0.105634
TRIPTOPHENOLIDE	-0.11735
QUINALIZARIN	-0.21139
TOMATINE	-0.07974
FENBENDAZOLE	0.646859
GITOXIN	-0.2239
alpha-MANGOSTIN	-1.47223
CANTHARIDIN	0.081654
MEFENAMIC ACID	-0.16079
CLOTRIMAZOLE	-0.23182
RHODOMYRTOXIN	1.508112
DIHYDROCELASTROL	0.9328
CICLOPIROX OLAMINE	0.831324
2,3,4-TRIHYDROXY-4'-ETHOXYBENZOPHENONE	0.29438
METHAZOLAMIDE	0.39282
CINCHONIDINE	Dead
ROTENONE	-0.88666
CELASTROL	-0.48844
OXIBENDAZOLE	0.138023
METHYLBENZETHONIUM CHLORIDE	0.302485
PEUCEDANIN	0.207656
LAWSONE	0.900563
ORTHOTHYMOTINIC ACID	0.280902
MUNDULONE	Dead
ETHAVERINE HYDROCHLORIDE	0.955627
THIOXOLONE	0.108306
ATORVASTATIN CALCIUM	-1.36484
PODOFILOX	0.386172
PERILLIC ACID (-)	-0.56323
ROTENONIC ACID, METHYL ETHER	1.145131
LASALOCID SODIUM	0.419734
STREPTOMYCIN SULFATE	Dead
DIHYDROROTENONE	Dead
5,7-DIHYDROXY-4-METHYLCOUMARIN	0.512356
MICONAZOLE NITRATE	-0.45384

Table 5.2: Table of the SSMD scores for all the compounds screened at 1µM after showing double deaths when screened at 10µM. Compounds in Blue showed fluorescence activation, compounds in yellow show weak fluorescence inhibition and in green are strong fluorescence inhibitors.

5.6 Fluorescent activators secondary screening

Secondary screens were performed on DsRed stress response activators to identify molecules which were up-regulating the heat shock pathway whilst not causing increased stress to the fish or which were themselves fluorescent compounds within the DsRed spectrum. To identify these compounds behavioural assays, high-quality imaging and repeat of the fluorescence assay to identify key compounds were carried out. The first step was to repeat the studies on positive compounds to identify molecules that reliably and reproducibly elicited an activation of fluorescence over multiple repeats.

MOLENAME	Run 1	Run 2	Run 3	Run 4	Run 5	Run 6	Run 7	Run 8	Run 9	Run 10	Average
HOMIDIUM BROMIDE	6.396827	6.689371	21.73816	21.44723	Dead	3.471581	4.788994	5.158843	15.10147	11.8838	10.74181
CALCEIN	3.997016	2.785236	9.999373	9.694776	2.009453	1.658812	3.42658	5.496258	2.395518	4.71864	4.618166
RUTILANTINONE	2.999166	3.916562	4.814146	12.90389	1.215844	0.835649	2.529274	2.151867	-0.73832	Dead	3.40312
CHLORPROMAZINE	1.488583	1.066245	2.772024	7.994029	0.060597	Dead	-1.39422	Dead	1.004166	3.141461	2.016611
LIMONIN	1.122029	-0.03397	5.097054	4.145069	0.651337	-0.13047	-0.69939	-0.28813	6.45468	Dead	1.813134
PHYSOSTIGMINE SALICYLATE	0.0776	1.528533	3.586798	3.454775	-0.19193	0.538117	0.192971	0.078021	Dead	-0.01934	1.027283
CIANIDANOL	0.397759	1.048939	3.887623	1.688016	-0.69614	0.924993	0.26294	1.149957	0.345305	0.366343	0.937574
PROPARGITE	1.285883	-0.59972	3.015325	2.071356	-0.87872	1.956186	Dead	-1.17835	1.737798	Dead	0.926219
CARNOSINE	1.050965	0.473795	1.978939	3.215246	0.287735	-1.29658	1.384113	-0.45397	0.377927	-0.02956	0.698861
NILUTAMIDE	0.086437	-0.92154	4.772653	2.964873	-1.16332	-0.41605	-0.08654	0.346422	-0.63908	1.997213	0.694108
DIBENZOTHIOPHENE	-0.32338	-0.2768	1.415953	2.78334	0.167473	0.053839	-0.911	-0.30293	0.683806	3.168134	0.645842
ACTINONIN	0.266308	-0.28969	1.810138	4.858468	0.699677	-0.12704	-0.63374	-0.95399	Dead	-0.20957	0.602286
PROCYCLIDINE HYDROCHLORIDE	1.993583	1.331541	3.208645	3.015796	-1.12629	-3.11901	-0.81584	0.641847	0.547598	0.246074	0.592394
PERUVOSIDE	1.713007	-0.58002	1.693203	3.119057	0.056298	-1.82361	0.082093	Dead	0.384315	0.054683	0.522113
VERATRIDINE	1.260292	Dead	0.906316	0.299598	0.56998	1.883464	-0.20722	-0.34827	-0.13347	-0.44743	0.420361
alpha-CYANO-3-HYDROXYCINNAMIC ACID	0.415802	1.106564	0.681808	1.249509	0.143074	-0.48593	-1.06231	-0.33316	1.296681	0.357584	0.336962
LYCORINE	-0.38303	1.157746	0.796736	0.064862	-0.7829	1.155138	-1.39522	-2.10306	-0.20178	0.524601	-0.11669
RHOIFOLIN	-0.24348	0.264283	0.551793	-1.15153	-1.99778	-1.43523	0.367523	-0.34494	0.656539	0.393259	-0.29396
COSMOSIIN	-0.51688	-0.05422	-1.47677	-0.2432	0.35064	0.339185	-0.3064	-0.53848	-1.17592	Dead	-0.40245
MANDELIC ACID, METHYL ESTER	1.158298	0.562533	-0.30309	-0.19808	-0.29247	-2.85894	-0.11597	-4.51125	0.036285	-0.25195	-0.67746

Table 5.3: Replicate screen of the twenty compounds that led to the strongest fluorescence activation. The table shows the fluorescence readout from ten G93Ros10 zebrafish dosed with the respective compound from 48hpf to 6dpf. Dead fish are highlighted in Red and compounds with an SSMD of >1.0 highlighted in blue.

It was found that a majority of the compounds which repeatedly showed a significant increase in fluorescence were naturally orange and red in nature and therefore expressed a natural fluorescence which overlapped with the emission spectrum of DsRed. Compounds such as Calcein (commonly used as an orange dye) and Homidium bromide (Red colour) showed up as having a strong signal but this was most likely due to the compound being taken up by the fish and building up or staining the fish tissue rather than an increase in hsp70 leading to DsRed overexpression. Further work is needed on the activators to identify which compounds are having a genuine effect in increasing the DsRed fluorescence via hsp70 and which compounds are just inducing stress or are fluorescent. One potential experiment would be to plate the DsRed protein and measure baseline fluorescence before adding the activator compounds to the plate. The genuine hsp70 inducers and compounds that cause stress should have no effect on the fluorescence as there is no target to act on, but any fluorescent molecules will lead to an increase in fluorescence which can be detected and these compounds can be disregarded from further analysis. This assay could also be used to identify compounds that are quenching the fluorescence signal rather than reducing stress.

5.7 Utilising a derivative of Arimoclomol to investigate heat shock protein activation

An amine derivative of Arimoclomol, an activator of the heat shock proteins highlighted as a potential future therapeutic for ALS, was synthesised and screened in the zebrafish. Unfortunately Arimoclomol was not available at the time of the study and so a derivative was used. The aim was to show if this derivative of Arimoclomol induced an increase in fluorescence via activation of the heat shock response. The difference between the derivative used and Arimoclomol was an amine group was present instead of the chlorine group as shown.

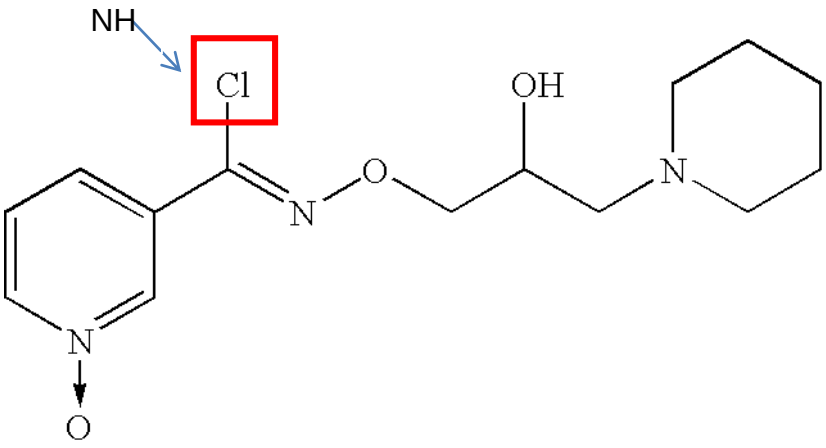

Fig 5.16: Chemical structure for Arimoclomol with the amine for chlorine swap highlighted as is present in the derivative used for this screen. Arimoclomol chemical name is N-{[(2*R*)-2-hydroxy-3-piperidin-1-propyl]oxy}pyridine-3-carboximidoyl chloride 1-oxide, $C_{14}H_{20}ClN_3O_3$, MW-313.78g/mol.

When the drug was screened in the hsp-GFP fish to show that the compound was increasing the fluorescence via the heat shock pathway, no increase in fluorescence was seen at any concentration. This is shown in fig 5.17 where there is no difference in hsp-GFP expression between DMSO treated, 1µM, 10µM and 100µM treatment from 48h-6dpf. All the fish in the experiment were developmentally normal and the compound had no anaesthetic effect. The compound was also screened in the G93Ros10 and WTos4 Sod1 zebrafish to identify an increase in DsRed or a mutant Sod1 specific effect of the Arimoclomol derivative. Both of these transgenic lines showed no increase in hsp70-DsRed expression and the G93Ros10 zebrafish showed no increase in fluorescence when sonicated and analysed. When treated with the derivative, no increase in hsp70 is detected which suggests that this arimoclomol derivative has no effect on the heat shock pathway in zebrafish. The next step to investigate this is to synthesise the halide form of Arimoclomol and check if it has the potential to activate the heat shock response which would be very informative on chemical structures and heat shock protein binding. One potential reason for the lack of effect is that Arimoclomol is a co-inducer of the HSR and is known to stabilise Hsf1 in its tri-merised active form (Kiernan et al, 2004). The compound was screened in a wild type model with only a normal background stress, meaning that active

Hsf1 levels would be very low and thus no large increase would be seen. This experiment should be repeated in the mutant Sod1model in which active Hsf1 levels will be much higher and by stabilisation with Arimoclomol, an increase in heat shock activation will be seen.

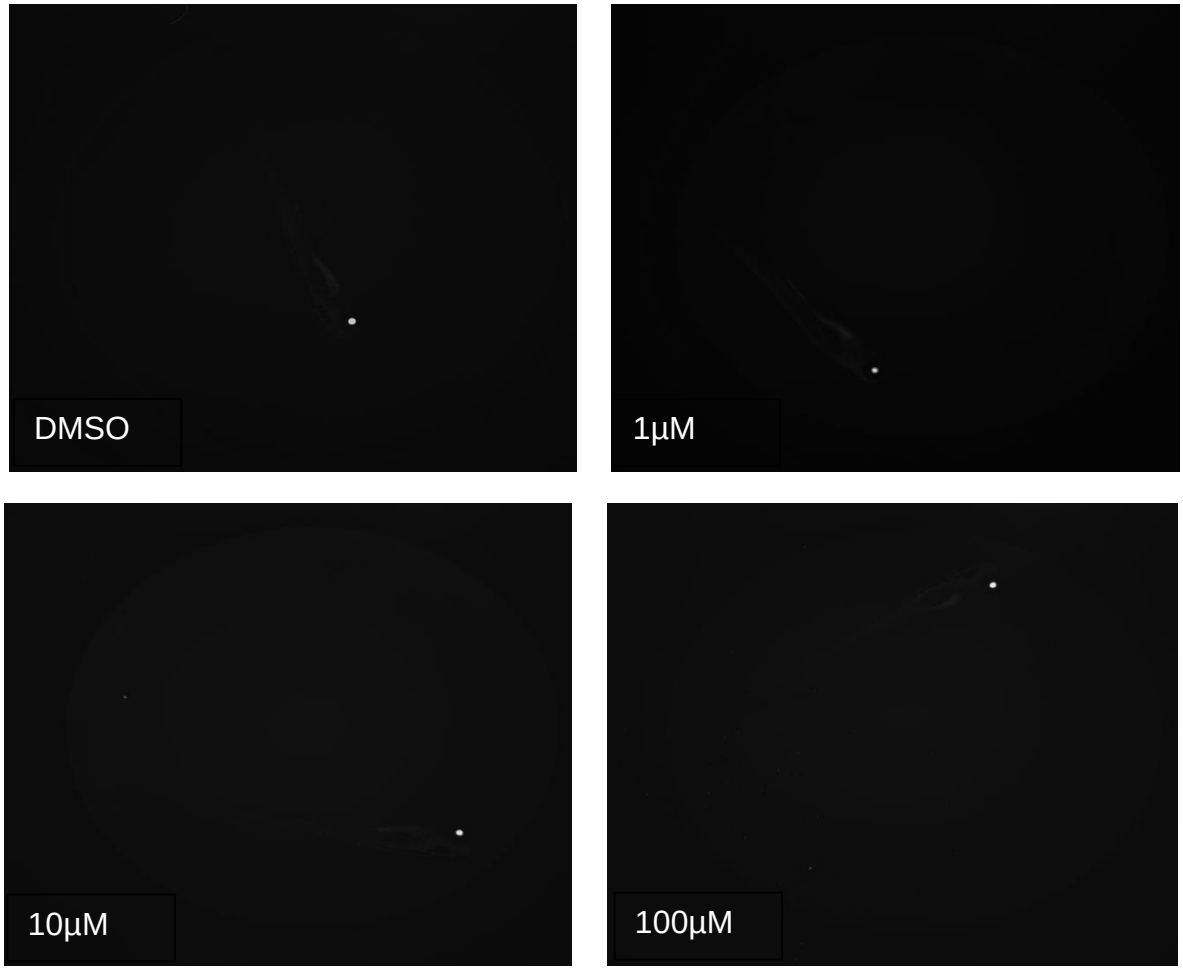

Fig 5.17: Image of hsp-GFP zebrafish dosed with an Arimoclomol derivative from 48hpf-6dpf. No increase in GFP expression is present and the only detectable GFP is in the eye which shows stable expression between all the doses.

5.8 Discussion

In this chapter the aim was to further characterise hit compounds arising from the primary screen on 2000 compounds from the Spectrum library. This is a key part of screening as it involves taking the positive compounds from a high-throughput screen and further validating their activity via multiple techniques to confirm that the drug effect seen in the primary screen was a real effect and not a false positive. Secondary screens have the advantage of a lower number of pre-selected lead compounds and therefore a larger number of low-throughput and intensive screens can be performed to investigate the drug effects. The cost implications of false positives being taken forward are huge and therefore secondary screens to confirm drug effect are essential.

The first confirmation assay was to investigate the fluorescence inhibitors by repeating studies on the best lead compounds (ten times) to confirm that the result from the primary screen was reproducible. Compounds causing a reduction in fluorescence are of particular interest as these may be indicative of a reduction in neuronal stress and therefore hit compounds may have neuroprotective effects within the CNS. The ten repeats were combined with heartbeat measurements and careful inspection for any developmental toxicity to ensure no toxicity or death had occurred which was missed in the original screen. We set our criteria for a hit as showing an inhibition of fluorescence in 9/10 experiments and no more than one death. These criteria were based on Riluzole where 9/10 experiments showed a significant inhibition of fluorescence. This 90% hit ratio is a strong threshold for hit selection. We have shown (Table 5.1) that the majority of the compounds did not show a reproducible effect to match our hit criteria. A large proportion of the compounds showed an increase in fluorescence, a probable side effect of toxicity. Many of the zebrafish that died after being treated with the compounds appeared normal upon visual inspection but were found to have no heartbeat which may explain why they showed low fluorescence in the original screen and were taken forward as hits originally. Based upon the

criteria for hit selection, only one compound was identified as a potential lead compound: Selamectin.

Sold under the trade names Revolution and Stronghold, Selamectin is a topical parasiticide and anti-helminthic compound that is used in the treatment of infections from heartworms, fleas, ear mites, sarcoptic mange and ticks. Selamectin is part of a family of compounds known as macrocyclic lactones and they are widely used in vetinary medicine for the treatment of parasitic diseases (Shoop et al 1995). Many macrocyclic lactones are commercially available for the treatment of parasites in cats and dogs such as the Avermectins, including Ivermectin (HEARTGARD) and Selamectin (STRONGHOLD, REVOLUTION), and the milbemycins such as Moxidectin (ADVOCATE, ADVANTAGE MULTI) and milbemycin oxime (MILBEMAX, PROGRAM PLUS) (Geyer et al 2009).Macrocyclic lactones are generated via semi synthesis from natural fermentation of the by-products from Streptomycetes bacteria.

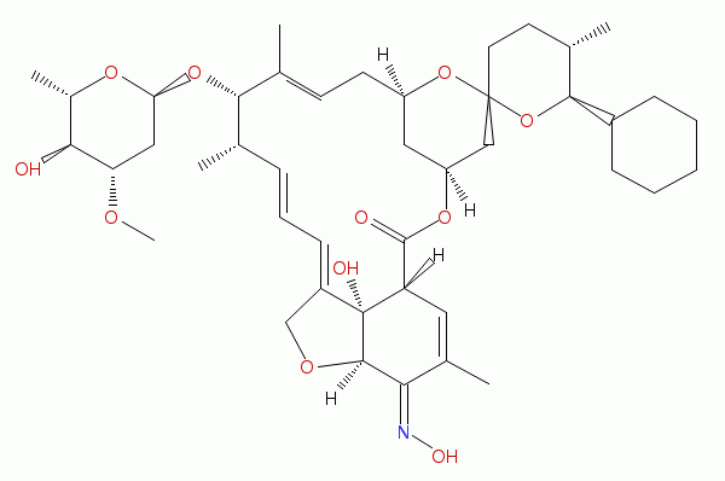

Fig 5.16: Chemical structure of Selamectin. Selamectin formula: $C_{43}H_{63}NO_{11}$. MW: 769.96g/mol (Drawn using www.emolecules.com)

Macrocyclic lactones are thought to have a mechanism of action in treating parasitic infection by inducing neuronal toxicity. It is thought they bind and block GABA gated chloride channels in the central nervous system leading to death (Dawson et al 2000, Sigel & Baur 1987) and activate glutamate-activated chloride ion channels which has been found to lead to ataxia and

death in arthropods (Bloomquist 2003, Martin 1997). In Arthopods the macrocyclic lactones have been shown to interfere with transport along nervous and muscle cells by inhibiting the GABA receptors at the neuromuscular junction in both vertebrates and invertebrates but with 100x more affinity for invertebrate receptors (Schaeffer & Haines 1989). Ivermectin, a compound from the same family as Selamectin, has previously been highlighted as a possible treatment for amyotrophic lateral sclerosis. It was shown that Ivermectin had the ability to reduce AMPA mediated toxicity in cultured rat neurons, a pathway highlighted as leading to ALS disease progression (Andries et al 2007). These authors found in neuronal cultures from 14 day old Wistar rats an 8h pre-incubation treatment with Ivermectin at 1µM led to an almost complete protection from neuronal death by 300µM kainate treatment to induce excitotoxicity. SOD1 mutant G93A mice were then dosed with Ivermectin from 50days of age (Symptom onset) in the drinking water. With 4.8mg/l and 12mg/l of Ivermectin in the drinking water an extension in survival of 8.7 days (6.2%) and 12.8 days (9.1%) respectively was seen. In the lumbar spinal cord, ivermectin was shown to significantly increase the numbers of large ventral neurons and the average root area occupied by neurons.

Ivermectin and other members of the avermectin family of compounds have been shown to bind the glycine receptor chloride channel leading to activation in a dose dependent manner (Lynagh et al 2011).They interestingly found that Selamectin showed a much weaker potency for activation of the α1 glycine receptor compared to Ivermectin and the other related compounds. The study found that Selamectin needed concentrations of 30µM to activate a glycine current in wild type glycine receptors. However they did show that Selamectin potentiates glycine currents suggesting that selamectin binds the receptor with an equal affinity to Ivermectin, but does not have the same affinity to activate the receptor (Lynagh et al 2011). This may suggest that rather than direct activation of the receptor, Selamectin may have more of a modulatory role to control glycine currents.

Macrocyclic lactones are generally regarded as safe for the treatment of mammals as P-glycoprotein efficiency has been shown to restrict the penetration of the blood brain barrier (Schinkel et al 1994). P-Glycoproteins were identified in the mid 1970's and were found to be a drug efflux transporter which is located within the plasma membrane (Juliano & Ling 1976). P-glycoproteins are 170-kDa proteins with six trans-membrane spanning domains and an intracellular ATP binding site which is well conserved and a member of the ABC superfamily of transporters (Borst & Elferink 2002, Higgins 1992). They are expressed in many tissues, with high expression in the major organs of drug absorption, distribution and excretion. Some of the tissues which express high levels of P-glycoprotein include the intestinal epithelial cells, hepatocytes, kidney proximal tubule cells, luminal membrane capillary cells and cells within the blood brain barrier (Thiebaut et al 1987). This has been shown in MDR1 P-glycoprotein negative dogs which showed lower tolerance and higher toxicity to treatment with macrocytic lactone compounds. The studies found that treatment with Ivermectin and Doramectin at 0.2-1.0 mg/kg leading to neurotoxicity, tremor and ataxia (Geyer et al 2007, Hopper et al 2002, Paul et al 1987). This is in contrast to Selamectin, Moxidectin and Milbemycin which at therapeutic doses did not lead to any toxicity in the MDR1 reduced dogs (Bishop et al 2000, Novotny et al 2000, Tranquilli et al 1991).

These data suggest that the different macrocyclic lactones have different affinities for the P-glycoproteins or that they bind different proteins based upon their structure. *In vitro* studies have shown equal transportation of Selamectin and Ivermectin by P-glycoproteins expressing Caco-2 monolayers (human intestinal epithelial cell monolayers) and canine peripheral blood lymphocytes (PBL) which suggests that the difference is not due to affinity for the P-glycoproteins (Griffin et al 2005). This was not confirmed by mdr1a,b P-glycoprotein deficient knockout mice which reported that Selamectin accumulation (5-10 fold higher) in the brain was massively reduced compared to Ivermectin accumulation (36-60 fold higher) in the P-glycoprotein knockout (Geyer et al 2009). This supports a further study which showed that Ivermectin had a much higher ability to modulate the ATPase

activity of P-glycoproteins when compared to Selamectin (Lespine et al 2007). The difference in receptor affinity may be due to the structural differences between Selamectin and Ivermectin. Selamectin has a monosaccharide group whereas Ivermectin has a disaccharide group on the macrocycle which may lead to different abilities to cross the blood brain barrier.

Based upon the literature and the ability to repeatedly reduce the neuronal stress to a similar level as Riluzole, Selamectin was taken forward as a lead molecule for secondary screening. A dose response experiment was undertaken utilising Selamectin to identify the optimal working dose. The dose response showed that Selamectin has no effect on DsRed fluorescence levels at concentrations below 1µM and death was seen at concentrations above 10µM. The IC_{50} was between 3-4µM with a maximum reduction in DsRed fluorescence at 7µM.

These data suggest that the Selamectin has a working concentration range similar to that of Riluzole. For further confirmation of the similarities between Riluzole and Selamectin treatments, 23 embryos treated with DMSO, Riluzole and Selamectin were imaged using the InCell system, analysed using the Pherastar system and overall fluorescence measure using the OMEGAstar system. Fig 5.2 shows when the fish were sonicated and overall fluorescence measured a reduction in DsRed fluorescence of around 50% was seen in both the Riluzole and Selamectin treated (10µm) G93Ros10 zebrafish. Prior to sonication the Pherastar system was used as it is a higher sensitivity system. Fig 5.4 shows the final fluorescence readout from the Pherastar showing a reduction in fluorescence with Riluzole (10µM) of 78% and a reduction in Selamectin (10µM) of 65%. Another interesting observation from the Pherastar using the heat maps of DsRed generated from the 15x15 well scan mode highlighted the high DsRed expression visible in the head region of DMSO treated G93Ros10 zebrafish (fig 5.5). The Selamectin and Riluzole treated zebrafish did not show a strong activation of the DsRed expression in the head region which suggests that these compounds are having an acting in this area and are leading to reduced neuronal stress and heat shock activation.

To further investigate the DsRed expression, the InCell images were analysed to identify which particular cell types and anatomical structures showed the largest reduction in fluorescence. As fig 5.9 shows, the Selamectin and Riluzole treated zebrafish at 10µM had significantly reduced neuronal stress throughout the zebrafish, with the strongest reduction in the hindbrain, spinal cord and eye compared to the DMSO. This reduction in fluorescence was not present in the 1µM Riluzole treated zebrafish which shows that the drug effect is mediated in a dose dependent manner. The hindbrain and spinal cord are key areas of neurodegeneration in ALS with high levels of neuronal stress and loss seen in these areas. Identification of a reduction in hsp70/DsRed activation in these areas is a key indicator that both of these compounds are having a neuroprotective role at these sites and are reducing the neuronal stress leading to lower DsRed expression. Validating that these drugs are acting at these sites provides evidence that both of these compounds are having a positive role within the CNS and are actively working against the Sod1 mediated toxicity and are protecting the stressed neurons.

Further evidence for an effect at a neuronal level is the anaesthetic effect seen using the Viewpoint system. When the behaviour of Selamectin and Riluzole fish at 10µM was measured in light and dark conditions, no movement was seen, suggesting a strong sedative effect of the compounds. Riluzole has sedative effect in both mice and rats with a known role in altering the glutamate neurotransmitter system (Mantz et al 1992). Selamectin is also a known neuromodulator that is known to replace glutamate at the synapse and at high enough concentrations leads to neuromuscular paralysis (Bishop et al 2000). This is of concern when investigating a treatment that may be used for a number of years, so the possibility of combinatorial dosing or Riluzole and Selamectin together at sub sedative doses while maintaining the positive reduction in neuronal stress was investigated. Combination dosing of the compounds identified a range of combinations that had the ability to reduce the fluorescence signal to a comparable level with Selamectin and Riluzole at 10µM (Fig 5.12). This means that side effects could be reduced as lower drug concentrations are

being used and the positive benefit of two compounds effects could mean multiple disease pathways are ameliorated leading to a stronger therapeutic effect. Also the ability of the fish dosed with a lower combination dose to continue to swim shows that in combination the drugs are having less of a sedative effect, suggesting the side effects are being reduced. It also opens up the opportunity to perform adult dosing studies as the fish will be able to swim and feed.

From the primary screen 142 drugs were identified that had a strong toxic effect and led to death in the high-throughput screen. Death from compound toxicity is a sign of developmental toxicity and general zebrafish toxicity which can be observed with many compounds at high concentrations. However these data do not exclude the possibility that the agents may show activity at lower (non-toxic) concentrations. A lower dose of compound is also more beneficial, as giving lower concentrations of drugs as a general rule leads to less unwanted side effects. We re-screened all the compounds that caused death in both primary replicates at 1µM. A small number of the compounds showed death at both concentrations suggesting that these agents are generally toxic to zebrafish and thus they were excluded from any further screens. A number of compounds at the lower dose led to an increase in fluorescence, suggesting that they are still having a toxic effect on the zebrafish but that the effect is not strong enough to cause death, just an increase in stress leading to hsp70 activation. The majority of the compounds led to a non-significant effect which suggests at 1µM dose they are no longer inducing stress via toxicity but also have no role in reducing neuronal stress as they did not achieve a significant SSMD score. A small collection of the compounds at 1µM did achieve a significant reduction in fluorescence. These compounds are of interest as they have the potential to be used at lower concentrations where they may show reduced toxicity. The next step for these compounds will be to repeat the screen multiple times to ensure the reproducibility of these results and that a true effect was seen, before dose response studies carried out to identify an optimal therapeutic window. It is important to be careful with any results from these compounds as they are toxic at higher concentrations and care must be taken to ensure

that it is not toxicity to the fish that gives rise to the reduction in DsRed expression, rather than a reduction in neuronal stress resulting in lower hsp70 activation.

Activators of the heat shock response are of interest as they potentially hold the key to helping the cell protect itself from neuronal stress (Kalmar & Greensmith 2009). Compounds that induce a big increase in the heat shock response may allow the cell to overcome the Sod1 mediated toxicity and use the cells own mechanisms to protect it from neuronal stress. The heat shock response has been highlighted as a possible pathway in neuroprotection and in ALS. Heatshock proteins including HSP70 have a role in preventing protein aggregation and the formation of non-functional proteins and thus have a key role in preventing the cells from damage and stress, both seen in ALS (Takeuchi et al 2002). HSP70 overexpression has been shown to be neuroprotective in mice with delayed symptom onset, increased survival and maintained function, while treatment with Arimoclomol, an activator of HSP70, also showed similar results (Gifondorwa et al 2012, Kalmar et al 2008).

Based upon the positive effect of activation of the heat shock response seen in other ALS models, activators of the fluorescence in our screen were taken forward for secondary analysis to identify true heat shock activators. The top twenty strongest activators of fluorescence from both replicates were taken forward for secondary analysis to identify true activators of fluorescence. The majority of the compounds screened had large variability in inducing the heat shock response which suggests they were more likely inducing mild toxicity to increase fluorescence rather than an increase in heat shock activation. Also, some induced death in a large number of the repeats also suggesting a toxic function of the compound in the zebrafish. Four compounds had the ability to repeatedly induce a large increase in fluorescence in the G93Ros10 model. These four activators of fluorescence revealed natural fluorescence in the orange-red spectra. Homidium Bromide, has intense orange fluorescence as does Rutilantinone which is bright red in colour. Calcein is another fluorescent dye which has the appearance of orange crystals. Chlorpromazine is an interesting candidate molecule as it is a dopamine

antagonist used in psychotic disorders with known antiadrenergic, anticholinergic and anti-serotonergic effects and has a role in the CNS. In the replicates secondary screen Chlorpromazine led to a few deaths and thus the compound was not taken forward for secondary screening although it is of interest as it is a compound with known CNS effects. In general the activators are a difficult group of compounds to validate as an increase in fluorescence can translate too many different biochemical changes, not all of which are beneficial.

In future work the secondary assays must be carefully designed and developed to give the assays the ability to distinguish between fluorescent molecules, toxic compounds leading to neuronal stress and true activators of the heat shock response. It is more likely that the strongest activators of fluorescence are not the key group to investigate as these are more likely due to side effects of the compound or natural fluorescence which leads to an abnormally large increase in DsRed expression. Some of the weaker activators are possibly much more likely to be having a real effect on heat shock protein levels by inducing a moderate increase in fluorescence which is more indicative of an increase in heat shock protein rather than general stress due to off target effects. Another key experiment that needs to be performed for all hit compounds is to confirm that the reduction in fluorescence is not as a result of toxicity and neuronal loss. If the cells are dying then a false readout of a reduction in stress will be seen. To confirm that the drug is not having a toxic effect cell counts and TUNEL assays can be performed to ensure that the level of cell death/loss is comparable between mutant and WT fish.

Arimoclomol is a compound that has been shown to activate the heat shock response and has been shown to have a neuroprotective effect in mutant SOD1 mice (Kalmar et al 2008). The compound was identified as a potential validation compound to show activation of the heat shock response and could be used as a potential positive control for activators. Unfortunately the compound is currently in clinical trials (Clincialtrials.gov No: NCT00706147) and obtaining the compound from any source was not possible. The compound was synthesised as per the protocol stated within the patent but

the final synthesis step, swapping the amine for chlorine, was not completed. Unfortunately the Arimoclomol derivative showed no effect in multiple zebrafish lines with and without mutant Sod1. This raises some interesting questions based upon the chemical structure and difference between Arimoclomol and the derivative. The next step in this project is to synthesise the halide version of Arimoclomol and see if this has the ability to activate the heat shock response in the zebrafish. If the compound has no effect, then it demonstrates that this class of chemical does not have the ability to induce the heat shock response in zebrafish. If activation is seen with Arimoclomol, it will be very informative about the chemistry of the compound and the importance of the chlorine in binding heat shock proteins as well as identifying a positive control for screening activators using the hsp70-DsRed readout.

In conclusion we have identified a compound showing a genuine effect in reducing fluorescence to a similar level as the current treatment for ALS, Riluzole. In repeated screening Selamectin showed an ability to reduce neuronal stress consistently and had a dose dependent effect.

Chapter 6: Discussion

The need for new and improved models that more closely mimic the human aspects of disease is a constant theme in many neurodegenerative disorders, but particularly in ALS. Many of the current models have limitations that impact on their applicability for modelling disease and for screening and identifying novel therapeutic compounds. The SOD1 G93A mouse was the first mouse model generated for ALS and it exhibits many of the physical symptoms of ALS such as hind limb tremor and muscular weakness, together with changes at the cellular level where motor neuron loss and NMJ defects are seen. One limitation of the mouse model is how early the symptoms become apparent which is followed by death within 4 months (normal life span is ~2years). As a result, many of the symptoms occur early in age compared to the disease progression seen in human ALS patients where the disease occurs in later life. This brings into question how applicable it is to use this mouse to model disease and identify therapeutics and highlights the continued need for new models of ALS. These mice have SOD1 activity approximately 11 times higher than normal due to the large gene copy numbers. In terms of drug discovery and development in ALS, the major disappointment of the mouse models has been the inability to translate a positive drug effect in the mouse to a positive effect in a human clinical trial. Many compounds have shown a positive effect in increasing survival and delaying onset in the mouse but have failed to show similar effects in humans. An analysis of over 30 compounds identified in mouse trials has failed to show a positive effect in a human clinical trial of ALS. Some of this poor translation may be attributed to poor study design and the limitations of the model. With clinical trials costing in excess of $100 million, few pharmaceutical houses are likely to embark on clinical studies based solely on the findings from the SOD1 transgenic mouse model.

In an attempt to ameliorate this issue we have developed and characterised a zebrafish model of motor neuron disease which closely resembles the human disease at both cellular and physiological levels. In the later stages of life this model shows reduced motor neurons numbers in the spinal cord

alongside increased numbers of abnormal neuromuscular junctions. Both of these features are seen in both the mouse and human disease. In the zebrafish this corresponds to reduced swimming ability which in mammalian models manifests as the decreased motor performance seen in mouse, rat and human SOD1 ALS patients. This is further validation that this zebrafish model closely mimics the phenotypes seen in both the mouse and human forms of SOD1 mediated ALS.

One of the major advantages of using zebrafish is the optical clarity of the embryos and the ability to image the tissues easily. This has allowed the investigation of the cellular changes occurring in the zebrafish in real time. An interesting finding from the zebrafish model was the identification of the stress response within the interneurons and not the motor neurons at the early stages. The motor neurons in the spinal cord did not show the stress response until later stages in adulthood. This raises the possibility that ALS is not primarily a disease of the motor neuron in the early stages, but an interneuron disorder. Normal interneuron function is to provide control to the motor neurons either by inhibitory or excitatory signals which control the firing properties of motor neurons. In ALS, interneurons have been postulated as being deregulated with evidence of widespread loss of GABA inhibitory interneurons in the motor cortex and fronto-temporal regions (Maekawa et al 2004, Nihei et al 1993).

Neurophysiological studies can be used to probe interneuron function by measuring the delivery of paired stimuli for a response time. In sporadic ALS cases this has been used to identify increased excitability in the cortical neurons which suggests a similar pathway to the Sod1 zebrafish data where loss of interneuron inhibition may lead to over excitation in the motor neurons (Yokota et al 1996). Longitudinal studies of asymptomatic SOD1 carriers show a big increase in excitability just before the onset of ALS symptoms (Vucic et al 2008). Further evidence for the role of interneurons in the disease pathway is seen in patients carrying D90A SOD1 mutations associated with slow disease progression that have preserved inhibitory interneuron circuits which suggests that the loss of inhibition by the

interneurons precedes the onset of the disease symptoms (Weber et al 2000, Wittstock et al 2007).

In ALS there is a broad range of evidence for inhibitory interneuron loss preceding motor neuron dysfunction as a key pathway in ALS pathogenesis. This zebrafish model along with patient data suggests that ALS is potentially an 'interneuronopathy' where the interneurons are most susceptible to the SOD1 toxicity and, once the interneurons are sufficiently stressed and dysfunctional, the motor neurons begin to develop problems and degenerate. This highlights the potential of targeting the interneurons therapeutically to try and ameliorate and delay the disease onset by improving the inhibitory influence, thus restoring the balance. This model has the advantage of being one of the first *in vivo* models to show an interneuronopathy phenotype in ALS.

Future experiments are planned, aiming to characterise the cell types affected to further understand exactly which cells are affected at each time point. This will also allow the identification of when the loss of interneurons is sufficient to lead to the activation of the stress response within motor neurons. It will also allow further investigation into the loss of interneurons, coinciding with the onset of motor symptoms in the zebrafish as was seen in the longitudinal patient studies. One advantage of the zebrafish that should be utilised is the generation of a stable interneuron marker transgenic line which would allow real time monitoring of interneurons in the Sod1 model over the disease course to truly monitor the cellular and neuronal network changes occurring in ALS. This could be correlated with the electrophysiological profiles of the glycine positive interneurons in the zebrafish and could give rise to a novel class of potential therapeutics that ameliorate the deterioration in synaptic firing seen in the interneurons.

Therapeutic testing of compounds using zebrafish has long been performed in multiple disciplines including cancer, cardiovascular science and development. It has led to the identification of many compounds that have a toxic effect in zebrafish, as well as compounds that have a positive role in modulating and ameliorating different conditions. In neuroscience, zebrafish

have not been utilised as extensively as in other disciplines. They have the potential to be an excellent model for neuroscience and particularly in CNS disorders as they have a similar neuronal network to humans in both the genetic and anatomical senses. The majority of the screens that have been performed have relied on having to use smaller numbers of compounds combined with difficult final readouts such as behavioural data (Vaccaro et al 2012) which, although informative of the effect of the compound, give little information on the role of the compound at a cellular level. Other investigators have performed large screens, but in a low throughput mechanism such as performing an *in situ* hybridisation or immunohistochemistry screen on every sample to look or for changes in expression of genes (Baxendale et al 2012). Both of these readouts are exciting and innovative ways of detecting compounds having a positive effect in a neurodegenerative model.

However, our mutant Sod1 zebrafish model has the advantage of utilizing an hsp70-DsRed stress marker to monitor cellular dysfunction in real-time. It allows real-time monitoring of drug effect by simple fluorescence microscopy which easily allows the detection of drug effect and the anatomical structures where the compound is acting. This has the potential for utilisation in many different disease models as the hsp70-DsRed construct is separate from the disease modifying gene and therefore can be applied in multiple disorders in neurodegeneration and other fields.

In the zebrafish mutant Sod1 model, the activation of the DsRed response in the absence of heatshock is specific to individual tissues and cell types whereas no activation is seen in the WT Sod1 line. Expression was also seen in the key anatomical areas and cell types affected in ALS and this is further evidence of the DsRed response being a viable readout of cellular toxicity in the model. Further support for utilising the Hsp70-DsRed measurement as readout of Sod1 toxicity is found by using Riluzole, the only compound licensed for the treatment of ALS. The demonstration of a reduction in activation of a key marker of cellular stress following administration of Riluzole is evidence that this model can be used to detect potential novel therapeutics. Riluzole has a modest effect in humans, with an

extension in survival of 3months on average, so the ability to show it having a role in the zebrafish model is key for validating this model. These experiments also highlight the specificity and sensitivity of this construct when used to detect cellular stress in specific tissues, together with the ability to show drug effects. This applicability should allow the DsRed readout to become a key marker in different zebrafish models for screening in the future.

Although no criteria exist for what is designated as a high-throughput screen, the assay outlined in this study is highly optimised, utilising multiple robotic systems to deliver a semi high-throughput compound screen using an *in vivo* model. New technologies have become available that can be implemented to improve throughput, which could give rise to a completely automated screen. The major advance in automation to improve the throughput would be to develop zebrafish handling systems that have the ability to load plates with embryos without the need for human intervention. Automated sorters that rapidly and accurately transfer embryos into assay plates are now becoming more affordable, but until these systems are combined with the technology to select zebrafish based upon DsRed fluorescence, the advantages of implementing these systems in this assay will be minimal as genotyping using the InCell Bioanalyser will still be required.

The high-throughput screen using the transgene as readout is one of the first examples of the utilisation of robotic systems to allow a significant increase in throughput which cannot be achieved with other readouts. Further improvements to the screen would be the adoption of *in silico* screening prior to utilisation of the zebrafish model. *In silico* screens utilise computer algorithms and historical data to predict the effect of a compound. In terms of drug screening, this may mean predicting that if a compound binds at a certain site on an enzyme it will show a response. With these methods, millions of compounds can be screened in a virtual setting for predicted effect. These assays will become more important as the algorithms improve.

Currently the major limitation of these assays is the data that the system begins with. By furthering our understanding of Sod1 and how it acts, then

the *in silico* screen will be improved as more functional data will be available. Screening in a high-throughput fashion is not possible in higher models such as mice due to the difficulty in obtaining high enough numbers of samples for significance, the cost implications and the duration of the assays. Cellular based assays and lower organisms allow high-throughput assays on well characterised systems but they lack the complexity of higher organisms with only single cell types or simple organisation of the nervous system. The zebrafish has advantages as a model as it has a CNS closer to that seen in humans together with rapid development, optical clarity, ease of compound administration plus the ability to obtain large numbers of embryos rapidly. All of these factors make zebrafish an excellent candidate as an *in vivo* model capable of bridging between cellular assays and higher mammalian organisms such as the mouse.

The zebrafish will not be able to replace therapeutic screening in the mouse but the zebrafish has the ability to compliment mouse models by rapidly providing information on how compounds may be acting, identifying efficacious dose ranges and at what anatomical sites the drug is acting, which means that subsequent mouse and/or human studies can be better designed. The zebrafish model also allows the identification of lead molecules which can be screened in the mouse, bridging the large jump in development and complexity between cell and mouse. Data from the zebrafish model will give greater confidence in mouse screens, as drugs will have previously shown effects in another *in vivo* model. This will reduce the time, cost and most importantly the number of mice needed to identify new therapeutic agents undergoing pre-clinical screening.

Riluzole was originally identified for its anaesthetic and anticonvulsant properties (Wokke 1996). Its ability to help treat ALS is most likely thought to stem from its anti-glutamatergic action by stopping the excitotoxicity from excessive glutamate. Further evidence for this mechanism comes from spinal cord injury models where glutamate excitotoxicity is known to cause problems and treatment with Riluzole has been shown to reduce the damage (Dumont et al 2001). Its anti-glutamatergic effect is thought to be mediated by inhibition of Na+ channels causing reduction of pre-synaptic

glutamate release (Chéramy et al 1992). This pathway has been brought into question by the failure of other anti-glutamatergic treatments that do not show the same effect as Riluzole in ALS or spinal cord injury. This suggests that Riluzole is acting by other mechanisms to prevent motor neuron loss. Elucidating these other pathways and developing a better understanding of how Riluzole is acting in ALS will facilitate the identification and development of future therapeutic agents.

Riluzole has been shown to upregulate glutamate transporters levels in glial cells suggesting a new role in glutamate uptake modulation (Carbone et al 2012). Riluzole treatments from 0.1µM- 10µM have been shown to increase glutamate receptor affinity while higher concentrations such as 100µM had no effect and even increased toxicity in response to acute glutamate exposure (Frizzo et al 2004).

Another potential therapeutic pathway for ALS is via suppression of neuronal excitability by modulation of the sodium current. Neuronal excitability has been postulated as a causative factor in ALS. The voltage gated sodium channels affected by Riluzole are abundant in interneurons and motor neurons (Harvey et al 2006, Tazerart et al 2007) and thus this may explain the beneficial effect of Riluzole in the zebrafish screen. Riluzole has been shown to modulate these neurons by stopping repetitive firing of action potentials. However, this pathway is brought into question as a sodium channel blocker, tetrodotoxin, failed to stop neurodegeneration induced by glutamate excitotoxicity (Mazzone & Nistri 2011).

One of the most important discoveries in the work of this thesis was the identification of Selamectin as a novel therapeutic agent for the treatment of ALS. There is a desperate need for new compounds to treat and delay the disease progression in ALS and Selamectin may have the ability to fulfil this role. Selamectin is a macrocyclic lactone, with a known modulator function for GABA and glutamate receptors. Selamectin and other macrocyclic lactones are currently marketed worldwide as a treatment for parasite infections in animals. Its proposed mechanism of action in disabling the

parasites is by replacing glutamate at the muscle synapse and activating chloride channel opening leading to neuromuscular paralysis. GABA is a major inhibitory neurotransmitter in the CNS and has a major role in controlling neuronal excitability, including in motor neurons. As previously discussed, inhibitory interneurons are implicated in the development of ALS and thus the known effects of Selamectin on these receptor subtypes suggest that it may have a beneficial role in protecting the interneurons. Selamectin is most likely re-establishing and boosting the capacity of the interneurons to provide inhibitory signals to the motor neurons. If this is the case then over time there should be a continued reduction in fluorescence and a protection of the motor neurons.

The mechanisms of action of Riluzole and Selamectin show lots of crossover and appear to act via similar pathways. Both are known to modulate AMPA receptors which are involved in excitotoxicity, a mechanism in ALS. Both are also implicated as modulators of GABA and glycine currents which have been implicated as involved in ALS disease progression. This highlights the strong pathway crossover of the compounds and highlights an excitotoxicity mechanism of action for both drugs. This does not mean that the drug should not be further investigated as it may be more potent, affect different receptors and has the potential to be used in combination with Riluzole.

It is important to remember that these treatments are focused on altering the disease in the early stages. The embryos are treated at 24h and 48h whereas a human patient will not begin treatment until the symptoms have manifested and are clear enough for a diagnosis on ALS. This is the true battle for ALS as many of the compounds which have a positive effect at the early pre-symptomatic stages may have no role once the motor neurons have been lost and the symptoms have begun. If the cells have already been lost due to SOD1 toxicity, then no drug can prevent disease progression. This highlights the need for the generation and identification of new and novel techniques as well as a panel of biomarkers to screen for ALS.

Biomarkers are measurable biological changes that reflect a specific disease state such as a change in gene expression or the presence of a specific

antibody. If a panel of specific ALS biomarkers could be identified for use with an easily accessible tissue sample such as blood or CSF then screening for pre-symptomatic ALS patients could be performed and treatments undertaken at earlier stages. This may mean that compounds such as Riluzole and Selamectin have a stronger effect as well the possibility that compounds which failed pervious trials may be effective at earlier stages.

One potential biomarker for ALS is from microRNAs (miRNAs) which are small RNA molecules with a regulatory role. They have been shown to have altered levels in multiple disease subtypes including in neurodegeneration. Multiple miRNAs have been shown to be up and/or down regulated in ALS as well as other diseases, so a panel would need to be designed which is specific to ALS and will allow the identification of the disease before symptom onset (Goodall et al 2013). Biomarkers, once validated, will also have the ability to show if a particular treatment regime is effective, as an efficacious treatment could lead to restored biomarker levels back to a baseline over time. Biomarkers are a rapidly advancing and exciting field of research and have great potential in the diagnosis and treatment of ALS, as well as for the development of therapeutics. ALS has the potential to become a manageable disease if biomarker monitoring is combined with personalised medicine. This could result in the disease being sufficiently slowed down so that it may never progress far enough for the onset of symptoms to occur. Thus ALS would become a ‘chronic’ disease whereby continuous therapy would enable the patient to live an extended or even normal lifespan.

A potential treatment option may be to use stem cells to replace the cells lost in ALS. Cell therapies and stem cells can be implemented to supply trophic support in an attempt to protect the stressed cells. The possibility of inserting stem cells into the affected spinal cord before using trophic factors to force differentiation into motor neurons could potentially allow the reversal of the ALS disease. This has been shown in mouse models where stem cell insertion into the spinal cord led to a significant delay in symptom onset and a significant increase in survival (Kim et al 2013).These therapies are still unproven as insertion has been shown to be safe into the spinal cord (Feldman et al 2014) but no positive effects on disease progression have

been seen In human patients and this may be due to the environment of insertion already being too toxic.

Zebrafish have a relatively well characterised capacity to regenerate, including within the CNS. This has been shown in multiple organs such as in limb wound models and in the heart where wounds are shown to quickly heal before regeneration occurs at the site of injury. Clearly this is not possible in humans. Multiple regeneration factors have been identified such as FGF-1 which can lead to regeneration of tissues that have been damaged or lost. This is a fascinating process that does not happen in the human. If these markers could be utilised in the human then there is the possibility of being able to induce regeneration by expressing these factors. The ability of the zebrafish to regenerate brings into question their ability to model a degenerative disorder. Although the Sod1 mutant zebrafish has the ability to regenerate, it is still possible to model the degeneration of motor neurons as can be seen by their loss in the adult spinal cord. The regeneration of the model may make it easier to model these diseases as the process of degeneration will be slowed and therefore easier to investigate. Further research into the effects of regeneration is required and it will be interesting to look at which regenerative factors/markers colocalise with the degeneration of the motor neurons.

Another potential intervention is gene therapy to knock down the expression of disease-causing mutant genes. This could be particularly useful in SOD1 mediated ALS where knockdown of SOD1 has been shown to slow disease progression. AAV9 viral mediated knockdown of mutant SOD1 led to increased survival and reduced disease progression in SOD1 mouse models (Foust et al 2013). AAV9 targets the knockdown to motor neurons specifically alongside astrocytes. There is evidence that knocking down mutant SOD1 in motor neurons and astrocytes protects against ALS. This is currently being further validated in primate models with the goal of starting clinical trials in humans in the near future.

Future work in this project is to take Selamectin and Riluzole forwards as a combination therapy for the treatment of ALS. Initial experiments should be

focused on elucidating the role of the compounds and the effect they have. A better understanding of the disease and how these compounds act to ameliorate the symptoms/progression will allow the design of better drugs. By using combination dosing, it may be possible to have the beneficial effects of both drugs to boost the neuroprotective effect while removing the negative sedative side effects known to arise from these compounds. The sedative effects arise from the inhibition of sodium channels which inhibit action potentials. Combinations of these drugs at lower concentrations has been shown to be less sedative than either drug at higher concentrations individually with the fish showing small amounts of movement in the absence of stimulus. This will allow long term treatments to study the benefit of prolonged exposure to the drugs. If Riluzole is having a sedative effect in human patients then by reducing this via combination with other therapies patients may give rise to improvement in their condition as sedation is reduced.

In conclusion we have designed, validated and implemented an innovative and novel high-throughput drug screen to identify novel therapeutics to treat ALS, using a zebrafish *in vivo* model. Utilising this model we have identified pathways involved in the disease progression, novel ways to screen drug effect in zebrafish and a potential new treatment for ALS.

References

Abhinav K, Stanton B, Johnston C, Hardstaff J, Orrell RW, et al. 2007. Amyotrophic lateral sclerosis in South-East England: a population-based study. The South-East England register for amyotrophic lateral sclerosis (SEALS Registry). *Neuroepidemiology* 29: 44-8

Adams MD, Celniker SE, Holt RA, Evans CA, Gocayne JD, et al. 2000. The genome sequence of Drosophila melanogaster. *Science* 287: 2185-95

Aggarwal S, Cudkowicz M. 2008. ALS drug development: reflections from the past and a way forward. *Neurotherapeutics* 5: 516-27

Andries M, Van Damme P, Robberecht W, Van Den Bosch L. 2007. Ivermectin inhibits AMPA receptor-mediated excitotoxicity in cultured motor neurons and extends the life span of a transgenic mouse model of amyotrophic lateral sclerosis. *Neurobiol Dis* 25: 8-16

Arai T, Hasegawa M, Akiyama H, Ikeda K, Nonaka T, et al. 2006. TDP-43 is a component of ubiquitin-positive tau-negative inclusions in frontotemporal lobar degeneration and amyotrophic lateral sclerosis. *Biochem Biophys Res Commun* 351: 602-11

Armon C. 2003. An evidence-based medicine approach to the evaluation of the role of exogenous risk factors in sporadic amyotrophic lateral sclerosis. *Neuroepidemiology* 22: 217-28

Armstrong GA, Drapeau P. 2013. Loss and gain of FUS function impair neuromuscular synaptic transmission in a genetic model of ALS. *Hum Mol Genet*

Arnold ES, Ling SC, Huelga SC, Lagier-Tourenne C, Polymenidou M, et al. 2013. ALS-linked TDP-43 mutations produce aberrant RNA splicing and adult-onset motor neuron disease without aggregation or loss of nuclear TDP-43. *Proc Natl Acad Sci U S A* 110: E736-45

Arundine M, Tymianski M. 2003. Molecular mechanisms of calcium-dependent neurodegeneration in excitotoxicity. *Cell Calcium* 34: 325-37

Ash PE, Bieniek KF, Gendron TF, Caulfield T, Lin WL, et al. 2013. Unconventional translation of C9ORF72 GGGGCC expansion generates insoluble polypeptides specific to c9FTD/ALS. *Neuron* 77: 639-46

Atkin JD, Farg MA, Turner BJ, Tomas D, Lysaght JA, et al. 2006. Induction of the unfolded protein response in familial amyotrophic lateral sclerosis and association of protein-disulfide isomerase with superoxide dismutase 1. *J Biol Chem* 281: 30152-65

Atkin JD, Farg MA, Walker AK, McLean C, Tomas D, Horne MK. 2008. Endoplasmic reticulum stress and induction of the unfolded protein response in human sporadic amyotrophic lateral sclerosis. *Neurobiol Dis* 30: 400-7

Ayala YM, De Conti L, Avendaño-Vázquez SE, Dhir A, Romano M, et al. 2011. TDP-43 regulates its mRNA levels through a negative feedback loop. *EMBO J* 30: 277-88

Baird GS, Zacharias DA, Tsien RY. 2000. Biochemistry, mutagenesis, and oligomerization of DsRed, a red fluorescent protein from coral. *Proc Natl Acad Sci U S A* 97: 11984-9

Barbeito LH, Pehar M, Cassina P, Vargas MR, Peluffo H, et al. 2004. A role for astrocytes in motor neuron loss in amyotrophic lateral sclerosis. *Brain Res Brain Res Rev* 47: 263-74

Barber SC, Higginbottom A, Mead RJ, Barber S, Shaw PJ. 2009. An in vitro screening cascade to identify neuroprotective antioxidants in ALS. *Free Radic Biol Med* 46: 1127-38

Basso M, Massignan T, Samengo G, Cheroni C, De Biasi S, et al. 2006. Insoluble mutant SOD1 is partly oligoubiquitinated in amyotrophic lateral sclerosis mice. *J Biol Chem* 281: 33325-35

Baxendale S, Holdsworth CJ, Meza Santoscoy PL, Harrison MR, Fox J, et al. 2012. Identification of compounds with anti-convulsant properties in a zebrafish model of epileptic seizures. *Dis Model Mech* 5: 773-84

Beck J, Poulter M, Hensman D, Rohrer JD, Mahoney CJ, et al. 2013. Large C9orf72 hexanucleotide repeat expansions are seen in

multiple neurodegenerative syndromes and are more frequent than expected in the UK population. *Am J Hum Genet* 92: 345-53

Beers DR, Henkel JS, Zhao W, Wang J, Appel SH. 2008. CD4+ T cells support glial neuroprotection, slow disease progression, and modify glial morphology in an animal model of inherited ALS. *Proc Natl Acad Sci U S A* 105: 15558-63

Benatar M. 2007. Lost in translation: treatment trials in the SOD1 mouse and in human ALS. *Neurobiol Dis* 26: 1-13

Bensimon G, Lacomblez L, Meininger V. 1994. A controlled trial of riluzole in amyotrophic lateral sclerosis. ALS/Riluzole Study Group. *N Engl J Med* 330: 585-91

Bento-Abreu A, Van Damme P, Van Den Bosch L, Robberecht W. 2010. The neurobiology of amyotrophic lateral sclerosis. *Eur J Neurosci* 31: 2247-65

Bergemalm D, Forsberg K, Jonsson PA, Graffmo KS, Brannstrom T, et al. 2009. Changes in the spinal cord proteome of an amyotrophic lateral sclerosis murine model determined by differential in-gel electrophoresis. *Mol Cell Proteomics* 8: 1306-17

Bertrandy S, Burlet P, Clermont O, Huber C, Fondrat C, et al. 1999. The RNA-binding properties of SMN: deletion analysis of the zebrafish orthologue defines domains conserved in evolution. *Hum Mol Genet* 8: 775-82

Bilsland LG, Nirmalananthan N, Yip J, Greensmith L, Duchen MR. 2008. Expression of mutant SOD1 in astrocytes induces functional deficits in motoneuron mitochondria. *J Neurochem* 107: 1271-83

Bishop BF, Bruce CI, Evans NA, Goudie AC, Gration KA, et al. 2000. Selamectin: a novel broad-spectrum endectocide for dogs and cats. *Vet Parasitol* 91: 163-76

Bloomquist JR. 2003. Chloride channels as tools for developing selective insecticides. *Arch Insect Biochem Physiol* 54: 145-56

Boillée S, Yamanaka K, Lobsiger CS, Copeland NG, Jenkins NA, et al. 2006. Onset and progression in inherited ALS determined by motor neurons and microglia. *Science* 312: 1389-92

Borasio GD, Gelinas DF, Yanagisawa N. 1998. Mechanical ventilation in amyotrophic lateral sclerosis: a cross-cultural perspective. *J Neurol* 245 Suppl 2: S7-12; discussion S29

Bordet T, Buisson B, Michaud M, Drouot C, Galea P, et al. 2007. Identification and characterization of cholest-4-en-3-one, oxime (TRO19622), a novel drug candidate for amyotrophic lateral sclerosis. *The Journal of pharmacology and experimental therapeutics* 322: 709-20

Borst P, Elferink RO. 2002. Mammalian ABC transporters in health and disease. *Annu Rev Biochem* 71: 537-92

Bosco DA, Morfini G, Karabacak NM, Song Y, Gros-Louis F, et al. 2010. Wild-type and mutant SOD1 share an aberrant conformation and a common pathogenic pathway in ALS. *Nat Neurosci* 13: 1396-403

Bourke SC, Bullock RE, Williams TL, Shaw PJ, Gibson GJ. 2003. Noninvasive ventilation in ALS: indications and effect on quality of life. *Neurology* 61: 171-7

Bowman TV, Zon LI. 2010. Swimming into the future of drug discovery: in vivo chemical screens in zebrafish. *ACS Chem Biol* 5: 159-61

Boyd JD, Lee-Armandt JP, Feiler MS, Zauur N, Liu M, et al. 2013. A High-Content Screen Identifies Novel Compounds That Inhibit Stress-Induced TDP-43 Cellular Aggregation and Associated Cytotoxicity. *J Biomol Screen*

Bretaud S, Allen C, Ingham PW, Bandmann O. 2007. p53-dependent neuronal cell death in a DJ-1-deficient zebrafish model of Parkinson's disease. *J Neurochem* 100: 1626-35

Brotherton TE, Li Y, Cooper D, Gearing M, Julien JP, et al. 2012. Localization of a toxic form of superoxide dismutase 1 protein to pathologically affected tissues in familial ALS. *Proc Natl Acad Sci U S A* 109: 5505-10

Cai H, Lin X, Xie C, Laird FM, Lai C, et al. 2005. Loss of ALS2 function is insufficient to trigger motor neuron degeneration in knock-out mice but predisposes neurons to oxidative stress. *J Neurosci* 25: 7567-74

Campbell WA, Yang H, Zetterberg H, Baulac S, Sears JA, et al. 2006. Zebrafish lacking Alzheimer presenilin enhancer 2 (Pen-2) demonstrate excessive p53-dependent apoptosis and neuronal loss. *J Neurochem* 96: 1423-40

Carbone M, Duty S, Rattray M. 2012. Riluzole elevates GLT-1 activity and levels in striatal astrocytes. *Neurochem Int* 60: 31-8

Chang G, Guo Y, Jia Y, Duan W, Li B, et al. 2010. Protective effect of combination of sulforaphane and riluzole on glutamate-mediated excitotoxicity. *Biol Pharm Bull* 33: 1477-83

Chang Q, Martin LJ. 2011. Glycine receptor channels in spinal motoneurons are abnormal in a transgenic mouse model of amyotrophic lateral sclerosis. *J Neurosci* 31: 2815-27

Cheah BC, Kiernan MC. 2010. Dexpramipexole, the R(+) enantiomer of pramipexole, for the potential treatment of amyotrophic lateral sclerosis. *IDrugs* 13: 911-20

Chéramy A, Barbeito L, Godeheu G, Glowinski J. 1992. Riluzole inhibits the release of glutamate in the caudate nucleus of the cat in vivo. *Neurosci Lett* 147: 209-12

Chia R, Tattum MH, Jones S, Collinge J, Fisher EM, Jackson GS. 2010. Superoxide dismutase 1 and tgSOD1 mouse spinal cord seed fibrils, suggesting a propagative cell death mechanism in amyotrophic lateral sclerosis. *PLoS One* 5: e10627

Chio A, Benzi G, Dossena M, Mutani R, Mora G. 2005. Severely increased risk of amyotrophic lateral sclerosis among Italian professional football players. *Brain* 128: 472-6

Chio A, Mora G, Calvo A, Mazzini L, Bottacchi E, Mutani R. 2009. Epidemiology of ALS in Italy: a 10-year prospective population-based study. *Neurology* 72: 725-31

Chuang DM, Leng Y, Marinova Z, Kim HJ, Chiu CT. 2009. Multiple roles of HDAC inhibition in neurodegenerative conditions. *Trends Neurosci* 32: 591-601

Ciura S, Lattante S, Le Ber I, Latouche M, Tostivint H, et al. 2013. Loss of function of C9orf72 causes motor deficits in a zebrafish model of Amyotrophic Lateral Sclerosis. *Ann Neurol*

Clement AM, Nguyen MD, Roberts EA, Garcia ML, Boillée S, et al. 2003. Wild-type nonneuronal cells extend survival of SOD1 mutant motor neurons in ALS mice. *Science* 302: 113-7

Colton CK, Kong Q, Lai L, Zhu MX, Seyb KI, et al. 2010. Identification of translational activators of glial glutamate transporter EAAT2 through cell-based high-throughput screening: an approach to prevent excitotoxicity. *J Biomol Screen* 15: 653-62

Cooper-Knock J, Hewitt C, Highley JR, Brockington A, Milano A, et al. 2012. Clinico-pathological features in amyotrophic lateral sclerosis with expansions in C9ORF72. *Brain* 135: 751-64

Costes SV, Daelemans D, Cho EH, Dobbin Z, Pavlakis G, Lockett S. 2004. Automatic and quantitative measurement of protein-protein colocalization in live cells. *Biophys J* 86: 3993-4003

Coyle JT, Puttfarcken P. 1993. Oxidative stress, glutamate, and neurodegenerative disorders. *Science* 262: 689-95

Cudkowicz ME, Andres PL, Macdonald SA, Bedlack RS, Choudry R, et al. 2009. Phase 2 study of sodium phenylbutyrate in ALS. *Amyotroph Lateral Scler* 10: 99-106

Cushman M, Johnson BS, King OD, Gitler AD, Shorter J. 2010. Prion-like disorders: blurring the divide between transmissibility and infectivity. *J Cell Sci* 123: 1191-201

Da Costa MM, Allen CE, Higginbottom A, Ramesh T, Shaw PJ, McDermott CJ. 2013. A new zebrafish model produced by TILLING of SOD1-related amyotrophic lateral sclerosis replicates key features of the disease and represents a tool for in vivo therapeutic screening. *Dis Model Mech*

Dawson GR, Wafford KA, Smith A, Marshall GR, Bayley PJ, et al. 2000. Anticonvulsant and adverse effects of avermectin analogs in mice are mediated through the gamma-aminobutyric acid(A) receptor. *The Journal of pharmacology and experimental therapeutics* 295: 1051-60

De Maio A. 1999. Heat shock proteins: facts, thoughts, and dreams. *Shock* 11: 1-12

De Vos KJ, Chapman AL, Tennant ME, Manser C, Tudor EL, et al. 2007. Familial amyotrophic lateral sclerosis-linked SOD1 mutants perturb fast axonal transport to reduce axonal mitochondria content. *Hum Mol Genet* 16: 2720-8

DeJesus-Hernandez M, Mackenzie IR, Boeve BF, Boxer AL, Baker M, et al. 2011. Expanded GGGGCC hexanucleotide repeat in noncoding region of C9ORF72 causes chromosome 9p-linked FTD and ALS. *Neuron* 72: 245-56

Devon RS, Helm JR, Rouleau GA, Leitner Y, Lerman-Sagie T, et al. 2003. The first nonsense mutation in alsin results in a homogeneous phenotype of infantile-onset ascending spastic paralysis with bulbar involvement in two siblings. *Clin Genet* 64: 210-5

Di Giorgio FP, Boulting GL, Bobrowicz S, Eggan KC. 2008. Human embryonic stem cell-derived motor neurons are sensitive to the toxic effect of glial cells carrying an ALS-causing mutation. *Cell Stem Cell* 3: 637-48

Doble A. 1996. The pharmacology and mechanism of action of riluzole. *Neurology* 47: S233-41

Dormann D, Haass C. 2011. TDP-43 and FUS: a nuclear affair. *Trends Neurosci*

Doyon Y, McCammon JM, Miller JC, Faraji F, Ngo C, et al. 2008. Heritable targeted gene disruption in zebrafish using designed zinc-finger nucleases. *Nat Biotechnol* 26: 702-8

Drapeau P, Ali DW, Buss RR, Saint-Amant L. 1999. In vivo recording from identifiable neurons of the locomotor network in the developing zebrafish. *J Neurosci Methods* 88: 1-13

Dumont RJ, Okonkwo DO, Verma S, Hurlbert RJ, Boulos PT, et al. 2001. Acute spinal cord injury, part I: pathophysiologic mechanisms. *Clin Neuropharmacol* 24: 254-64

Edgar JM, Nave KA. 2009. The role of CNS glia in preserving axon function. *Curr Opin Neurobiol* 19: 498-504

Eisen A. 2009. Amyotrophic lateral sclerosis: A 40-year personal perspective. *J Clin Neurosci* 16: 505-12

Ekins S, Olechno J, Williams AJ. 2013. Dispensing processes impact apparent biological activity as determined by computational and statistical analyses. *PLoS One* 8: e62325

Ezzi SA, Urushitani M, Julien JP. 2007. Wild-type superoxide dismutase acquires binding and toxic properties of ALS-linked mutant forms through oxidation. *J Neurochem* 102: 170-8

Feldman EL, Boulis NM, Hur J, Johe K, Rutkove SB, et al. 2014. Intraspinal Neural Stem Cell Injections in ALS Subjects: Phase I Trial Outcomes. *Ann Neurol*

Ferrante RJ, Browne SE, Shinobu LA, Bowling AC, Baik MJ, et al. 1997. Evidence of increased oxidative damage in both sporadic and familial amyotrophic lateral sclerosis. *J Neurochem* 69: 2064-74

Fischer LR, Culver DG, Tennant P, Davis AA, Wang M, et al. 2004. Amyotrophic lateral sclerosis is a distal axonopathy: evidence in mice and man. *Exp Neurol* 185: 232-40

Fischer LR, Li Y, Asress SA, Jones DP, Glass JD. 2012. Absence of SOD1 leads to oxidative stress in peripheral nerve and causes a progressive distal motor axonopathy. *Exp Neurol* 233: 163-71

Fitzmaurice PS, Shaw IC, Kleiner HE, Miller RT, Monks TJ, et al. 1996. Evidence for DNA damage in amyotrophic lateral sclerosis. *Muscle Nerve* 19: 797-8

Flaherty KM, DeLuca-Flaherty C, McKay DB. 1990. Three-dimensional structure of the ATPase fragment of a 70K heat-shock cognate protein. *Nature* 346: 623-8

Foran E, Trotti D. 2009. Glutamate transporters and the excitotoxic path to motor neuron degeneration in amyotrophic lateral sclerosis. *Antioxid Redox Signal* 11: 1587-602

Foust KD, Salazar DL, Likhite S, Ferraiuolo L, Ditsworth D, et al. 2013. Therapeutic AAV9-mediated Suppression of Mutant SOD1 Slows Disease Progression and Extends Survival in Models of Inherited ALS. *Mol Ther* 21: 2148-59

Frey D, Schneider C, Xu L, Borg J, Spooren W, Caroni P. 2000. Early and selective loss of neuromuscular synapse subtypes with low

sprouting competence in motoneuron diseases. *J Neurosci* 20: 2534-42

Frizzo ME, Dall'Onder LP, Dalcin KB, Souza DO. 2004. Riluzole enhances glutamate uptake in rat astrocyte cultures. *Cell Mol Neurobiol* 24: 123-8

Gassen M, Glinka Y, Pinchasi B, Youdim MB. 1996. Apomorphine is a highly potent free radical scavenger in rat brain mitochondrial fraction. *Eur J Pharmacol* 308: 219-25

Geyer J, Gavrilova O, Petzinger E. 2009. Brain penetration of ivermectin and selamectin in mdr1a,b P-glycoprotein- and bcrp- deficient knockout mice. *J Vet Pharmacol Ther* 32: 87-96

Geyer J, Klintzsch S, Meerkamp K, Wöhlke A, Distl O, et al. 2007. Detection of the nt230(del4) MDR1 mutation in White Swiss Shepherd dogs: case reports of doramectin toxicosis, breed predisposition, and microsatellite analysis. *J Vet Pharmacol Ther* 30: 482-5

Gifondorwa DJ, Jimenz-Moreno R, Hayes CD, Rouhani H, Robinson MB, et al. 2012. Administration of Recombinant Heat Shock Protein 70 Delays Peripheral Muscle Denervation in the SOD1(G93A) Mouse Model of Amyotrophic Lateral Sclerosis. *Neurol Res Int* 2012: 170426

Gifondorwa DJ, Robinson MB, Hayes CD, Taylor AR, Prevette DM, et al. 2007. Exogenous delivery of heat shock protein 70 increases lifespan in a mouse model of amyotrophic lateral sclerosis. *J Neurosci* 27: 13173-80

Gijselinck I, Van Langenhove T, van der Zee J, Sleegers K, Philtjens S, et al. 2012. A C9orf72 promoter repeat expansion in a Flanders-Belgian cohort with disorders of the frontotemporal lobar degeneration-amyotrophic lateral sclerosis spectrum: a gene identification study. *Lancet Neurol* 11: 54-65

Gómez-Tortosa E, Gallego J, Guerrero-López R, Marcos A, Gil-Neciga E, et al. 2013. C9ORF72 hexanucleotide expansions of 20-22 repeats are associated with frontotemporal deterioration. *Neurology* 80: 366-70

Gong YH, Parsadanian AS, Andreeva A, Snider WD, Elliott JL. 2000. Restricted expression of G86R Cu/Zn superoxide dismutase in astrocytes results in astrocytosis but does not cause motoneuron degeneration. *J Neurosci* 20: 660-5

Goodall EF, Heath PR, Bandmann O, Kirby J, Shaw PJ. 2013. Neuronal dark matter: the emerging role of microRNAs in neurodegeneration. *Front Cell Neurosci* 7: 178

Grad LI, Guest WC, Yanai A, Pokrishevsky E, O'Neill MA, et al. 2011. Intermolecular transmission of superoxide dismutase 1 misfolding in living cells. *Proc Natl Acad Sci U S A* 108: 16398-403

Griffin J, Fletcher N, Clemence R, Blanchflower S, Brayden DJ. 2005. Selamectin is a potent substrate and inhibitor of human and canine P-glycoprotein. *J Vet Pharmacol Ther* 28: 257-65

Grunnet ML, Leicher C, Zimmerman A, Zalneraitis E, Barwick M. 1989. Primary lateral sclerosis in a child. *Neurology* 39: 1530-2

Guo Y, Li C, Wu D, Wu S, Yang C, et al. 2010. Ultrastructural diversity of inclusions and aggregations in the lumbar spinal cord of SOD1-G93A transgenic mice. *Brain Res* 1353: 234-44

Gurney ME. 1994. Transgenic-mouse model of amyotrophic lateral sclerosis. *N Engl J Med* 331: 1721-2

Gurney ME, Cutting FB, Zhai P, Doble A, Taylor CP, et al. 1996. Benefit of vitamin E, riluzole, and gabapentin in a transgenic model of familial amyotrophic lateral sclerosis. *Ann Neurol* 39: 147-57

Hadano S, Hand CK, Osuga H, Yanagisawa Y, Otomo A, et al. 2001. A gene encoding a putative GTPase regulator is mutated in familial amyotrophic lateral sclerosis 2. *Nat Genet* 29: 166-73

Haidet-Phillips AM, Hester ME, Miranda CJ, Meyer K, Braun L, et al. 2011. Astrocytes from familial and sporadic ALS patients are toxic to motor neurons. *Nat Biotechnol* 29: 824-8

Harvey PJ, Li Y, Li X, Bennett DJ. 2006. Persistent sodium currents and repetitive firing in motoneurons of the sacrocaudal spinal cord of adult rats. *J Neurophysiol* 96: 1141-57

Hasegawa M, Nonaka T, Tsuji H, Tamaoka A, Yamashita M, et al. 2011. Molecular dissection of TDP-43 proteinopathies. *J Mol Neurosci* 45: 480-5

Henkel JS, Engelhardt JI, Siklós L, Simpson EP, Kim SH, et al. 2004. Presence of dendritic cells, MCP-1, and activated microglia/macrophages in amyotrophic lateral sclerosis spinal cord tissue. *Ann Neurol* 55: 221-35

Hetz C, Thielen P, Matus S, Nassif M, Court F, et al. 2009. XBP-1 deficiency in the nervous system protects against amyotrophic lateral sclerosis by increasing autophagy. *Genes Dev* 23: 2294-306

Hewamadduma CA, Grierson AJ, Ma TP, Pan L, Moens CB, et al. 2013. Tardbpl splicing rescues motor neuron and axonal development in a mutant tardbp zebrafish. *Hum Mol Genet* 22: 2376-86

Higashi S, Tsuchiya Y, Araki T, Wada K, Kabuta T. 2010. TDP-43 physically interacts with amyotrophic lateral sclerosis-linked mutant CuZn superoxide dismutase. *Neurochem Int* 57: 906-13

Higgins CF. 1992. ABC transporters: from microorganisms to man. *Annu Rev Cell Biol* 8: 67-113

Higgins CM, Jung C, Ding H, Xu Z. 2002. Mutant Cu, Zn superoxide dismutase that causes motoneuron degeneration is present in mitochondria in the CNS. *J Neurosci* 22: RC215

Hollmann M, Heinemann S. 1994. Cloned glutamate receptors. *Annu Rev Neurosci* 17: 31-108

Hopper K, Aldrich J, Haskins SC. 2002. Ivermectin toxicity in 17 collies. *J Vet Intern Med* 16: 89-94

Hortobagyi T, Troakes C, Nishimura AL, Vance C, van Swieten JC, et al. 2011. Optineurin inclusions occur in a minority of TDP-43 positive ALS and FTLD-TDP cases and are rarely observed in other neurodegenerative disorders. *Acta Neuropathol* 121: 519-27

Hoshino T, Murao N, Namba T, Takehara M, Adachi H, et al. 2011. Suppression of Alzheimer's disease-related phenotypes by expression of heat shock protein 70 in mice. *J Neurosci* 31: 5225-34

Howland DS, Liu J, She Y, Goad B, Maragakis NJ, et al. 2002. Focal loss of the glutamate transporter EAAT2 in a transgenic rat model of SOD1 mutant-mediated amyotrophic lateral sclerosis (ALS). *Proc Natl Acad Sci U S A* 99: 1604-9

Igaz LM, Kwong LK, Lee EB, Chen-Plotkin A, Swanson E, et al. 2011. Dysregulation of the ALS-associated gene TDP-43 leads to neuronal death and degeneration in mice. *J Clin Invest* 121: 726-38

Ihara R, Matsukawa K, Nagata Y, Kunugi H, Tsuji S, et al. 2013. RNA binding mediates neurotoxicity in the transgenic Drosophila model of TDP-43 proteinopathy. *Hum Mol Genet* 22: 4474-84

Irifune M, Kikuchi N, Saida T, Takarada T, Shimizu Y, et al. 2007. Riluzole, a glutamate release inhibitor, induces loss of righting reflex, antinociception, and immobility in response to noxious stimulation in mice. *Anesth Analg* 104: 1415-21, table of contents

Ito D, Seki M, Tsunoda Y, Uchiyama H, Suzuki N. 2011. Nuclear transport impairment of amyotrophic lateral sclerosis-linked mutations in FUS/TLS. *Ann Neurol* 69: 152-62

Ito H, Wate R, Zhang J, Ohnishi S, Kaneko S, et al. 2008. Treatment with edaravone, initiated at symptom onset, slows motor decline and decreases SOD1 deposition in ALS mice. *Exp Neurol* 213: 448-55

Jaarsma D, Teuling E, Haasdijk ED, De Zeeuw CI, Hoogenraad CC. 2008. Neuron-specific expression of mutant superoxide dismutase is sufficient to induce amyotrophic lateral sclerosis in transgenic mice. *J Neurosci* 28: 2075-88

Jaiswal MK, Keller BU. 2009. Cu/Zn superoxide dismutase typical for familial amyotrophic lateral sclerosis increases the vulnerability of mitochondria and perturbs Ca2+ homeostasis in SOD1G93A mice. *Mol Pharmacol* 75: 478-89

Jiang M, Schuster JE, Fu R, Siddique T, Heckman CJ. 2009. Progressive changes in synaptic inputs to motoneurons in adult sacral spinal cord of a mouse model of amyotrophic lateral sclerosis. *J Neurosci* 29: 15031-8

Johnson JO, Mandrioli J, Benatar M, Abramzon Y, Van Deerlin VM, et al. 2010. Exome sequencing reveals VCP mutations as a cause of familial ALS. *Neuron* 68: 857-64

Johnston CA, Stanton BR, Turner MR, Gray R, Blunt AH, et al. 2006. Amyotrophic lateral sclerosis in an urban setting: a population based study of inner city London. *J Neurol* 253: 1642-3

Johnston JA, Dalton MJ, Gurney ME, Kopito RR. 2000. Formation of high molecular weight complexes of mutant Cu, Zn-superoxide dismutase in a mouse model for familial amyotrophic lateral sclerosis. *Proc Natl Acad Sci U S A* 97: 12571-6

Joyce PI, Fratta P, Fisher EM, Acevedo-Arozena A. 2011. SOD1 and TDP-43 animal models of amyotrophic lateral sclerosis: recent advances in understanding disease toward the development of clinical treatments. *Mamm Genome*

Juliano RL, Ling V. 1976. A surface glycoprotein modulating drug permeability in Chinese hamster ovary cell mutants. *Biochim Biophys Acta* 455: 152-62

Jung C, Higgins CM, Xu Z. 2002. A quantitative histochemical assay for activities of mitochondrial electron transport chain complexes in mouse spinal cord sections. *J Neurosci Methods* 114: 165-72

Kalmar B, Greensmith L. 2009. Activation of the heat shock response in a primary cellular model of motoneuron neurodegeneration-evidence for neuroprotective and neurotoxic effects. *Cell Mol Biol Lett* 14: 319-35

Kalmar B, Novoselov S, Gray A, Cheetham ME, Margulis B, Greensmith L. 2008. Late stage treatment with arimoclomol delays disease progression and prevents protein aggregation in the SOD1 mouse model of ALS. *J Neurochem* 107: 339-50

Karch CM, Borchelt DR. 2008. A limited role for disulfide cross-linking in the aggregation of mutant SOD1 linked to familial amyotrophic lateral sclerosis. *J Biol Chem* 283: 13528-37

Karlovich CA, John RM, Ramirez L, Stainier DY, Myers RM. 1998. Characterization of the Huntington's disease (HD) gene homologue in the zebrafish Danio rerio. *Gene* 217: 117-25

Kato M, Han TW, Xie S, Shi K, Du X, et al. 2012. Cell-free formation of RNA granules: low complexity sequence domains form dynamic fibers within hydrogels. *Cell* 149: 753-67

Kaufman RJ. 2002. Orchestrating the unfolded protein response in health and disease. *J Clin Invest* 110: 1389-98

Keller AF, Gravel M, Kriz J. 2011. Treatment with minocycline after disease onset alters astrocyte reactivity and increases microgliosis in SOD1 mutant mice. *Exp Neurol* 228: 69-79

Kempster PA, Frankel JP, Stern GM, Lees AJ. 1990. Comparison of motor response to apomorphine and levodopa in Parkinson's disease. *J Neurol Neurosurg Psychiatry* 53: 1004-7

Kieran D, Kalmar B, Dick JR, Riddoch-Contreras J, Burnstock G, Greensmith L. 2004. Treatment with arimoclomol, a coinducer of heat shock proteins, delays disease progression in ALS mice. *Nat Med* 10: 402-5

Kim KS, Lee HJ, An J, Kim YB, Ra JC, et al. 2013. Transplantation of human adipose tissue-derived stem cells delays clinical onset and prolongs life span in ALS mouse model. *Cell Transplant*

King AE, Dickson TC, Blizzard CA, Foster SS, Chung RS, et al. 2007. Excitotoxicity mediated by non-NMDA receptors causes distal axonopathy in long-term cultured spinal motor neurons. *Eur J Neurosci* 26: 2151-9

Kipnis J, Avidan H, Caspi RR, Schwartz M. 2004. Dual effect of CD4+CD25+ regulatory T cells in neurodegeneration: a dialogue with microglia. *Proc Natl Acad Sci U S A* 101 Suppl 2: 14663-9

Kirby J, Goodall EF, Smith W, Highley JR, Masanzu R, et al. 2010. Broad clinical phenotypes associated with TAR-DNA binding protein (TARDBP) mutations in amyotrophic lateral sclerosis. *Neurogenetics* 11: 217-25

Klivenyi P, Ferrante RJ, Matthews RT, Bogdanov MB, Klein AM, et al. 1999. Neuroprotective effects of creatine in a transgenic animal model of amyotrophic lateral sclerosis. *Nat Med* 5: 347-50

Koppers M, van Blitterswijk MM, Vlam L, Rowicka PA, van Vught PW, et al. 2012. VCP mutations in familial and sporadic amyotrophic lateral sclerosis. *Neurobiol Aging* 33: 837 e7-13

Krajewski KM, Lewis RA, Fuerst DR, Turansky C, Hinderer SR, et al. 2000. Neurological dysfunction and axonal degeneration in Charcot-Marie-Tooth disease type 1A. *Brain* 123 (Pt 7): 1516-27

Kriz J, Nguyen MD, Julien JP. 2002. Minocycline slows disease progression in a mouse model of amyotrophic lateral sclerosis. *Neurobiol Dis* 10: 268-78

Kuo PH, Doudeva LG, Wang YT, Shen CK, Yuan HS. 2009. Structural insights into TDP-43 in nucleic-acid binding and domain interactions. *Nucleic Acids Res* 37: 1799-808

Kurji K, Payne M, Doyle H, LaMarca J. 2006. The lesser evils of battling round goby infiltration. *CMAJ* 174: 1557

Kwak MK, Wakabayashi N, Greenlaw JL, Yamamoto M, Kensler TW. 2003. Antioxidants enhance mammalian proteasome expression through the Keap1-Nrf2 signaling pathway. *Mol Cell Biol* 23: 8786-94

Kwiatkowski TJ, Jr., Bosco DA, Leclerc AL, Tamrazian E, Vanderburg CR, et al. 2009. Mutations in the FUS/TLS gene on chromosome 16 cause familial amyotrophic lateral sclerosis. *Science* 323: 1205-8

Lagier-Tourenne C, Polymenidou M, Hutt KR, Vu AQ, Baughn M, et al. 2012. Divergent roles of ALS-linked proteins FUS/TLS and TDP-43 intersect in processing long pre-mRNAs. *Nat Neurosci* 15: 1488-97

Lahnsteiner F. 2008. The effect of internal and external cryoprotectants on zebrafish (Danio rerio) embryos. *Theriogenology* 69: 384-96

Lemmens R, Van Hoecke A, Hersmus N, Geelen V, D'Hollander I, et al. 2007. Overexpression of mutant superoxide dismutase 1 causes a motor axonopathy in the zebrafish. *Hum Mol Genet* 16: 2359-65

Lerman-Sagie T, Filiano J, Smith DW, Korson M. 1996. Infantile onset of hereditary ascending spastic paralysis with bulbar involvement. *J Child Neurol* 11: 54-7

Lespine A, Martin S, Dupuy J, Roulet A, Pineau T, et al. 2007. Interaction of macrocyclic lactones with P-glycoprotein: structure-affinity relationship. *Eur J Pharm Sci* 30: 84-94

Li Q, Lau A, Morris TJ, Guo L, Fordyce CB, Stanley EF. 2004. A syntaxin 1, Galpha(o), and N-type calcium channel complex at a presynaptic nerve terminal: analysis by quantitative immunocolocalization. *J Neurosci* 24: 4070-81

Lincecum JM, Vieira FG, Wang MZ, Thompson K, De Zutter GS, et al. 2010. From transcriptome analysis to therapeutic anti-CD40L treatment in the SOD1 model of amyotrophic lateral sclerosis. *Nat Genet* 42: 392-9

Liu J, Shinobu LA, Ward CM, Young D, Cleveland DW. 2005. Elevation of the Hsp70 chaperone does not effect toxicity in mouse models of familial amyotrophic lateral sclerosis. *J Neurochem* 93: 875-82

Loizzo S, Pieri M, Ferri A, Carri MT, Zona C, et al. 2010. Dynamic NAD(P)H post-synaptic autofluorescence signals for the assessment of mitochondrial function in a neurodegenerative disease: monitoring the primary motor cortex of G93A mice, an amyotrophic lateral sclerosis model. *Mitochondrion* 10: 108-14

Lynagh T, Webb TI, Dixon CL, Cromer BA, Lynch JW. 2011. Molecular determinants of ivermectin sensitivity at the glycine receptor chloride channel. *J Biol Chem* 286: 43913-24

Mackenzie IR, Bigio EH, Ince PG, Geser F, Neumann M, et al. 2007. Pathological TDP-43 distinguishes sporadic amyotrophic lateral sclerosis from amyotrophic lateral sclerosis with SOD1 mutations. *Ann Neurol* 61: 427-34

Mackenzie IR, Rademakers R, Neumann M. 2010. TDP-43 and FUS in amyotrophic lateral sclerosis and frontotemporal dementia. *Lancet Neurol* 9: 995-1007

Maekawa S, Al-Sarraj S, Kibble M, Landau S, Parnavelas J, et al. 2004. Cortical selective vulnerability in motor neuron disease: a morphometric study. *Brain* 127: 1237-51

Majounie E, Renton AE, Mok K, Dopper EG, Waite A, et al. 2012. Frequency of the C9orf72 hexanucleotide repeat expansion in

patients with amyotrophic lateral sclerosis and frontotemporal dementia: a cross-sectional study. *Lancet Neurol* 11: 323-30

Mandrell D, Truong L, Jephson C, Sarker MR, Moore A, et al. 2012. Automated zebrafish chorion removal and single embryo placement: optimizing throughput of zebrafish developmental toxicity screens. *J Lab Autom* 17: 66-74

Mantovani S, Garbelli S, Pasini A, Alimonti D, Perotti C, et al. 2009. Immune system alterations in sporadic amyotrophic lateral sclerosis patients suggest an ongoing neuroinflammatory process. *J Neuroimmunol* 210: 73-9

Mantz J, Chéramy A, Thierry AM, Glowinski J, Desmonts JM. 1992. Anesthetic properties of riluzole (54274 RP), a new inhibitor of glutamate neurotransmission. *Anesthesiology* 76: 844-8

Martin RJ. 1997. Modes of action of anthelmintic drugs. *Vet J* 154: 11-34

Maruyama H, Morino H, Ito H, Izumi Y, Kato H, et al. 2010. Mutations of optineurin in amyotrophic lateral sclerosis. *Nature* 465: 223-6

Matsumoto G, Stojanovic A, Holmberg CI, Kim S, Morimoto RI. 2005. Structural properties and neuronal toxicity of amyotrophic lateral sclerosis-associated Cu/Zn superoxide dismutase 1 aggregates. *J Cell Biol* 171: 75-85

Mattiazzi M, D'Aurelio M, Gajewski CD, Martushova K, Kiaei M, et al. 2002. Mutated human SOD1 causes dysfunction of oxidative phosphorylation in mitochondria of transgenic mice. *J Biol Chem* 277: 29626-33

Mayer MP. 2013. Hsp70 chaperone dynamics and molecular mechanism. *Trends Biochem Sci*

Mazzocchio R, Rossi A. 2010. Role of Renshaw cells in amyotrophic lateral sclerosis. *Muscle Nerve* 41: 441-3

Mazzone GL, Nistri A. 2011. Delayed neuroprotection by riluzole against excitotoxic damage evoked by kainate on rat organotypic spinal cord cultures. *Neuroscience* 190: 318-27

McCombe PA, Henderson RD. 2010. Effects of gender in amyotrophic lateral sclerosis. *Gend Med* 7: 557-70

McGown A, McDearmid JR, Panagiotaki N, Tong H, Al Mashhadi S, et al. 2013. Early interneuron dysfunction in ALS: insights from a mutant sod1 zebrafish model. *Ann Neurol* 73: 246-58

Mead RJ, Higginbottom A, Allen SP, Kirby J, Bennett E, et al. 2013. S[+] Apomorphine is a CNS penetrating activator of the Nrf2-ARE pathway with activity in mouse and patient fibroblast models of amyotrophic lateral sclerosis. *Free Radic Biol Med* 61C: 438-52

Mecocci P, MacGarvey U, Kaufman AE, Koontz D, Shoffner JM, et al. 1993. Oxidative damage to mitochondrial DNA shows marked age-dependent increases in human brain. *Ann Neurol* 34: 609-16

Millan MJ, Maiofiss L, Cussac D, Audinot V, Boutin JA, Newman-Tancredi A. 2002. Differential actions of antiparkinson agents at multiple classes of monoaminergic receptor. I. A multivariate analysis of the binding profiles of 14 drugs at 21 native and cloned human receptor subtypes. *J Pharmacol Exp Ther* 303: 791-804

Mitchell JC, McGoldrick P, Vance C, Hortobagyi T, Sreedharan J, et al. 2013. Overexpression of human wild-type FUS causes progressive motor neuron degeneration in an age- and dose-dependent fashion. *Acta Neuropathol* 125: 273-88

Mitchell JD. 1987. Heavy metals and trace elements in amyotrophic lateral sclerosis. *Neurologic clinics* 5: 43-60

Moi P, Chan K, Asunis I, Cao A, Kan YW. 1994. Isolation of NF-E2-related factor 2 (Nrf2), a NF-E2-like basic leucine zipper transcriptional activator that binds to the tandem NF-E2/AP1 repeat of the beta-globin locus control region. *Proc Natl Acad Sci U S A* 91: 9926-30

Moreno JA, Halliday M, Molloy C, Radford H, Verity N, et al. 2013. Oral treatment targeting the unfolded protein response prevents neurodegeneration and clinical disease in prion-infected mice. *Sci Transl Med* 5: 206ra138

Mori K, Lammich S, Mackenzie IR, Forné I, Zilow S, et al. 2013a. hnRNP A3 binds to GGGGCC repeats and is a constituent of p62-positive/TDP43-negative inclusions in the hippocampus of patients with C9orf72 mutations. *Acta Neuropathol* 125: 413-23

Mori K, Weng SM, Arzberger T, May S, Rentzsch K, et al. 2013b. The C9orf72 GGGGCC repeat is translated into aggregating dipeptide-repeat proteins in FTLD/ALS. *Science* 339: 1335-8

Morimoto N, Nagai M, Ohta Y, Miyazaki K, Kurata T, et al. 2007. Increased autophagy in transgenic mice with a G93A mutant SOD1 gene. *Brain Res* 1167: 112-7

Nagai M, Aoki M, Miyoshi I, Kato M, Pasinelli P, et al. 2001. Rats expressing human cytosolic copper-zinc superoxide dismutase transgenes with amyotrophic lateral sclerosis: associated mutations develop motor neuron disease. *J Neurosci* 21: 9246-54

Nagai M, Re DB, Nagata T, Chalazonitis A, Jessell TM, et al. 2007. Astrocytes expressing ALS-linked mutated SOD1 release factors selectively toxic to motor neurons. *Nat Neurosci* 10: 615-22

Nagy D, Kato T, Kushner PD. 1994. Reactive astrocytes are widespread in the cortical gray matter of amyotrophic lateral sclerosis. *J Neurosci Res* 38: 336-47

Nalbandian A, Llewellyn KJ, Kitazawa M, Yin HZ, Badadani M, et al. 2012. The homozygote VCP($R^{155}H/R^{155}H$) mouse model exhibits accelerated human VCP-associated disease pathology. *PLoS One* 7: e46308

Neumann M, Sampathu DM, Kwong LK, Truax AC, Micsenyi MC, et al. 2006. Ubiquitinated TDP-43 in frontotemporal lobar degeneration and amyotrophic lateral sclerosis. *Science* 314: 130-3

Neymotin A, Calingasan NY, Wille E, Naseri N, Petri S, et al. 2011. Neuroprotective effect of Nrf2/ARE activators, CDDO ethylamide and CDDO trifluoroethylamide, in a mouse model of amyotrophic lateral sclerosis. *Free Radic Biol Med* 51: 88-96

Nihei K, McKee AC, Kowall NW. 1993. Patterns of neuronal degeneration in the motor cortex of amyotrophic lateral sclerosis patients. *Acta Neuropathol* 86: 55-64

Nishihira Y, Tan CF, Toyoshima Y, Yonemochi Y, Kondo H, et al. 2009. Sporadic amyotrophic lateral sclerosis: Widespread multisystem degeneration with TDP-43 pathology in a patient after long-term survival on a respirator. *Neuropathology* 29: 689-96

Novotny MJ, Krautmann MJ, Ehrhart JC, Godin CS, Evans EI, et al. 2000. Safety of selamectin in dogs. *Vet Parasitol* 91: 377-91

Okada Y, Sakai H, Kohiki E, Suga E, Yanagisawa Y, et al. 2005. A dopamine D4 receptor antagonist attenuates ischemia-induced neuronal cell damage via upregulation of neuronal apoptosis inhibitory protein. *J Cereb Blood Flow Metab* 25: 794-806

Pagala MK, Ravindran K, Namba T, Grob D. 1998. Skeletal muscle fatigue and physical endurance of young and old mice. *Muscle Nerve* 21: 1729-39

Papadeas ST, Kraig SE, O'Banion C, Lepore AC, Maragakis NJ. 2011. Astrocytes carrying the superoxide dismutase 1 (SOD1G93A) mutation induce wild-type motor neuron degeneration in vivo. *Proc Natl Acad Sci U S A* 108: 17803-8

Pasinelli P, Brown RH. 2006. Molecular biology of amyotrophic lateral sclerosis: insights from genetics. *Nature reviews* 7: 710-23

Paul AJ, Tranquilli WJ, Seward RL, Todd KS, DiPietro JA. 1987. Clinical observations in collies given ivermectin orally. *Am J Vet Res* 48: 684-5

Perlson E, Jeong GB, Ross JL, Dixit R, Wallace KE, et al. 2009. A switch in retrograde signaling from survival to stress in rapid-onset neurodegeneration. *J Neurosci* 29: 9903-17

Peterson RT, Shaw SY, Peterson TA, Milan DJ, Zhong TP, et al. 2004. Chemical suppression of a genetic mutation in a zebrafish model of aortic coarctation. *Nat Biotechnol* 22: 595-9

Phukan J, Pender NP, Hardiman O. 2007. Cognitive impairment in amyotrophic lateral sclerosis. *Lancet Neurol* 6: 994-1003

Plaut I. 2000. Effects of fin size on swimming performance, swimming behaviour and routine activity of zebrafish Danio rerio. *J Exp Biol* 203: 813-20

Pramatarova A, Laganière J, Roussel J, Brisebois K, Rouleau GA. 2001. Neuron-specific expression of mutant superoxide dismutase 1 in transgenic mice does not lead to motor impairment. *J Neurosci* 21: 3369-74

Pun S, Santos AF, Saxena S, Xu L, Caroni P. 2006. Selective vulnerability and pruning of phasic motoneuron axons in motoneuron disease alleviated by CNTF. *Nat Neurosci* 9: 408-19

Quinn N. 1995. Drug treatment of Parkinson's disease. *BMJ* 310: 575-9

Ramesh T, Lyon AN, Pineda RH, Wang C, Janssen PM, et al. 2010. A genetic model of amyotrophic lateral sclerosis in zebrafish displays phenotypic hallmarks of motoneuron disease. *Dis Model Mech* 3: 652-62

Ravits JM, La Spada AR. 2009. ALS motor phenotype heterogeneity, focality, and spread: deconstructing motor neuron degeneration. *Neurology* 73: 805-11

Reaume AG, Elliott JL, Hoffman EK, Kowall NW, Ferrante RJ, et al. 1996. Motor neurons in Cu/Zn superoxide dismutase-deficient mice develop normally but exhibit enhanced cell death after axonal injury. *Nat Genet* 13: 43-7

Reddy K, Zamiri B, Stanley SY, Macgregor RB, Pearson CE. 2013. The disease-associated r(GGGGCC)n repeat from the C9orf72 gene forms tract length-dependent uni- and multimolecular RNA G-quadruplex structures. *J Biol Chem* 288: 9860-6

Renton AE, Majounie E, Waite A, Simon-Sanchez J, Rollinson S, et al. 2011a. A hexanucleotide repeat expansion in C9ORF72 is the cause of chromosome 9p21-linked ALS-FTD. *Neuron* 72: 257-68

Renton AE, Majounie E, Waite A, Simón-Sánchez J, Rollinson S, et al. 2011b. A hexanucleotide repeat expansion in C9ORF72 is the cause of chromosome 9p21-linked ALS-FTD. *Neuron* 72: 257-68

Ringholz GM, Appel SH, Bradshaw M, Cooke NA, Mosnik DM, Schulz PE. 2005. Prevalence and patterns of cognitive impairment in sporadic ALS. *Neurology* 65: 586-90

Ritossa F. 1996. Discovery of the heat shock response. *Cell Stress Chaperones* 1: 97-8

Robinson MB, Tidwell JL, Gould T, Taylor AR, Newbern JM, et al. 2005. Extracellular heat shock protein 70: a critical component for motoneuron survival. *J Neurosci* 25: 9735-45

Rohde G, Kermer P, Reed JC, Bahr M, Weishaupt JH. 2008. Neuron-specific overexpression of the co-chaperone Bcl-2-associated athanogene-1 in superoxide dismutase 1(G93A)-transgenic mice. *Neuroscience* 157: 844-9

Rosen DR, Bowling AC, Patterson D, Usdin TB, Sapp P, et al. 1994. A frequent ala 4 to val superoxide dismutase-1 mutation is associated with a rapidly progressive familial amyotrophic lateral sclerosis. *Hum Mol Genet* 3: 981-7

Rosen DR, Siddique T, Patterson D, Figlewicz DA, Sapp P, et al. 1993. Mutations in Cu/Zn superoxide dismutase gene are associated with familial amyotrophic lateral sclerosis. *Nature* 362: 59-62

Rushmore TH, Morton MR, Pickett CB. 1991. The antioxidant responsive element. Activation by oxidative stress and identification of the DNA consensus sequence required for functional activity. *J Biol Chem* 266: 11632-9

Saari WS, King SW. 1973. Synthesis and biological activity of (6aS)-10,11-dihydroxyaporphine, the optical antipode of apomorphine. *J Med Chem* 16: 171-2

Sakowski SA, Lunn JS, Busta AS, Oh SS, Zamora-Berridi G, et al. 2012. Neuromuscular effects of G93A-SOD1 expression in zebrafish. *Mol Neurodegener* 7: 44

Sarlette A, Krampfl K, Grothe C, Neuhoff N, Dengler R, Petri S. 2008. Nuclear erythroid 2-related factor 2-antioxidative response element signaling pathway in motor cortex and spinal cord in amyotrophic lateral sclerosis. *J Neuropathol Exp Neurol* 67: 1055-62

Sasaki S. 2011. Autophagy in spinal cord motor neurons in sporadic amyotrophic lateral sclerosis. *J Neuropathol Exp Neurol* 70: 349-59

Saxena S, Cabuy E, Caroni P. 2009. A role for motoneuron subtype-selective ER stress in disease manifestations of FALS mice. *Nat Neurosci* 12: 627-36

Saxena S, Caroni P. 2011. Selective neuronal vulnerability in neurodegenerative diseases: from stressor thresholds to degeneration. *Neuron* 71: 35-48

Schaeffer JM, Haines HW. 1989. Avermectin binding in Caenorhabditis elegans. A two-state model for the avermectin binding site. *Biochem Pharmacol* 38: 2329-38

Schiffer D, Fiano V. 2004. Astrogliosis in ALS: possible interpretations according to pathogenetic hypotheses. *Amyotroph Lateral Scler Other Motor Neuron Disord* 5: 22-5

Schinkel AH, Smit JJ, van Tellingen O, Beijnen JH, Wagenaar E, et al. 1994. Disruption of the mouse mdr1a P-glycoprotein gene leads to a deficiency in the blood-brain barrier and to increased sensitivity to drugs. *Cell* 77: 491-502

Schmid B, Hruscha A, Hogl S, Banzhaf-Strathmann J, Strecker K, et al. 2013. Loss of ALS-associated TDP-43 in zebrafish causes muscle degeneration, vascular dysfunction, and reduced motor neuron axon outgrowth. *Proc Natl Acad Sci U S A* 110: 4986-91

Shamovsky I, Nudler E. 2008. New insights into the mechanism of heat shock response activation. *Cell Mol Life Sci* 65: 855-61

Sharp PS, Akbar MT, Bouri S, Senda A, Joshi K, et al. 2008. Protective effects of heat shock protein 27 in a model of ALS occur in the early stages of disease progression. *Neurobiol Dis* 30: 42-55

Shaw CE. 2010. Capturing VCP: another molecular piece in the ALS jigsaw puzzle. *Neuron* 68: 812-4

Shaw PJ, Forrest V, Ince PG, Richardson JP, Wastell HJ. 1995. CSF and plasma amino acid levels in motor neuron disease: elevation of CSF glutamate in a subset of patients. *Neurodegeneration* 4: 209-16

Shibata N, Hirano A, Kobayashi M, Sasaki S, Kato T, et al. 1994. Cu/Zn superoxide dismutase-like immunoreactivity in Lewy body-like inclusions of sporadic amyotrophic lateral sclerosis. *Neurosci Lett* 179: 149-52

Shoop WL, Mrozik H, Fisher MH. 1995. Structure and activity of avermectins and milbemycins in animal health. *Vet Parasitol* 59: 139-56

Sigel E, Baur R. 1987. Effect of avermectin B1a on chick neuronal gamma-aminobutyrate receptor channels expressed in Xenopus oocytes. *Mol Pharmacol* 32: 749-52

Skradski S, White HS. 2000. Topiramate blocks kainate-evoked cobalt influx into cultured neurons. *Epilepsia* 41 Suppl 1: S45-7

Song JH, Huang CS, Nagata K, Yeh JZ, Narahashi T. 1997. Differential action of riluzole on tetrodotoxin-sensitive and tetrodotoxin-resistant sodium channels. *The Journal of pharmacology and experimental therapeutics* 282: 707-14

Soriano ME, Scorrano L. 2010. The interplay between BCL-2 family proteins and mitochondrial morphology in the regulation of apoptosis. *Adv Exp Med Biol* 687: 97-114

Sotelo-Silveira JR, Lepanto P, Elizondo V, Horjales S, Palacios F, et al. 2009. Axonal mitochondrial clusters containing mutant SOD1 in transgenic models of ALS. *Antioxid Redox Signal* 11: 1535-45

Sreedharan J, Blair IP, Tripathi VB, Hu X, Vance C, et al. 2008. TDP-43 mutations in familial and sporadic amyotrophic lateral sclerosis. *Science* 319: 1668-72

Stephens B, Navarrete R, Guiloff RJ. 2001. Ubiquitin immunoreactivity in presumed spinal interneurones in motor neurone disease. *Neuropathol Appl Neurobiol* 27: 352-61

Takeuchi H, Kobayashi Y, Yoshihara T, Niwa J, Doyu M, et al. 2002. Hsp70 and Hsp40 improve neurite outgrowth and suppress intracytoplasmic aggregate formation in cultured neuronal cells expressing mutant SOD1. *Brain Res* 949: 11-22

Tavaria M, Gabriele T, Kola I, Anderson RL. 1996. A hitchhiker's guide to the human Hsp70 family. *Cell Stress Chaperones* 1: 23-8

Tazerart S, Viemari JC, Darbon P, Vinay L, Brocard F. 2007. Contribution of persistent sodium current to locomotor pattern generation in neonatal rats. *J Neurophysiol* 98: 613-28

Thiebaut F, Tsuruo T, Hamada H, Gottesman MM, Pastan I, Willingham MC. 1987. Cellular localization of the multidrug-resistance gene product P-glycoprotein in normal human tissues. *Proc Natl Acad Sci U S A* 84: 7735-8

Tiloca C, Ratti A, Pensato V, Castucci A, Soraru G, et al. 2012. Mutational analysis of VCP gene in familial amyotrophic lateral sclerosis. *Neurobiol Aging* 33: 630 e1-2

Tollervey JR, Curk T, Rogelj B, Briese M, Cereda M, et al. 2011. Characterizing the RNA targets and position-dependent splicing regulation by TDP-43. *Nat Neurosci* 14: 452-8

Tran TC, Sneed B, Haider J, Blavo D, White A, et al. 2007. Automated, quantitative screening assay for antiangiogenic compounds using transgenic zebrafish. *Cancer Res* 67: 11386-92

Tranquilli WJ, Paul AJ, Todd KS. 1991. Assessment of toxicosis induced by high-dose administration of milbemycin oxime in collies. *Am J Vet Res* 52: 1170-2

Trotti D, Rossi D, Gjesdal O, Levy LM, Racagni G, et al. 1996. Peroxynitrite inhibits glutamate transporter subtypes. *J Biol Chem* 271: 5976-9

Tumer Z, Bertelsen B, Gredal O, Magyari M, Nielsen KC, et al. 2012. Novel heterozygous nonsense mutation of the OPTN gene segregating in a Danish family with ALS. *Neurobiol Aging* 33: 208 e1-5

Turner BJ, Talbot K. 2008. Transgenics, toxicity and therapeutics in rodent models of mutant SOD1-mediated familial ALS. *Prog Neurobiol* 85: 94-134

Urushitani M, Ezzi SA, Julien JP. 2007. Therapeutic effects of immunization with mutant superoxide dismutase in mice models of amyotrophic lateral sclerosis. *Proc Natl Acad Sci U S A* 104: 2495-500

Urushitani M, Sik A, Sakurai T, Nukina N, Takahashi R, Julien JP. 2006. Chromogranin-mediated secretion of mutant superoxide dismutase proteins linked to amyotrophic lateral sclerosis. *Nat Neurosci* 9: 108-18

Vaccaro A, Patten SA, Ciura S, Maios C, Therrien M, et al. 2012. Methylene blue protects against TDP-43 and FUS neuronal toxicity in C. elegans and D. rerio. *PLoS One* 7: e42117

Valdmanis PN, Daoud H, Dion PA, Rouleau GA. 2009. Recent advances in the genetics of amyotrophic lateral sclerosis. *Curr Neurol Neurosci Rep* 9: 198-205

Van Den Bosch L, Van Damme P, Bogaert E, Robberecht W. 2006. The role of excitotoxicity in the pathogenesis of amyotrophic lateral sclerosis. *Biochim Biophys Acta* 1762: 1068-82

Van Den Bosch L, Vandenberghe W, Klaassen H, Van Houtte E, Robberecht W. 2000. Ca(2+)-permeable AMPA receptors and selective vulnerability of motor neurons. *J Neurol Sci* 180: 29-34

Van Langenhove T, van der Zee J, Van Broeckhoven C. 2012. The molecular basis of the frontotemporal lobar degeneration-amyotrophic lateral sclerosis spectrum. *Ann Med* 44: 817-28

van Zundert B, Peuscher MH, Hynynen M, Chen A, Neve RL, et al. 2008. Neonatal neuronal circuitry shows hyperexcitable disturbance in a mouse model of the adult-onset neurodegenerative disease amyotrophic lateral sclerosis. *J Neurosci* 28: 10864-74

Vance C, Rogelj B, Hortobagyi T, De Vos KJ, Nishimura AL, et al. 2009. Mutations in FUS, an RNA processing protein, cause familial amyotrophic lateral sclerosis type 6. *Science* 323: 1208-11

Vargas MR, Johnson DA, Sirkis DW, Messing A, Johnson JA. 2008. Nrf2 activation in astrocytes protects against neurodegeneration in mouse models of familial amyotrophic lateral sclerosis. *J Neurosci* 28: 13574-81

Vijayalakshmi K, Alladi PA, Ghosh S, Prasanna VK, Sagar BC, et al. 2011. Evidence of endoplasmic reticular stress in the spinal motor neurons exposed to CSF from sporadic amyotrophic lateral sclerosis patients. *Neurobiol Dis* 41: 695-705

Voigt A, Herholz D, Fiesel FC, Kaur K, Müller D, et al. 2010. TDP-43-mediated neuron loss in vivo requires RNA-binding activity. *PLoS One* 5: e12247

Volterra A, Trotti D, Tromba C, Floridi S, Racagni G. 1994. Glutamate uptake inhibition by oxygen free radicals in rat cortical astrocytes. *J Neurosci* 14: 2924-32

Vucic S, Nicholson GA, Kiernan MC. 2008. Cortical hyperexcitability may precede the onset of familial amyotrophic lateral sclerosis. *Brain* 131: 1540-50

Waibel S, Reuter A, Malessa S, Blaugrund E, Ludolph AC. 2004. Rasagiline alone and in combination with riluzole prolongs survival in an ALS mouse model. *J Neurol* 251: 1080-4

Wang J, Farr GW, Hall DH, Li F, Furtak K, et al. 2009. An ALS-linked mutant SOD1 produces a locomotor defect associated with aggregation and synaptic dysfunction when expressed in neurons of Caenorhabditis elegans. *PLoS Genet* 5: e1000350

Wang Y, Li M, Xu X, Song M, Tao H, Bai Y. 2012. Green tea epigallocatechin-3-gallate (EGCG) promotes neural progenitor cell proliferation and sonic hedgehog pathway activation during adult hippocampal neurogenesis. *Mol Nutr Food Res* 56: 1292-303

Watson MR, Lagow RD, Xu K, Zhang B, Bonini NM. 2008. A drosophila model for amyotrophic lateral sclerosis reveals motor neuron damage by human SOD1. *J Biol Chem* 283: 24972-81

Watts DJ, Strogatz SH. 1998. Collective dynamics of 'small-world' networks. *Nature* 393: 440-2

Weber M, Eisen A, Stewart HG, Andersen PM. 2000. Preserved slow conducting corticomotoneuronal projections in amyotrophic lateral sclerosis with autosomal recessive D90A CuZn-superoxide dismutase mutation. *Brain* 123 (Pt 7): 1505-15

Weger BD, Weger M, Jung N, Lederer C, Bräse S, Dickmeis T. 2013. A chemical screening procedure for glucocorticoid signaling with a zebrafish larva luciferase reporter system. *J Vis Exp*

Weisskopf MG, O'Reilly EJ, McCullough ML, Calle EE, Thun MJ, et al. 2005. Prospective study of military service and mortality from ALS. *Neurology* 64: 32-7

Westerfield M, ZFIN. 2000. The zebrafish book a guide for the laboratory use of zebrafish Danio (Brachydanio) rerio. Univ. of Oregon Press, Eugene, OR

Williamson TL, Cleveland DW. 1999. Slowing of axonal transport is a very early event in the toxicity of ALS-linked SOD1 mutants to motor neurons. *Nat Neurosci* 2: 50-6

Wittstock M, Wolters A, Benecke R. 2007. Transcallosal inhibition in amyotrophic lateral sclerosis. *Clin Neurophysiol* 118: 301-7

Wokke J. 1996. Riluzole. *Lancet* 348: 795-9

Wong PC, Pardo CA, Borchelt DR, Lee MK, Copeland NG, et al. 1995. An adverse property of a familial ALS-linked SOD1 mutation causes motor neuron disease characterized by vacuolar degeneration of mitochondria. *Neuron* 14: 1105-16

Xu YF, Gendron TF, Zhang YJ, Lin WL, D'Alton S, et al. 2010. Wild-type human TDP-43 expression causes TDP-43 phosphorylation, mitochondrial aggregation, motor deficits, and early mortality in transgenic mice. *J Neurosci* 30: 10851-9

Yamanaka K, Miller TM, McAlonis-Downes M, Chun SJ, Cleveland DW. 2006. Progressive spinal axonal degeneration and slowness in ALS2-deficient mice. *Ann Neurol* 60: 95-104

Yamanaka K, Vande Velde C, Eymard-Pierre E, Bertini E, Boespflug-Tanguy O, Cleveland DW. 2003. Unstable mutants in the peripheral endosomal membrane component ALS2 cause early-onset motor neuron disease. *Proc Natl Acad Sci U S A* 100: 16041-6

Yin HZ, Nalbandian A, Hsu CI, Li S, Llewellyn KJ, et al. 2012. Slow development of ALS-like spinal cord pathology in mutant valosin-containing protein gene knock-in mice. *Cell Death Dis* 3: e374

Yokota T, Yoshino A, Inaba A, Saito Y. 1996. Double cortical stimulation in amyotrophic lateral sclerosis. *J Neurol Neurosurg Psychiatry* 61: 596-600

Yu J, Jia Y, Guo Y, Chang G, Duan W, et al. 2010. Epigallocatechin-3-gallate protects motor neurons and regulates glutamate level. *FEBS Lett* 584: 2921-5

Zhang XD. 2011. Illustration of SSMD, z score, SSMD*, z* score, and t statistic for hit selection in RNAi high-throughput screens. *J Biomol Screen* 16: 775-85

Zhou H, Huang C, Chen H, Wang D, Landel CP, et al. 2010. Transgenic rat model of neurodegeneration caused by mutation in the TDP gene. *PLoS Genet* 6: e1000887